

THE EFFECTS OF SUPEROXIDE DISMUTASE ON
OSTEOARTICULAR CELLS AND STRUCTURAL
ANALYSIS OF OCHRONOSIS, IN A DISEASE MODEL
OF ALKAPTONURIA

By

Vishnu Dinesh Kammath

A Thesis Submitted to Lancaster University

For the Degree of MSc by Research

Supervisors: Dr Adam M. Taylor and Dr Marwan Bukhari

July 2017

Acknowledgments

I would like to thank Dr Adam Taylor for his excellent guidance and patience throughout this project, and Dr Marwan Bukhari for his support.

Dr Jemma Kerns provided invaluable guidance on Raman spectroscopy, without which this part of the project would not have been possible.

I would like to thank The Pathological Society for providing the funding for this project.

Finally, I would like to thank my family and Christie, who continue to support me and have helped me get this far.

Declaration

I hereby declare that this thesis is my own work and has not been submitted anywhere else for any other award. Where other sources of information have been used, they have been acknowledged.

Abstract

Introduction: Alkaptonuria (AKU) is a rare autosomal recessive condition resulting from deficiency of homogentisate 1,2 dioxygenase, causing inability to metabolise homogentisic acid (HGA). Over time HGA polymerises and deposits as a dark pigment within collagenous tissues; this process is ochronosis. Ochronosis causes rapid and early onset joint arthropathy, mimicking osteoarthritis in presentation. Ochronosis causes damage to the extracellular matrix and chondrocyte death. It is hypothesised that superoxide dismutase (SOD) may have a beneficial effect on chondrocytes and limit this polymerisation process. This research aims to observe the effects of SOD in an *in vitro* model of ochronosis, and identify structural changes in this model via Raman spectroscopy.

Methods: Immortalised human chondrocytes (C20) and osteosarcoma (MG63) cell lines were cultured in DMEM containing HGA, SOD or a combination of both for up to 14 days. Cell viability was assessed using trypan blue assay. Pigmentation was quantified using Schmorl's staining technique. A dimethylmethylene blue assay was performed to assess damage to proteoglycans. Structural analysis was then performed on an *in vitro* model of ochronosis via Raman spectroscopy.

Results: Addition of SOD to the culture medium indicates there is little effect on percentage viability of osteoarticular cells. All C20 cultures suggest a decrease in pigmentation upon addition of SOD by day 14. Pigmentation analysis of MG63 cultures indicate contrasting results at different magnification settings. In C20 and MG63 cells, there does not appear to be a difference in levels of sulphated glycosaminoglycan release between these treatment

groups. Results from Raman spectroscopy identify structural differences between control and HGA treated cultures.

Conclusion: The results indicate that SOD does have a role in the prevention of ochronosis. This suggests that SOD has the potential to be used as a therapeutic approach in the prevention of ochronosis in articular cartilage. Raman spectroscopy is able to highlight structural differences caused by ochronosis. This has implications for the use of Raman spectroscopy as a potential diagnostic tool in AKU, in the future.

Contents

| | |
|---|-----------|
| Acknowledgements | 2 |
| Declaration | 3 |
| Abstract | 4 |
| Contents | 6 |
| List of Abbreviations | 10 |
| List of Figures | 12 |
| List of Tables | 15 |
| Chapter 1 – Introduction | 16 |
| 1.1 Alkaptonuria | 16 |
| 1.2 History of AKU | 17 |
| 1.3 Pathogenesis and Clinical Features | 19 |
| 1.4 Management of AKU | 23 |
| 1.4.1 Low Tyrosine Diet | 23 |
| 1.4.2 Ascorbic Acid | 23 |
| 1.4.3 N-acetylcysteine | 23 |
| 1.4.4 Nitisinone | 24 |
| 1.4.5 Palliative Care | 24 |
| 1.5 Bone Ultrastructure | 25 |
| 1.6 Cartilage Ultrastructure | 26 |
| 1.7 MG63 and C20 | 29 |
| 1.8 OA | 29 |
| 1.9 The Role of Superoxide Dismutase in AKU Pathogenesis..... | 32 |

| | |
|---|-----------|
| 1.10 Raman Spectroscopy | 35 |
| 1.11 Summary | 36 |
| 1.14 Statement of Aims | 38 |
| Chapter 2 – Materials and Methods | 39 |
| 2.1 Materials | 39 |
| 2.1.1 Phosphate Buffer Solution Preparation | 39 |
| 2.1.2 SOD Preparation | 39 |
| 2.1.3 HGA Preparation | 40 |
| 2.2 Cell Culture | 40 |
| 2.3 Experiment I – The Effects of SOD on C20 and MG63 Cell Lines | 41 |
| 2.3.1 Preparation of Samples | 41 |
| 2.3.2 Trypan Blue Exclusion Assay to Assess Cell Viability | 42 |
| 2.3.3 Statistical Analysis | 43 |
| 2.4 Experiment II - The Effects of SOD on an <i>in vitro</i> Model of Ochronosis | 44 |
| 2.4.1 Effects of SOD and HGA on Cell Viability | 44 |
| 2.4.2 Statistical Analysis | 45 |
| 2.4.3 Identification and Quantitation of Ochronotic Pigment Deposition <i>in vitro</i> | 45 |
| 2.4.3.1 Preparation of 10% Phosphate Buffered Formalin Solution | 45 |
| 2.4.3.2 Preparation of Schmorl’s Stain | 46 |
| 2.4.3.3 Schmorl’s Staining and Analysis of Samples | 46 |
| 2.4.4 Statistical Analysis | 47 |
| 2.5 Experiment III – Analysis of Sulphated GAG Release in an <i>in vitro</i> Model of Ochronosis, Following Treatment with SOD | 48 |
| 2.5.1 Preparation of Dimethylmethylene Blue | 48 |

| | |
|--|-----------|
| 2.5.2 DMMB Assay | 48 |
| 2.5.3 Statistical Analysis | 49 |
| 2.6 Experiment IV - Raman Spectroscopy of an <i>in vitro</i> Model of Ochronosis | 50 |
| 2.6.1 Preparation of Samples for Raman Spectroscopy Analysis | 50 |
| 2.6.2 Raman Spectroscopy Instrumentation and Analysis | 50 |
| 2.6.3 Data Pre-Processing and Statistical Analysis | 51 |
| Chapter 3 – Results I | 53 |
| 3.1 The Effects of SOD on C20 and MG63 Cell Lines | 53 |
| 3.2 Summary of Results | 56 |
| Chapter 4– Results II | 58 |
| 4.1 The Effects of SOD on an <i>in vitro</i> Model of Ochronosis | 58 |
| 4.1.1 C20 – Cell Viability and Histological Analysis | 59 |
| 4.1.2 MG63 – Cell Viability and Histological Analysis | 65 |
| 4.2 Summary of Results | 71 |
| Chapter 5 – Results III | 72 |
| 5.1 Analysis of Sulphated GAG Release in an <i>in vitro</i> Model of Ochronosis, Following Treatment with SOD | 72 |
| 5.1.1 C20 – DMMB Assay | 73 |
| 5.1.2 MG63 – DMMB Assay | 78 |
| 5.2 Summary of Results | 83 |
| Chapter 6 – Results IV..... | 84 |
| 6.1 Raman Spectroscopy of an <i>in vitro</i> Model of Ochronosis | 84 |
| 6.2 Summary of Results | 96 |
| Chapter 7 – Discussion | 97 |

| | |
|---|------------|
| 7.1 The Effects of SOD on C20 and MG63 Cell Lines | 97 |
| 7.2 The Effects of SOD on an <i>in vitro</i> Model of Ochronosis | 99 |
| 7.3 Analysis of Sulphated GAG Release in an <i>in vitro</i> Model of Ochronosis, Following Treatment with SOD..... | 102 |
| 7.4 Raman Spectroscopy of an <i>in vitro</i> Model of Ochronosis | 104 |
| 7.5 Conclusion | 109 |
| References | 113 |

List of Abbreviations

| | |
|------------------|-------------------------------------|
| AKU | Alkaptonuria |
| ANOVA | Analysis of Variance |
| ASC | Ascorbic Acid |
| BQA | Benzoquinone Acetic Acid |
| CaF ₂ | Calcium Fluoride |
| CS | Chondroitin Sulphate |
| DMEM | Dulbecco's Modified Eagle's Medium |
| DMMB | Dimethylmethylene Blue |
| ECM | Extracellular Matrix |
| FCS | Foetal Calf Serum |
| FDA | Food and Drug Administration |
| GAG | Glycosaminoglycan |
| HA | Hyaluronic Acid |
| HGA | Homogentisic Acid |
| HGD | Homogentisate 1,2 Dioxygenase |
| HPPD | 4-Hydroxyphenylpyruvate Dioxygenase |
| IGF-1 | Insulin-Like Growth Factor |
| IL-1 | Interleukin 1 |
| IL-4 | Interleukin 4 |
| IL-6 | Interleukin 6 |
| IL-10 | Interleukin 10 |

| | |
|---------------|---------------------------------------|
| LDA | Linear Discriminant Analysis |
| MMP | Matrix Metalloproteinase |
| NAC | N-acetylcysteine |
| OA | Osteoarthritis |
| PBS | Phosphate Buffer Solution |
| PC | Principle Component |
| PBFS | Phosphate Buffered Formalin Solution |
| PCA | Principle Component Analysis |
| P/S | Penicillin/Streptomycin |
| ROS | Reactive Oxygen Species |
| SEM | Standard Error of Mean |
| SOD | Superoxide Dismutase |
| TGF- β | Transforming Growth Factor β |
| TIMP | Tissue Inhibitor of Metalloproteinase |
| TNF- α | Tumour Necrosis Factor α |

List of Figures

Chapter 1

| | | |
|------------|--|----|
| 1.1 | The Distribution of Patients Identified with AKU | 17 |
| 1.2 | Tyrosine Degradation Pathway | 19 |
| 1.3 | Zonal Layers of Articular Cartilage | 28 |
| 1.4 | Cytokines Which Influence Anabolic and Catabolic Activities | 30 |
| 1.5 | Components Involved in the Breakdown of Cartilage in OA | 32 |
| 1.6 | The role of superoxide anions in the initiation of ochronosis. | 35 |

Chapter 2

| | | |
|------------|--|----|
| 2.1 | Mammalian Cell Counting Formula | 41 |
| 2.2 | Dilution Factor Formula | 43 |
| 2.3 | Percentage Viability Formula | 43 |
| 2.4 | The Dehydration Process for Schmorl's Staining | 47 |
| 2.5 | Spectral Acquisition Settings | 51 |

Chapter 3

| | | |
|------------|---|----|
| 3.1 | Percentage Viability of C20 Cells Using a Range of Concentrations of SOD | 54 |
| 3.2 | Percentage Viability of MG63 Cells Using a Range of Concentrations of SOD | 55 |

Chapter 4

| | | |
|------------|---|----|
| 4.1 | Percentage Viability of C20 Cultures (Day 7) | 59 |
| 4.2 | Percentage Viability of C20 Cultures (Day 14) | 59 |
| 4.3 | Microscopy Images of C20 Cultures (x10) | 60 |
| 4.4 | Pigment count of C20 Cultures (Day 7) (x10) | 61 |

| | | |
|-------------|--|----|
| 4.5 | Pigment count of C20 Cultures (Day 14) (x10) | 61 |
| 4.6 | Microscopy Images of C20 Cultures (x40) | 62 |
| 4.7 | Pigment count of C20 Cultures (Day 7) (x40) | 63 |
| 4.8 | Pigment count of C20 Cultures (Day 14) (x40) | 63 |
| 4.9 | Percentage Viability of MG63 Cultures (Day 7) | 65 |
| 4.10 | Percentage Viability of MG63 Cultures (Day 14) | 65 |
| 4.11 | Microscopy Images of MG63 Cultures (x10) | 66 |
| 4.12 | Pigment count of MG63 Cultures (Day 7) (x10) | 67 |
| 4.13 | Pigment count of MG63 Cultures (Day 14) (x10) | 67 |
| 4.14 | Microscopy Images of MG63 Cultures (x40) | 68 |
| 4.15 | Pigment count of MG63 Cultures (Day 7) (x40) | 69 |
| 4.16 | Pigment count of MG63 Cultures (Day 14) (x40) | 69 |

Chapter 5

| | | |
|------------|--|----|
| 5.1 | Concentration of Sulphated GAGs in C20 Culture Medium (Day 4) | 73 |
| 5.2 | Concentration of Sulphated GAGs in C20 Culture Medium (Day 8) | 73 |
| 5.3 | Concentration of Sulphated GAGs in C20 Culture Medium (Day 12) | 74 |
| 5.4 | Concentration of Sulphated GAGs in C20 Culture Medium (Day 14) | 74 |
| 5.5 | Comparison of Sulphated GAG Concentrations in C20 Control Cultures | 75 |
| 5.6 | Comparison of Sulphated GAG Concentrations in C20 HGA Cultures | 75 |
| 5.7 | Comparison of Sulphated GAG Concentrations in C20 SOD Cultures | 76 |
| 5.8 | Comparison of Sulphated GAG Concentrations in C20 HGA+SOD Cultures | 76 |
| 5.9 | Concentration of Sulphated GAGs in MG63 Culture Medium (Day 4) | 78 |

| | | |
|------------------|--|----|
| 5.10 | Concentration of Sulphated GAGs in MG63 Culture Medium (Day 8) | 78 |
| 5.11 | Concentration of Sulphated GAGs in MG63 Culture Medium (Day 12) | 79 |
| 5.12 | Concentration of Sulphated GAGs in MG63 Culture Medium (Day 14) | 79 |
| 5.13 | Comparison of Sulphated GAG Concentrations in MG63 Control Cultures | 80 |
| 5.14 | Comparison of Sulphated GAG Concentrations in MG63 HGA Cultures | 80 |
| 5.15 | Comparison of Sulphated GAG Concentrations in MG63 SOD Cultures | 81 |
| 5.16 | Comparison of Sulphated GAG Concentrations in MG63 HGA+SOD Cultures | 81 |
| Chapter 6 | | |
| 6.1 | Average Spectra of C20 Control and HGA Cultures | 86 |
| 6.2 | Average Spectra of MG63 Control and HGA Cultures | 87 |
| 6.3 | PCA Analysis of all C20 and MG63 Cultures | 88 |
| 6.4 | PCA-LDA Analysis of all C20 and MG63 Cultures | 88 |
| 6.5 | Loadings Plot of LD1 Following PCA-LDA analysis of all C20 and MG63 Cultures | 89 |
| 6.6 | Loadings Plot of LD3 Following PCA-LDA analysis of all C20 and MG63 Cultures | 90 |
| 6.7 | PCA-LDA Analysis of C20 Control and HGA Cultures | 91 |
| 6.8 | Loadings Plot of LD1 Following PCA-LDA analysis of C20 Control and HGA Cultures | 91 |
| 6.9 | PCA-LDA Analysis of MG63 Control and HGA Cultures | 92 |
| 6.10 | Loadings Plot of LD1 Following PCA-LDA analysis of MG63 Control and HGA Cultures | 92 |

List of Tables

Chapter 1

| | | |
|------------|---------------------------------------|----|
| 1.1 | Signs and Symptoms Associated With OA | 30 |
|------------|---------------------------------------|----|

Chapter 2

| | | |
|------------|---|----|
| 2.1 | Concentration Range of SOD Used in Experiment 1 | 42 |
| 2.2 | Volumes of Reagents Used in Experiment 1 | 42 |
| 2.3 | Concentrations of HGA and/or SOD Used in Experiment 2 | 44 |
| 2.4 | Volume of Reagents Used in Experiment 2 | 45 |
| 2.5 | Serial Dilution of CS in DMEM | 49 |

Chapter 1 – Introduction

1.1 Alkaptonuria

Alkaptonuria (AKU) is an autosomal recessive, metabolic disease resulting from mutations to the homogentisate 1,2 dioxygenase (HGD) gene. This genetic defect results in an accumulation of homogentisic acid (HGA), which undergoes polymerisation and deposits in cartilages, leading to an extreme and debilitating form of osteoarthropathy. This condition was the first to demonstrate a Mendelian pattern of inheritance and was also used to coin the term “inborn errors of metabolism” by Archibald Garrod (1, 2).

The prevalence of AKU is extremely low. It is estimated there are approximately 950 people diagnosed with the condition worldwide, from 61 identified countries (3). However, areas such as the Dominican Republic and Slovakia show a relatively higher prevalence, estimated to be 1: 19,000. Two hundred and eight patients have been diagnosed with AKU in Slovakia, of which 110 are children (Fig. 1.1) (4). More recently, countries such as Jordan and India have seen a rise in the number of diagnosed cases of AKU. This suggests that there are still numerous unidentified cases and the current prevalence of the condition is underestimated (3, 5). The recent rise in the number of cases of AKU in Jordan for example, can be attributed to increased awareness of the condition among health care providers and high rates of consanguineous marriages, suggesting a founder effect (3, 5). This raised profile of the condition has enabled the identification of more HGD gene variants, with at least 129 mutations currently identified, enabling studies in genotype-phenotype correlation in AKU (3).

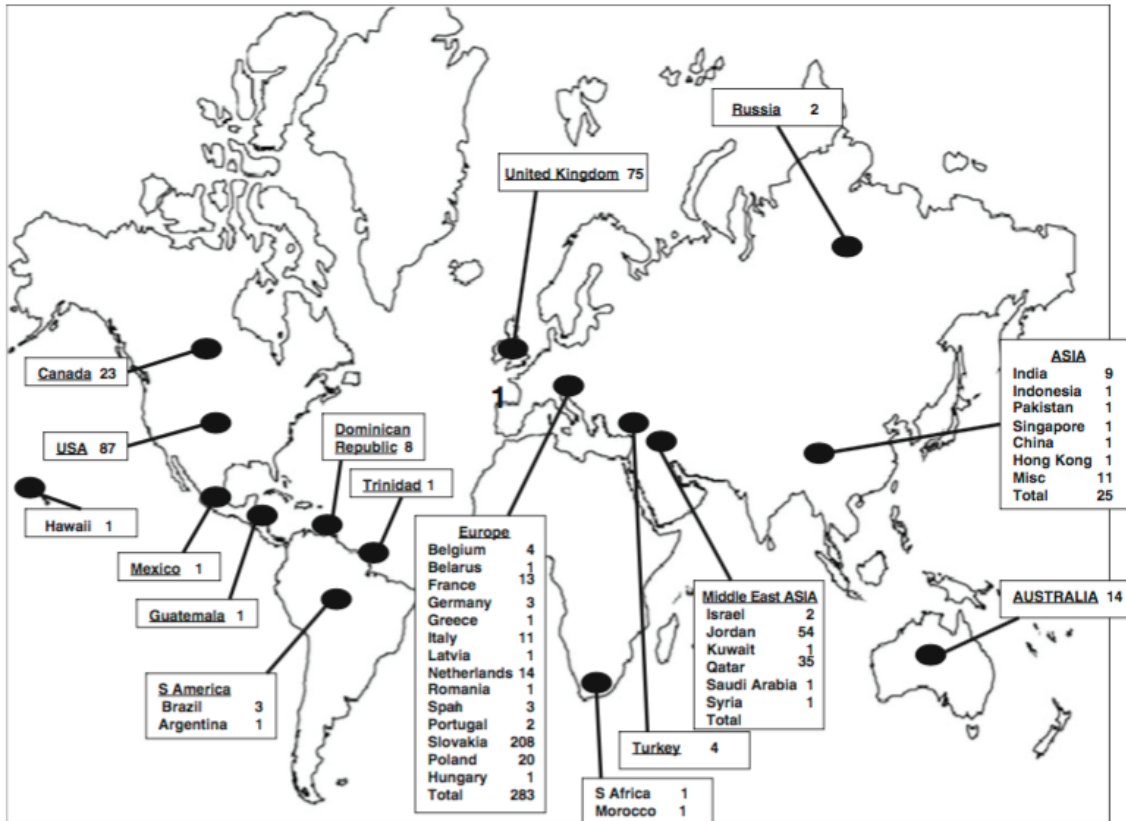


Fig. 1.1. Taken from reference (4). The distribution of patients identified with AKU, worldwide in 2011.

1.2 History of AKU

The earliest documented case of AKU was by Scribonius in 1586, of a school boy who excreted black urine. The cause of this phenomena, however, was not known as the boy appeared otherwise well (6). It was not until Boedeker, that the term *Alkaptonuria* was associated with black urine. At the time, there was confusion between AKU and diabetes, as many thought AKU was an atypical form of diabetes. Boedeker attempted to identify glucose in an AKU urine sample, but instead noticed that a reduction reaction was occurring in alkaline conditions. He therefore termed the causative substance “Alkapton”; a combination of the Arabic word

meaning alkali and the Greek word meaning “to suck up” oxygen greedily in alkali. *Alkaptonuria* was therefore the term used to describe the condition (2, 6, 7).

The term ochronosis was coined by Virchow, who during an autopsy, noticed dark pigment deposits in the cartilage of a sixty-seven-year-old male. When he took some samples and put them under the microscope, they displayed an “ochre” (yellow) colour (8, 9). Ochronosis was not linked to AKU until Albrecht, in 1902, showed that a patient known to have AKU also demonstrated ochronosis. Further evidence to link ochronosis to AKU was provided by Osler, who demonstrated that two brothers with AKU showed pigmentation in cartilaginous areas, such as the eyes, ears and nose (6, 7).

Wolkow and Bauman were the first to isolate and identify the structural formula of the pigment that undergoes ochronosis. Their results showed that the chemical compound shared a similar structure to the salicylic acid metabolite, gentisic acid, hence they termed the compound *homogentisic acid* in 1891. It was then Archibald Garrod, who by using the term “inborn error of metabolism”, suggested that there was a specific enzyme defect causing ochronosis. Fifty years later this was proven by La Du who showed that the enzyme involved was HGD (2, 6, 7, 10).

In recent years, several advances have been made in AKU research. The Egyptian mummy Harwa, dated back to 1500 B.C. was verified as the earliest case of AKU (11). The defective gene was identified and located on chromosome 3q2, enabling identification of the various mutations attributed to AKU (3, 8). An *in vitro* model synonymous with the human condition was also established. This model has enabled research into the pathological process of AKU,

and assessment of possible therapeutic interventions (12, 13). Despite this, there are still gaps in the understanding of AKU pathology, with current treatment only being palliative (14).

1.3 Pathogenesis and Clinical Features

AKU is caused by a genetic defect to the gene coding for the HGD enzyme. This defect results in a lack of production of HGD. Normally present in the liver, HGD is involved in the tyrosine degradation pathway (Fig. 1.2) (2). It is responsible for the breakdown of HGA to maleylacetoacetic acid. A lack of this enzyme, therefore causes an accumulation of HGA, resulting in the clinical features associated with AKU (15).

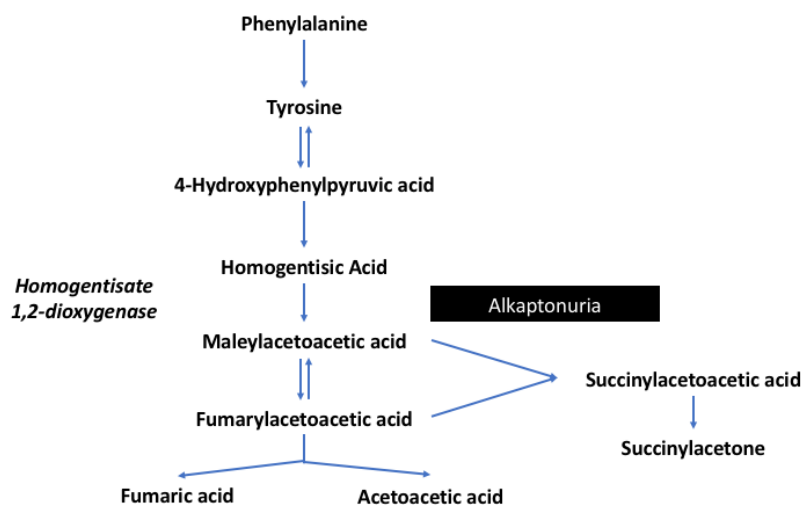


Fig. 1.2. Adapted from reference (2). The image shows the Tyrosine degradation pathway. AKU (highlighted) is the condition that can occur if the HGD enzyme (left of pathway) is deficient.

The earliest clinical feature that often appears is urine which turns dark on standing. HGA, present from birth, is excreted in urine. HGA undergoes spontaneous oxidation in air, resulting in the formation of benzoquinone acetic acid (BQA), an intermediary which undergoes polymerisation into ochronotic pigment. Whilst it is possible for this reaction to occur by itself,

it is enhanced in an alkaline environment (15, 16). Although dark urine is a characteristic symptom of the disease, it has been shown that other tyrosine metabolites in excess can darken urine (17, 18). It is therefore usually confirmed using a technique known as high performance liquid chromatography, which has been shown to be a highly specific and sensitive way of detecting the condition (19, 20).

The conversion of HGA into ochronotic pigment also occurs inside the body. The deposition of pigments in connective tissues occurs around the third decade, and is known as ochronosis (8, 20). The reaction is the same as when HGA in urine undergoes spontaneous oxidation in air, except Zannoni *et al* have shown that the whole reaction is catalysed by an enzyme, termed homogentisic acid polyphenol oxidase (21). This implies that even those without the genetic defect carry this enzyme, which would not incur any evolutionary advantage. Taylor *et al* therefore postulated that Tyrosinase, an enzyme involved in melanin synthesis, is responsible for producing the melanin like ochronotic pigment. This is because the melanin synthesis pathway and HGA polymerisation pathway share remarkable similarities (8). Ochronosis in connective tissue is only seen from around the third decade of life. This raises the question as to why pigmentation does not occur earlier, suggesting there are physiological changes which must occur to enable ochronosis. What these physiological changes are is not currently known. One hypothesis is that it is linked with a decline in kidney function and a reduction in plasma pH, accelerating the rate of ochronosis (8, 22-24). Inflammation and reactive oxygen species (ROS) have also been theorised to be involved in the pathogenesis of AKU. Results have shown that interleukin 6 (IL-6) and oxygen free radicals have been present alongside HGA in AKU patients (25).

Ochronosis is found in a variety of collagenous tissues. HGA polymerises into ochronotic pigment, which preferentially binds to cartilage in joints and aortic valves (26). Discolouration can also be noticed clearly in the sclera of eyes and pinna of ears and can affect the renal system via formation of stones (2). AKU has significant implications on the cardiovascular system, due to its role in the formation of stenotic valves in the aorta. It has been reported that patients require valve replacement surgery to alleviate symptoms. Pigmentation has also been noticed in the arteriolar section of the cardiovascular system, whilst there have been no reports with regards to venous pigmentation. This could have implications for the pathogenesis of AKU, suggesting that mechanical forces may have a role in the initiation of ochronosis (2, 27-29).

Chronic ochronosis in joints results in the third clinical feature, ochronotic osteoarthropathy. Patients commonly appear with progressive degeneration of their spine and weight-bearing joints. The clinical and radiological features that often appear first are associated with the spine. X-rays show features similar to osteoarthritis (OA), including joint space narrowing, subchondral sclerosis and subchondral cysts. Clinically, the patient presents with sharp debilitating back pain which progresses with time to peripheral weight bearing joints such as the hips and knees (7, 30). Symptoms then continue to develop; thoracic kyphosis and reduced chest expansion due to osteoarthropathy of the spine are seen after the fourth decade. Whilst AKU does not reduce mortality it is clear to see that it affects morbidity. Patients are often left with severe disabilities having significant impacts on their activities of daily living (20).

There are still gaps however in the understanding of the pathogenesis of ochronosis and ochronotic osteoarthropathy. The initiating factor/factors of ochronosis are currently unknown. It has been observed that there is an initial period where connective tissue is resistant to ochronosis. This is known because ochronosis isn't seen until early adulthood (1, 31). This therefore suggests there are protective mechanisms in connective tissue preventing ochronosis, which are currently unknown. It is hypothesised that the tissue undergoes stresses which remove protective factors such as proteoglycans, enabling ochronotic polymers to bind to collagen fibres in specific areas, as shown by Taylor *et al* (1, 32). Whilst the stressors are currently unknown, inferences can be made. IL-6 is a catabolic cytokine, released during an inflammatory response. Research has shown that IL-6 plays a role in the pigmentation process. IL-6 has been shown to dysregulate antioxidant defences in chondrocytes. Mechanical insult to chondrocytes results in an inflammatory response and therefore the release of IL-6 (25, 33, 34). HGA during the polymerisation process produces ROS, which overwhelm inhibited antioxidant defences (15, 25, 35). It is proposed that these ROS inflict damage to the protective barriers in collagen, resulting in the collagen strand being exposed. This exposed collagen hypothesis therefore suggests that the lack of a protective barrier, such as proteoglycans, enables pigment polymers to bind to collagen. This changes the biochemical and biomechanical properties of collagen, causing further damage and continued release of IL-6, leading to further loss of protective barriers and therefore a nucleation event (1).

1.4 Management of AKU

1.4.1 Low Tyrosine Diet

Approximately six percent of dietary proteins undergo degradation via the HGA pathway. It therefore makes sense to reduce the intake of dietary proteins, to decrease the amount of HGA produced. Unfortunately, trials have shown this method as being ineffective and impractical. If this treatment is implemented, intensive specialist supervision is required during the growth period. As well as this, endogenous catabolism of protein results in tyrosine production regardless of dietary restrictions. The lack of efficacy associated with this treatment means that it is no longer considered in clinical practice and research is directed at pharmacological interventions (2, 20, 30).

1.4.2 Ascorbic acid

HGA is converted to an ochronotic polymer in an oxidative process. It was thought that in high doses, ascorbic acid (ASC), a type of vitamin-C could prevent the conversion of HGA into BQA. Whilst this was shown, it also increased levels of serum HGA. ASC was also shown to be a cofactor to 4-hydroxyphenylpyruvate dioxygenase (HPPD), which further increases HGA production. The presence of HGA is known to contribute to the formation of renal oxalate stones. Using ASC therefore increases the risk of renal stone formation and therefore renal damage, in patients who are already at risk. Studies also showed that ASC displayed variable treatment efficacy. With variable clinical efficacy and risk of harm to the patient, it was deemed that ASC was not an appropriate treatment option for AKU patients (2, 24, 30, 36).

1.4.3 N-acetylcysteine

Recent research however is looking at alternative antioxidants which are not cofactors to

HPPD. N-acetylcysteine (NAC), a drug already in use in the management for paracetamol overdose and in respiratory disease, has been shown to inhibit the oxidation of HGA to BQA (20, 37, 38).

1.4.4 Nitisinone

Nitisinone, a HPPD inhibitor, acts by preventing HGA production. Nitisinone therefore acts as a preventative treatment, by aims of preventing ochronosis. It is already an established treatment, approved by the Food and Drug Administration (FDA), in the management of hereditary tyrosinemia type I. The first round of trials for AKU have shown promising results with urinary HGA levels decreasing in a dose dependant manner. Although it is an FDA approved treatment, there are still safety concerns with Nitisinone. Some of the side effects have the potential to cause ocular and neurological complications, such as corneal irritation, corneal epithelial damage, ataxia, delayed development, and intellectual impairment. A short-term study exists which states that those with AKU, treated by the medication for a few months experienced no complications. To further assess the long-term efficacy however, a large-scale trial is currently underway (2, 14, 39).

1.4.5 Palliative Care

As there is no licensed therapy for AKU, management is achieved via physiotherapy, joint replacement and pain relief (2). Physiotherapy aims to improve range of movements in joints, whilst pain management is achieved via medications and physical interventions such as acupuncture. Whilst these treatments do not target ochronosis, they aim to improve a patient's quality of life. The most definitive treatment currently available is joint replacement and spinal surgery, which can prevent complications such as cauda equina syndrome or joint

failure (20). As the enzyme HGD is mainly present in the liver, a liver transplant has shown a partial or complete resolution of AKU. However, due to the difficulty of the operation and potential to develop severe complications, this is not considered an ideal solution (8, 20, 40).

1.5 Bone Ultrastructure

Bone is classified as a type of connective tissue and therefore shares similar histological features to other connective tissues (41). There is a widespread extracellular matrix (ECM) surrounding the cells, of which there are relatively few. Unlike other connective tissues, the ECM of bone contains inorganic salts as well as an organic matrix. The inorganic component is approximately 60 percent of the bone matrix and is constituted mainly of calcium hydroxyapatite crystals. These crystals surround the collagen fibres (organic matrix) in a process known as mineralisation. The type I collagen fibres form about 90 percent of the bone's organic material. The collagen-crystal combination gives the bone the ability to withstand compressive and tensile forces (42).

Osteoblasts are the cells which deposit new bone matrix by secreting collagen fibres around the cell, initiating the calcification process. By depositing collagen fibres around themselves, osteoblasts transition into osteocytes, cells which are responsible for maintaining the ECM. The final type of cell present, is known as an osteoclast, responsible for the breakdown of old ECM. These cells work in homeostasis with osteoblasts to ensure that removal and production of bone are kept in balance. Any disturbances to this balanced process can result in pathology (43, 44).

Histologically, bone tissue is known to have two variations; cortical (compact) bone, and trabecular (cancellous) bone. In cortical bone the building blocks are known as osteons. Around a central canal are layers of concentric lamellae. Within these lamellae are osteocytes which have become embedded. The osteocytes communicate with each other through small channels known as canaliculi. Blood vessels run through the central canal and reach osteocytes via transverse perforating canals known as Volkmann's canals. Trabecular bone is always located on the inside, surrounded by cortical bone. The basic units of trabecular bone are trabeculae which are composed of lamella, forming a three-dimensional interconnecting lattice. The lattice is aligned along lines of stress and has gaps between each lamella, which contain bone marrow. The purpose of trabecular bone is to reduce bone density, to enable movement of bone (41-43).

1.6 Cartilage Ultrastructure

Cartilage is an avascular connective tissue, which is composed of cells known as chondrocytes and a specialised ECM. Three types of cartilage exist with varied compositions, relating to their function and location in the body (41). Ochronosis occurs in all collagenous connective tissues, but occurs predominantly in weight bearing joints (32). As hyaline cartilage coats the articular surfaces of these joints, it will be described in greater detail (45). Articular cartilage is present on the surface of joints for its ability to provide a smooth surface. This facilitates movement between joints and evenly distributes the load to the underlying subchondral bone (46). The strength and resilience of articular cartilage is achieved through complex interactions between collagen, proteoglycans, chondrocytes and water (46).

Chondrocytes are responsible for collagen synthesis. Collagen is present in large quantities (90%) in the ECM, and makes up 60% of the dry weight of articular cartilage. Type II collagen is the main type of collagen present in articular cartilage. Other types of collagen are also present, and they aid in forming and maintaining the structure of type II collagen. Three proteoglycan chains, present within each collagen fibril, arrange themselves into a triple helical molecule, formed by disulphide bonds between and within the chains. These triple helix structures provide articular cartilage with sheer and tensile strength (45, 46).

Proteoglycans are macromolecules which exist in the ECM of articular cartilage, making up 10% of the wet weight. Aggrecan is the main proteoglycan found in articular cartilage. Several chondroitin sulphate (CS) and keratan sulphate glycosaminoglycan (GAG) molecules, are attached to a core protein via sugar bonds to form the proteoglycan molecule. These molecules are highly negatively charged; this attracts cations and, due to an increase in osmotic pressure, attracts water. Water is the main contributing factor to articular cartilage, making up approximately 80% of the wet weight of cartilage. Water is known to withstand high pressures. Therefore, this arrangement serves to provide the cartilage with compressive strength (45-47). Hyaluronic acid (HA) another GAG, is another important component of the ECM (41). The aggrecan molecule, via a link protein, binds non-covalently to HA. HA therefore acts as a binding site for several aggrecan molecules resulting in a large proteoglycan aggregate (45).

Histologically articular cartilage consists of four zones (I-IV) (Fig. 1.3). The superficial zone (zone I) is responsible for protecting the lower layers from sheer stress, and acts as a barrier preventing large molecules from entering the cartilage. The collagen fibrils are arranged

parallel to the articular surface, and are coated by a thin film of lubricating synovial fluid. This arrangement provides a smooth gliding surface for the cartilage. Damage to this structure results in changes to the mechanical property of cartilage, which is thought to be a contributing factor to the pathogenesis of OA. The transitional zone (zone II) has its collagen fibrils arranged at an oblique angle, enabling the compressive forces to be transferred to the deep layer. The deep radial zone (zone III) has collagen fibres arranged perpendicular to the articular surface, enabling them to resist compressive forces and evenly distribute load. The chondrocytes in zones II and III are spherical, unlike zone I where they are flat and arranged in a layer. The calcified zone (zone IV), the final layer, has a distinct boundary between the calcified and uncalcified cartilage, known as the tidemark. Zone IV is responsible for fixing cartilage to the subchondral bone. The chondrocytes in this zone are hypertrophic in appearance and produce type X collagen (45-47).

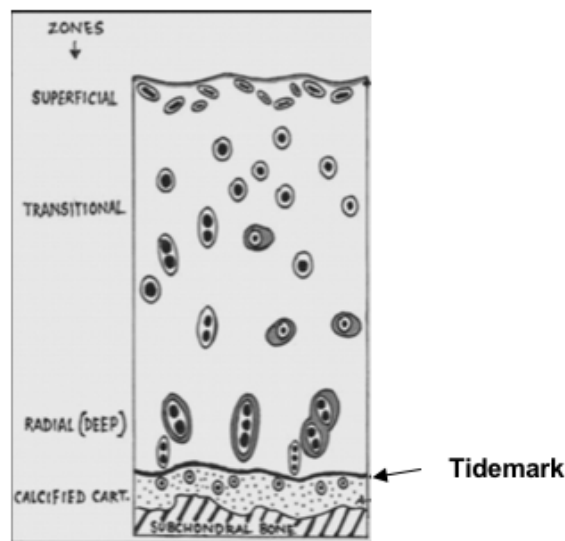


Fig. 1.3. Adapted from reference (47). Image shows the zonal layers of articular cartilage.

1.7 MG63 and C20

For the purposes of this research two cell lines will be used as *in vitro* models to demonstrate the pathogenesis of AKU. C20 cells are immortalised human chondrocytes, which characterise the properties of cartilage. Previous experiments have shown that pigment deposition is observed intra- and extracellularly, which replicates the pathological picture of articular cartilage *in vivo* (2, 25). MG63 cells are osteosarcoma cell lines. They have been used as an *in vitro* model to investigate ochronosis. Unlike *in vivo*, these cells have shown that they pigment both intra- and extracellularly, like the C20 cell line. It is thought this is due to the lack of mineralizing agents which bind to collagen. This finding therefore suggests that mineralisation of collagen serves as a protective mechanism against AKU (2, 48).

1.8 OA

OA is the most common form of arthritis, commonly associated with ageing (49). OA is a clinical diagnosis, often confirmed by observing structural changes radiographically. The changes that are often seen include: loss of joint space due to loss of cartilage, subchondral sclerosis, osteophyte (new bone) formation at joint margins, and subchondral cysts (50, 51). Patients typically present with joint pain, exacerbated during exercise and alleviated by rest. Short periods of stiffness are also common, differentiating the condition from Rheumatoid Arthritis (51, 52). Table 1.1 summarises the signs and symptoms that are often associated with OA:

| Signs | Symptoms |
|--|---|
| <ul style="list-style-type: none"> • Crepitus | <ul style="list-style-type: none"> • Joint pain |
| <ul style="list-style-type: none"> • Joint effusion +/- inflammation | <ul style="list-style-type: none"> • Short lasting morning stiffness |
| <ul style="list-style-type: none"> • Joint instability and muscle wasting | <ul style="list-style-type: none"> • Limitations in movements |

Table 1.1. Adapted from reference (52). Table lists the signs and symptoms associated with OA.

The aetiology of OA is currently unknown, which is mainly due to multiple identified causes (50, 52). The initiation of OA can be thought to occur in either of two ways: when an abnormal load is placed on articular cartilage of normal structure, or when a normal load is placed on articular cartilage with an abnormal structure (53). This results in an imbalance between anabolic and catabolic activities of chondrocytes (Fig. 1.4) (54).

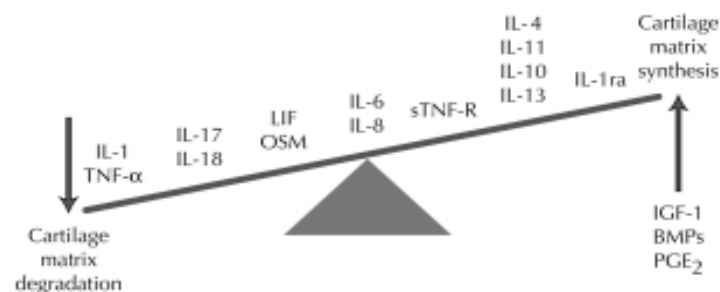


Fig. 1.4. Figure taken from reference (54). Cytokines which influence anabolic and catabolic activities in chondrocytes.

It is suggested that stress on cartilage results in damage to the ECM, inducing a breakdown of proteoglycans and type II collagen. It is thought that the breakdown products of these molecules stimulate the production of inflammatory mediators, specifically interleukin 1 (IL-1) and tumour necrosis factor α (TNF- α) (55). It has been shown that these are pro-catabolic

mediators, which upregulate and activate matrix metalloproteinase (MMP) (56). MMPs are a group of enzymes produced by chondrocytes and are responsible for degrading collagen and proteoglycans. Specifically, it is the collagenase, gelatinase, stromelysin and membrane type 1 families that are involved in this process (52, 57). In normal cartilage, MMP activity is kept in balance by inhibitory enzymes and anabolic growth factors (Fig. 1.5). Examples of inhibitory enzymes are tissue inhibitor of metalloproteinase (TIMP), interleukin 4 (IL-4) and interleukin 10 (IL-10). Examples of anabolic growth factors include insulin-like growth factor (IGF-1) and transforming growth factor β (TGF- β). In OA, due to repetitive mechanical stress, there is an imbalance resulting in greater expression of MMP. This outmatches inhibitory and anabolic factors resulting in the pathogenesis of OA (54, 57, 58).

There is an initial compensation period by chondrocytes, where there is an overproduction of ECM content and cloning of chondrocytes in an attempt to prevent an overall loss of ECM. However, these cells eventually fail to match the degradation of articular ECM, resulting in an overall degradation of cartilage (59). This imbalance between anabolic and catabolic activity results in loss of proteoglycans and cleavage of type II collagen. This leads to an influx of water into the cartilage, resulting in loss of function of articular cartilage. No longer having the ability to withstand tensile stresses and compression, articular cartilage undergoes physical changes, leading to the characteristic radiographic appearance of OA (49, 54).

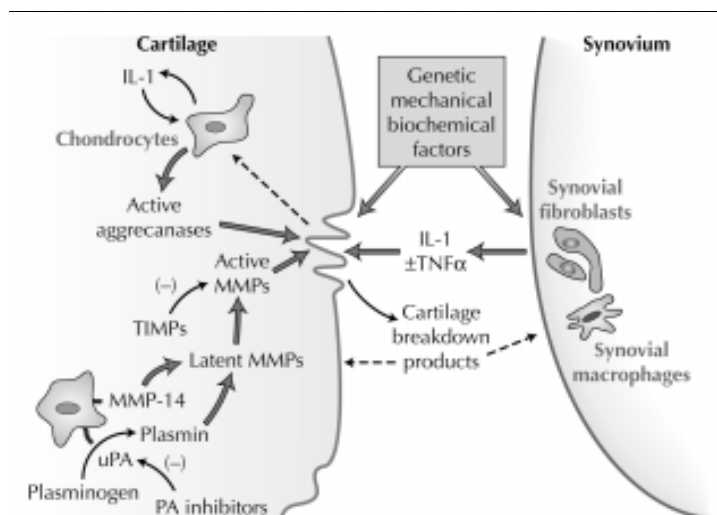


Fig. 1.5. Taken from Reference (54). Components involved in the breakdown of cartilage in OA.

OA and AKU share some common clinical characteristics. Ochronotic osteoarthropathy can be viewed as an extreme form of OA. Therefore, it is theorised that by using an *in vitro* model to study AKU, novel discoveries can be made in relation to OA (1, 60).

1.9 The Role of Superoxide Dismutase in AKU Pathogenesis

Superoxide Dismutase (SOD) are enzymes found in a wide variety of living organisms, and are responsible for the conversion of superoxide free radicals into hydrogen peroxide and oxygen. Three variants of SOD exist within the body, and work as part of the cellular antioxidant defence mechanism. SOD 1 (CuZnSOD) and SOD 2 (MnSOD) are found intracellularly; SOD 1 is present in the cytoplasm and SOD 2 in mitochondria. SOD 3 (extracellular SOD) is found in the ECM, bound to negatively charged proteoglycans and collagen fibril. The role of SOD is to prevent the over-accumulation of ROS, specifically the superoxide anion. Whilst superoxide anions are important for cellular metabolism and intercellular signalling, overproduction can lead to loss of cellular integrity and in some cases, apoptosis (61-63).

Superoxide anions are the ROS primarily produced in the body as a by-product of cellular metabolism and inflammatory processes. SOD is therefore produced in a variety of tissues, including articular cartilage, with the aim of maintaining superoxide anions at a viable level (63-65). OA and AKU share similar pathophysiological mechanisms. It has been shown that in human joints affected with OA, there is an overproduction of superoxide anions during the inflammatory process. Experiments in mice have also shown an accumulation of ROS prior to structural changes in cartilage. This accumulation was accompanied by an early decrease in SOD, suggesting that it is implicated in the early initiation of OA. It can therefore be hypothesised that a potential deficit of SOD in articular cartilage of patients with AKU, may be a contributing factor to its pathogenesis (1, 60, 63, 65).

It is currently not known where in the body ochronosis is initiated. Studies however, have shown that fresh serum and urine samples from AKU patients only contain HGA molecules. These results suggest that *in vivo*, HGA is a stable molecule and that polymerisation only occurs in collagenous areas such as articular cartilage (8, 66, 67). During the polymerisation process, HGA is oxidised to form BQA (7). However, normal articular cartilage is avascular and therefore has a hypoxic environment (45, 68). It is possible that HGA utilises ROS to initiate the polymerisation process (69). Trauma or focal damage to articular cartilage is thought to be a key factor in the initiation of ochronosis. The resultant inflammatory process is known to produce superoxide anions in excess. This would suggest that superoxide anions are likely to be the ROS utilised by HGA (1, 65). If this is the case, it is plausible to hypothesise the use of SOD in the prevention of ochronosis.

As previously stated, in patients with AKU there are thought to be protective factors which are removed in the third and fourth decades of life, resulting in the clinical manifestations of AKU (1, 30, 60). SOD may be one of those protective factors which is inhibited by IL-6 during mechanical stress (25, 33, 34). This enables ROS produced by polymerisation of HGA to damage proteoglycans. Loss of proteoglycans from the ECM is thought to enable pigmentation (1, 15). This hypothesis can be further supported as there has been no published evidence of ochronotic pigment deposition in skeletal muscle or lung tissue. This can be thought of as an anomaly, as ochronotic pigment has an affinity for collagenous tissue (32). It therefore appears there are factors present which prevent ochronosis in the collagen of skeletal and lung ECM (70, 71). Both tissues require high levels of aerobic cellular activity, which produces ROS as a by-product. To prevent accumulation of ROS, high levels of SOD are present within these cells to maintain a fine balance. It could be suggested that this high level of SOD protects proteoglycans in skeletal and lung ECM from ochronosis. This provides further reason to suggest SOD as a viable protective mechanism in cartilage against AKU (61, 64, 72-74). It can therefore be suggested that SOD may not only have a preventative role, by preventing the initiation of ochronosis, but it may also have a protective role, by preventing pigments from binding to collagen fibrils (Fig. 1.6).

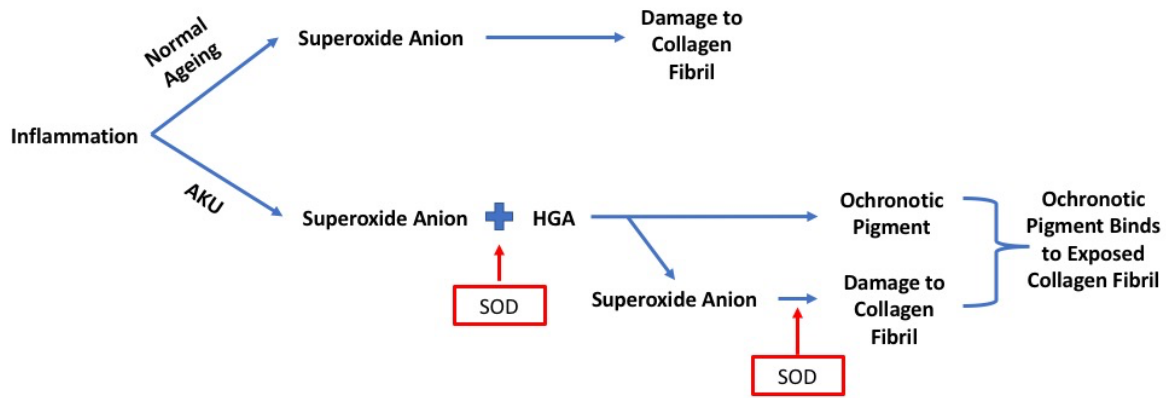


Fig. 1.6. Schematic representation of the proposed role superoxide anions have in the initiation of ochronosis, and their role in enabling the binding of ochronotic pigment to collagen fibrils. In normal aging superoxide anions are involved in cartilage degradation, suggesting its role in the pathogenesis of OA. In AKU this process is accelerated due to the polymerisation of HGA in conjunction with normal aging processes. The diagram indicates the reactions SOD is likely to target to prevent the process of ochronosis from occurring.

For the purposes of this research SOD from bovine erythrocytes was used, due to its suitability for cell culture. Erythrocytes contain cytoplasm but lack organelles, and therefore lack mitochondria. CuZnSOD is therefore the SOD used in these experiments. This SOD is extracted from erythrocytes, purified and stored in powder form. It is not known where this enzyme acts, however due to the intact membranes of live cultured cells, it is likely to act mainly in the ECM. Therefore, for the purposes of the following experiments SOD is speculated to act in a similar manner to extracellular SOD (43, 75).

1.10 Raman Spectroscopy

Raman spectroscopy is a non-destructive spectroscopic method which provides quantitative and qualitative information of samples (76, 77). A laser beam of single wavelength interacts

with samples, causing light to scatter upon contact (76). Scattering can be either elastic or inelastic in nature (78).

Elastic scattering occurs when there is no exchange of energy between the sample and incident light. This means the scattered light has the same amount of energy as the incident light. Elastic scattering is termed Rayleigh scattering, and the majority of light is scattered in this fashion. Inelastic scattering, known as Raman scattering, is also generated. This type of scattering is used to generate a detailed chemical analysis of a sample's structure. Raman scattering results from an exchange of energy between the incident light and sample. This means that the scattered light has less energy (stokes scatter), or more energy (anti-stokes scatter) than the incident light. Change in energy results in an associated change in wavelength of scattered light. The changes in wavelength are dependent on the molecular bonds present within the sample, resulting in a unique fingerprint for each sample (77-79).

The wavelengths of the Raman scatter are plotted as a spectrum of intensity (a.u) against wavenumbers (cm^{-1}) (79). Qualitative analysis provides details about the structure of the sample studied, while quantitative analysis provides information about the relative amounts of analyte present in the sample (77). Therefore, using this spectral technique, it is thought that structural changes, if present, can be identified in an *in vitro* model of AKU.

1.11 Summary

AKU is a rare autosomal recessive condition, resulting in a triad of clinical manifestations (2). Homogentisic aciduria is the earliest clinical feature of AKU (8, 15). Pigment formation then

begins to occur within the body, from the third decade onwards. Ochronosis occurs in a variety of collagenous tissues. HGA polymerises into ochronotic pigment, and preferentially binds to cartilage in joints (2, 26). Chronic ochronosis in joints results in the third clinical feature, ochronotic osteoarthropathy (30). Ochrotonic osteoarthropathy can be viewed as an extreme form of OA. The similarities between these two conditions have been demonstrated with novel cartilage and bone phenotypes observed in both conditions (31, 80). This means that discoveries made from research in AKU can also have potential implications for the understanding of the pathophysiology of OA.

Many advances have been made in the study and understanding of AKU. The defective gene has been identified and located on chromosome 3q2 (1, 8). *In vitro* and mouse models have been established, which are synonymous with the human condition (12, 48). These recent discoveries have enabled the evaluation of joint pathology and testing of novel therapeutic interventions, such as Nitisinone, currently undergoing human trials (13, 14).

SOD is an enzyme responsible for the conversion of superoxide free radicals into hydrogen peroxide and oxygen (61). Studies have shown that ROS are involved in the OA disease process due to a decrease in SOD (63). Due to OA and AKU sharing similar pathophysiological mechanisms, it can be hypothesised that a potential deficit/inactivity of SOD in articular cartilage of patients with AKU, may be a contributing factor to its pathogenesis (1, 25).

Structural analysis has enabled significant advancement in AKU research, such as the discovery of novel cartilage and bone phenotypes (80). It is therefore likely that using a novel analytical technique will provide new insights into the pathogenesis of AKU. Raman

spectroscopy, a non-destructive spectroscopic method, will therefore be used to observe chemical changes in an *in vitro* model of ochronosis (76, 77).

1.14 Statement of Aims

This study will aim to further existing knowledge of AKU. This will be achieved by:

1. Observing the effects of SOD in an AKU disease model.
2. Observing any structural changes to cell cultures in a disease model of AKU via Raman spectroscopy.

An *in vitro* model will be used to observe the effect of different concentrations of SOD on MG63 and C20 cell lines. This experiment will aim to assess the highest concentration of SOD that can maintain cell viability. Using the concentration determined from this experiment, another experiment will be set up to see if pigmentation occurs in cell lines with and without SOD, upon addition of HGA. This may give some novel insights into the pathophysiological mechanism of ochronosis, and lend evidence to suggest that SOD is a protective mechanism which prevents ochronosis. If this is the case, SOD may have implications to future therapeutic approaches in AKU.

An *in vitro* model of each cell line will be set up and treated with HGA. Raman spectroscopy will then be used in an attempt to identify structural changes to cells and their matrix upon addition of HGA. If there are structural differences, it may be possible to implement Raman spectroscopy in a clinical setting as a diagnostic tool.

Chapter 2 - Materials and Methods

2.1 Materials

Dulbecco's modified eagle's medium (DMEM) for MG63 and DMEM with Hams F12 1:1 for C20, were purchased pre-mixed with 5ml (1%) L-Glutamine (Sigma Aldrich, UK). Both mediums were then supplemented with 50ml (10%) foetal calf serum (FCS) (Appleton Woods), and 5ml (1%) penicillin/streptomycin (P/S) (Sigma Aldrich, UK), in sterile conditions. All DMEM was stored at 2- 4°C. FCS was aliquoted into 25ml universals (Appleton Woods) and P/S aliquoted into 5ml bijoux (Appleton Woods). Both were stored at -20°C until further required.

Trypsin EDTA (Sigma Aldrich, UK) was aliquoted into 5ml bijoux and stored at -20°C until further required.

25cm³ cell culture flasks were obtained from laboratory store supplies.

2.1.1 Phosphate Buffer Solution Preparation

10M stock of phosphate buffer solution (PBS) was made in the laboratory and stored at room temperature. When required this solution was diluted down to 1M PBS and autoclaved.

2.1.2 SOD Preparation

SOD from bovine erythrocytes (Sigma Aldrich, UK) was prepared as detailed in the supplier's instructions and aliquoted into Eppendorf's at 2000 units per ml. One unit of SOD is defined as the number of enzymes needed to convert 50% of superoxide anions into hydrogen

peroxide and water, preventing the reduction of cytochrome c (75). SOD was stored at -20°C until further required.

2.1.3 HGA Preparation

HGA stock solution was prepared by adding 100mg of HGA crystalline (Sigma Aldrich, UK) to 5.95ml of PBS, resulting in 0.1M HGA solution. This was stored at -20°C until further required.

2.2 Cell Culture

C20 immortalised chondrocytes were a kind gift from Dr. Mary B. Goldring (Hospital for Special Surgery, NY, USA)(81). MG63 osteosarcoma cells were obtained from laboratory stocks. Both cell lines were cultured in 25cm³ culture flasks containing DMEM for MG63, and DMEM with Hams F12 1:1 for C20.

Cells were passaged every three days in a clean laminar flow hood. The DMEM was removed from both cell lines and the plates were washed once with PBS. 2.5ml of trypsin EDTA was added to the cultures and then incubated at 37°C, to detach the cell layer from the base of the flasks. The action of trypsin EDTA was halted by adding 12.5ml of DMEM or DMEM with Hams F12 1:1, to the respective culture flasks. This 15ml cell suspension was then vortexed to remove any cell clumps, and then distributed evenly (5ml) into three new 25cm³ culture flasks. The flasks were then supplemented with 5ml of fresh medium each. The flasks were stored in an incubator in a humidified atmosphere of 95% air and 5% CO₂ for three days, until the point of confluency, before being passaged again (82).

2.3 Experiment I - The Effects of SOD on C20 and MG63 Cell Lines

2.3.1 Preparation of Samples

Following the incubation period, one flask of each cell type displaying greater than 80% confluence was selected. The culture medium was removed and the cells were washed with 10mls of PBS and incubated for 5 minutes with 2.5ml of trypsin EDTA. This cell suspension was then placed in a centrifuge and spun at 900rpm, for 5 minutes at 18°C, resulting in the sedimentation of cells. The trypsin EDTA supernatant was removed and 1ml of culture medium was added to re-suspend the cell lines, using a vortex. 10µL of cell suspension was injected into a disposable C-Chip haemocytometer (Labtech), and cells were counted under a light microscope. The mammalian cell counting formula (Fig. 2.1) was then used to provide the appropriate number of cells per ml. Cells from each cell line were plated at 5×10^3 cells per well, into a 24 well plate each. Cells were left to culture for three days.

$$\text{Cells per ml} = \frac{\text{cells in 5 large squares}}{5} \times \text{dilution factor} \times 10^4$$

Fig. 2.1. Taken from reference (83). Mammalian cell counting formula. A dilution factor of 1 was used when preparing samples.

After 3 days, the plates were treated with medium supplemented with varying concentrations of SOD (Table 2.1 and 2.2). The cells were cultured in these conditions for seven days, with a medium change after three days. All supernatants were pipetted into labelled sterile Eppendorf's and stored at -20°C for further analysis (84).

| | 1 | 2 | 3 | 4 | 5 | 6 |
|---|---------|-----------------|----------------|---------------|------------------|------------------|
| A | Control | 500 units/ml | 50 units/ml | 5 units/ml | 0.5 units /ml | 0.05 units/ml |
| B | | | | | | |
| C | | | | | | |
| D | | | | | | |

Table 2.1. Concentrations of SOD used for each column of cultured C20 and MG63 cells.

| | 1 | 2 | 3 | 4 | 5 | 6 |
|---|----------------|--|--|---------------------------------------|--------------------------------------|--|
| A | 4000µl DMEM | 1000µl SOD stock + 3000µl DMEM | 100µl SOD stock + 3900µl DMEM | 10µl SOD stock + 3990µl DMEM | 1µl SOD stock + 3999µl DMEM | 0.1µl SOD stock + 3999.9µl DMEM |
| B | | | | | | |
| C | | | | | | |
| D | | | | | | |

Table 2.2. The volume of medium and stock SOD used to achieve the required concentrations listed in Table 2.1. Solutions were prepared in 5ml bijou jars prior to being aliquoted into each well of the corresponding column at 1ml/well.

2.3.2 Trypan Blue Exclusion Assay to Assess Cell Viability

Following treatment for seven days, the supernatant was removed and stored in sterile Eppendorf's for further analysis. 0.5ml of trypsin EDTA was added to each well to detach cells from the bottom of the well. The culture plate was then incubated for 5 minutes to enable optimal conditions for the enzyme. The cell suspensions from each of the wells with the same treatment were pipetted into a labelled 25ml universal. The universal was then spun down in a balanced centrifuge at 900rpm at 18°C for 5 minutes.

The trypsin EDTA supernatant was poured off and the remaining cell pellets were re-suspended with PBS, at a ratio of 1ml/well. 0.1ml of this cell suspension was mixed with 0.1ml of trypan blue, in a sterile Eppendorf, resulting in a dilution factor of 2 (Fig. 2.2). 10µl of this

mixture was pipetted into a C-Chip haemocytometer, and a mammalian cell count was performed under a light microscope of the total number of cells and blue stained cells.

$$\frac{\text{Volume of cells} + \text{volume of Trypan Blue}}{\text{Volume of Cells}}$$

Fig. 2.2. Formula for calculating the dilution factor for trypan blue exclusion assay.

2.3.3 Statistical Analysis

The cell counts were used to determine percentage viability (Fig. 2.3). The experiment used one biological replicate for each cell line. Each treatment group was set up as a technical replicate of four in the 24-well plate. The mean and standard error of the mean (SEM) were calculated for each treatment group, using the four technical replicates from the same cell line (n=1). The analysis was performed using GraphPad Prism 7 software (GraphPad Software Inc. USA).

$$\% \text{ viable cells} = \left[1.00 - \left(\frac{\text{Number of blue cells}}{\text{Number of total cells}} \right) \right] * 100$$

Fig. 2.3. Formula for calculation of percentage viability following trypan blue exclusion assay.

2.4 Experiment II – The Effects of SOD on an *in vitro* Model of Ochronosis

2.4.1 Effects of SOD and HGA on Cell Viability

Each cell line was seeded into a 24 well plate at a density of 5×10^3 cells per well as described above, and allowed to grow for 3 days prior to treatment. Cells were treated with medium supplemented with HGA and/or SOD (Table 2.3 and Table 2.4). The supplemented medium was aliquoted at 1ml/well, with each row of the 24 well plate considered as one treatment arm. The treatment medium was changed after every third day and the supernatants spun down and stored at -20°C in labelled sterile Eppendorf's, until further required. Cells were grown for either 7 or 14 days. At these time points cell layers were washed, trypsinised and counted, using disposable C-Chip haemocytometers. Trypan blue exclusion assay was used to determine cell viability.

| | A | B | C | D | E | F |
|---|--|---|---|---|---|---|
| 1 | Control – DMEM with Ham's F12 (1:1) or DMEM dependant on cell line | | | | | |
| 2 | HGA – DMEM with Ham's F12 (1:1) or DMEM dependant on cell line + HGA at $33\mu\text{M}$ | | | | | |
| 3 | SOD - DMEM with Ham's F12 (1:1) or DMEM dependant on cell line + SOD at 0.5units/ml | | | | | |
| 4 | HGA + SOD - DMEM with Ham's F12 (1:1) or DMEM dependant on cell line + HGA at $33\mu\text{M}$ + SOD at 0.5units/ml | | | | | |

Table 2.3. Concentrations of HGA and/or SOD used for each row of cultured C20 and MG63 cells.

| | A | B | C | D | E | F |
|---|--|---|---|---|---|---|
| 1 | Control – 13ml DMEM | | | | | |
| 2 | HGA – 4.29µl HGA stock + 12 996.75µl DMEM | | | | | |
| 3 | SOD – 3.25µl SOD stock + 12 996.74µl DMEM | | | | | |
| 4 | HGA + SOD - 4.29µl HGA stock + 3.25µl SOD stock + 12 992.46µl DMEM | | | | | |

Table 2.4. The volume of medium, stock HGA and stock SOD used to achieve the required concentrations listed in Table 2.3. Solutions were prepared in 25ml universals prior to being aliquoted into each well of the corresponding row at 1ml/well. The solution was aliquoted into 2 X 24 well plates. One plate was used to assess cell viability, the other plate was used for quantification of pigment deposition using Schmorl's stain.

2.4.2 Statistical Analysis

The cell counts were used to determine percentage viability. The experiment used one biological replicate for each cell line. Each treatment group was set up as a technical replicate of three in the 24-well plate for day 7 and day 14. The mean and SEM were calculated for each treatment group, using the three technical replicates from the same cell line (n=1). The analysis was performed using GraphPad Prism 7 software.

2.4.3 Identification and Quantitation of Ochronotic Pigment Deposition *in vitro*

2.4.3.1 Preparation of 10% Phosphate Buffered Formalin Solution

- 100ml formalin (37-40% stock solution)
- 900ml water
- 4g/L NaH₂PO₄ (monobasic)
- 6.5g/l Na₂HPO₄ (dibasic)

Materials were purchased from Sigma Aldrich, UK.

2.4.3.2 Preparation of Schmorl's Stain

- 37.5ml ferric chloride solution 1% (freshly prepared)
- 5ml potassium ferricyanide solution 1%
- 7.5ml distilled water

Mix the above and use within one hour (85). Materials were purchased from Sigma Aldrich, UK.

2.4.3.3 Schmorl's Staining and Analysis of Samples

The cell lines were each seeded at a density of 5×10^3 cells per well, into 24 well plates containing sterile 13mm glass cover slips at the bottom of each well. These plates were setup and were treated as described previously (Table 2.3 and 2.4). At day 7 and day 14 the medium was spun down and stored at -20°C , in labelled sterile Eppendorf's for further analysis. The glass cover slips were rinsed with PBS and then fixed in 10% phosphate buffered formalin solution (PBFS). Following fixation, cells were stored at $2-4^{\circ}\text{C}$ for at least 24 hours. The PBFS was then removed and the cover slips were rinsed with 1ml of PBS and left for another 12 hours at $2-4^{\circ}\text{C}$, prior to staining and mounting.

The cover slips were removed from the well plates and rinsed. They were then immersed in freshly prepared Schmorl's reagent for 10 minutes. The cover slip was washed again in distilled water to remove any residual ferricyanide and then counterstained using nuclear fast red (Sigma Aldrich, UK) for 5 minutes. The cover slips then went through a dehydration process in graded levels of alcohol and xylene (Fig 2.4), and were then mounted onto labelled

glass slides using DPX microscopy mountant (Sigma Aldrich, UK). These slides were then left for 24 hours on a flat surface to dry prior to microscopic analysis.



Fig. 2.4. Adapted from reference (86). The dehydration process for Schmorl's staining, using ethanol and xylene.

Digital images of all coverslips were obtained using an Olympus light microscope at x10 and x40 magnification settings. Five random areas of each cover slip were photographed, two of which were selected for each cover slip. Grids were overlain on each of these two digital images:

- At X10 magnification, 6 grids were overlain on each image, each grid covering 30,000 μm^2 .
- At X40 magnification, 3 grids were overlain on each image, each grid covering 10,000 μm^2 .

The number of blue pigment deposits within the grids were counted for each of the two images. The number of pigment deposits were then averaged and expressed per unit area for each image. This resulted in six average counts of pigment deposits expressed per unit area, for each treatment group, for each day and magnification (25, 48, 85).

2.4.4 Statistical Analysis

The experiment used one biological replicate for each cell line. Each treatment group was set up as a technical replicate of three in the 24-well plate for day 7 and day 14. The mean and

SEM for the number of pigment deposits were derived for each treatment group, using the three technical replicates from the same cell line (n=1). The analysis was performed using GraphPad Prism 7 software.

2.5 Experiment III - Analysis of Sulphated GAG Release in an *in vitro* Model of Ochronosis, Following Treatment with SOD

2.5.1 Preparation of Dimethylmethylene Blue

- 1L water
- 3.04g glycine
- 2.37g NaCl
- 95ml 0.1M HCl
- 16mg dimethylmethylene blue (DMMB) reagent - 1,9-dimethylmethylene blue

The solution was thoroughly mixed and stored at room temperature in a brown bottle wrapped in foil, to prevent interactions with background light (87). Materials were purchased from Sigma Aldrich, UK.

2.5.2 DMMB Assay

Two 5ml samples of 4mg/ml CS solution were first prepared by mixing CS A sodium salt (Sigma Aldrich, UK), with DMEM with Hams F12 1:1 and DMEM. The samples were prepared 24 hours prior to analysis, enabling the CS to fully dissolve. These solutions were then diluted to prepare a working solution of 50µg/ml of CS. This solution was then used to prepare serial dilutions to generate a standard curve (Table 2.5). The dilutions were aliquoted at 20µL, as

duplicates, into a 96 well plate. The supernatants collected from experiment II were defrosted, and 20 μ L pipetted into 96 well plates. 180 μ L of DMMB solution was aliquoted into each well using a multichannel pipette. The absorbance was measured at 530nm using a photospectrometer (87).

| Volume of 50 μ g/mL stock solution (μ L) | Volume of DMEM (μ L) | Concentration (μ g/mL) |
|---|---------------------------|-----------------------------|
| 0 | 20 | 0 |
| 2.5 | 17.5 | 6.25 |
| 5 | 15 | 12.5 |
| 7.5 | 12.5 | 18.75 |
| 10 | 10 | 25 |
| 12.5 | 7.5 | 31.25 |
| 17.5 | 2.5 | 43.75 |
| 20 | 0 | 50 |

Table 2.5. Serial dilutions of CS in DMEM used to generate a standard curve for DMMB assay.

2.5.3 Statistical Analysis

The supernatants obtained from experiment II were used for this assay. The supernatants were therefore derived from one biological replicate for each cell line. At days 4 and 8 the supernatant was derived from a technical replicate of 6, for each treatment group (n=1). At days 12 and 14 the supernatant was derived from a technical replicate of three, for each treatment group (n=1). The measured absorbance values were interpolated using a standard curve to obtain corresponding concentration values of CS. The mean and SEM of the

concentrations of CS for each treatment group were then calculated using GraphPad Prism 7 software.

2.6 Experiment IV – Raman Spectroscopy of an *in vitro* Model of Ochronosis

2.6.1 Preparation of Samples for Raman Spectroscopy Analysis

Prior to passaging cells, sterilised calcium fluoride (CaF₂) disks were placed into 25cm³ sterile culture flasks. Each cell line was then passaged as described above into two flasks, each containing a CaF₂ disk. One flask was left untreated as a control. The other flask upon passaging was treated with HGA. The cell medium was pre-mixed with HGA in sterile universals, to ensure a concentration of 33µM of HGA. Cells were then left for three days which ensured cells adhered to and achieved confluency on the CaF₂ disks. Cells were then gently rinsed with PBS solution and immersed in fresh PBS on an open petri dish. Raman spectroscopy produces weak signals for PBS (88). This process therefore ensures minimal interference from culture medium, and allows cells to maintain structural integrity and viability during the spectral acquisition period.

2.6.2 Raman Spectroscopy Instrumentation and Analysis

Spectroscopic measurements were carried out using a Renishaw inVia Raman spectrometer (Renishaw Plc. UK). A laser with 785nm bandwidth was used for all spectral acquisitions. The instrument was calibrated using silicon, which has a spectral band at 520.5cm⁻¹, and confirmed using polystyrene at the spectral bands of 1001.4cm⁻¹ and 1031.0cm⁻¹. Spectral acquisition settings were determined using a spare CaF₂ disk, using C20 cells grown in confluence. Various settings were trialled with consideration to quality of data generated and time taken for each spectral acquisition. Visual analysis for the optimal signal to noise ratio,

showed that the most appropriate setting was 20 seconds, with six accumulations, at 100% intensity, with a X60 immersion objective (Fig. 2.5). The spectra were measured across the wavelengths 593.00cm^{-1} to 1704.00cm^{-1} , where biological molecules are most likely to be detected (89). These settings were applied to both C20 and MG63 cell lines for all measurements. The experiment used one biological replicate for each cell line, with a technical replicate of 15 spectral acquisitions for each treatment group. 15 areas were randomly selected for spectral acquisition on each CaF_2 disk, to ensure a representative sampling of cell and matrix. A total of 60 spectra were acquired for the purposes of this experiment.

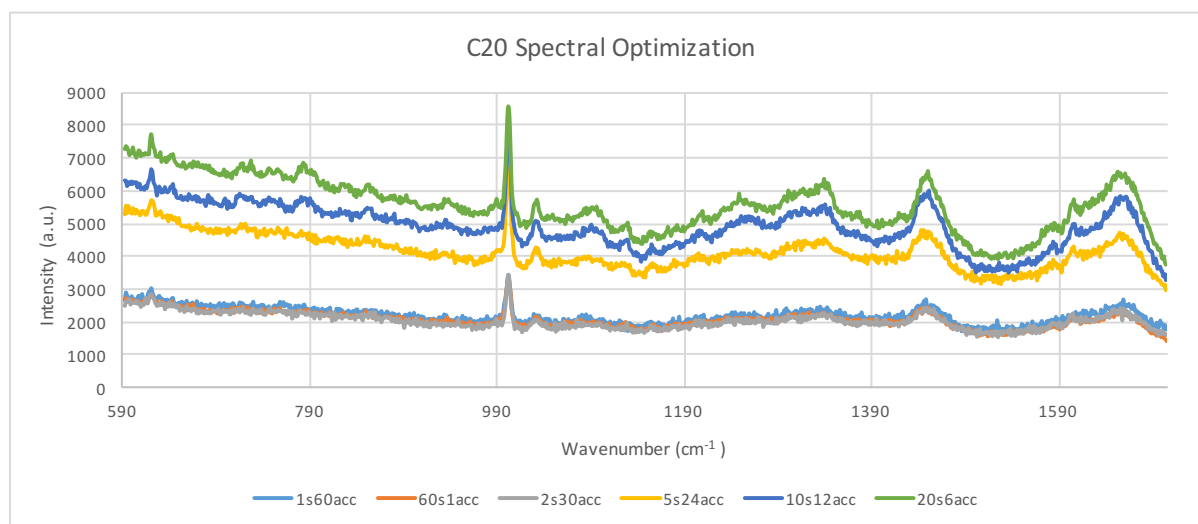


Fig. 2.5. Graph displaying various spectral acquisition settings attempted, using an immersion objective. Visual analysis was then performed to identify the setting with the best signal to noise ratio. The most appropriate setting was 20 seconds with six accumulations (green).

2.6.3 Data Pre-Processing and Statistical Analysis

The spectra were first baseline corrected with an 11th order polynomial, using WiRE software (Renishaw Plc. UK), to minimise fluorescence interference in all spectral acquisitions. A min max normalization was applied using peaks at 1150cm^{-1} and 1003cm^{-1} (arising from the

Phenylalanine group), as these bands did not fluctuate in signal strength across all spectra. Normalization of sample spectra ensures the concentration and thickness of samples are accounted for to enable comparability (79, 90, 91).

Multivariate analysis using principle component analysis (PCA) and linear discriminant analysis (LDA) was then performed using MATLAB software (The MathWorks, USA). PCA is an unsupervised technique used to find the most variance in the dataset. It is a method of compressing several datasets (wavenumbers) into a visually representable dataset, by focusing on the wavenumbers with the greatest amount of variance. The degrees of variance are termed principle component (PC) and the axis with most variance is termed PC 1, the axis with the second highest variance is then termed PC 2. This continues until the number of PCs are the same or less than the number of variables. The first three PCs are used, as they are likely to contain 99% of all variances (79, 90). LDA is then used on top of PCA. LDA is a supervised technique which is used to discriminate different categories. LDA aims to maximise the differences between groups (cell type and cell treatment) whilst minimising inter-category variance. A loadings plot is then displayed, which shows the contribution of each wavenumber to the linear discrimination produced by a PCA-LDA plot (90, 92).

Chapter 3 – Results I

3.1 The Effects of SOD on C20 and MG63 Cell Lines

The aim of this experiment was to observe the effects of SOD on immortalised human chondrocytes and osteosarcoma cell lines. Studies have shown SOD to be present at high levels in human cartilage samples (63). However, no studies have been conducted to assess the dose response relationship of SOD in chondrocytes. Therefore, it is not known if the presence of SOD at certain concentrations creates a beneficial or detrimental environment in articular cartilage.

This experiment was based on work published by Mistry *et al* with modifications (84). The experiment utilises an *in vitro* model to test various concentrations of SOD, to assess cell viability. As AKU primarily effects articular cartilage, C20 human immortalised chondrocytes were chosen (84). MG63 cell lines produce an un-mineralised collagen matrix, known to become pigmented when treated with HGA. This lends to further evidence that HGA deposits in collagenous matrix, and that there are protective factors such as mineralisation of bone which prevent ochronosis (48).

This experiment will aim to determine a viable concentration of SOD, for an *in vitro* model containing osteoarticular cells. This will enable further work into observing the effects of SOD on an *in vitro* model of ochronosis.

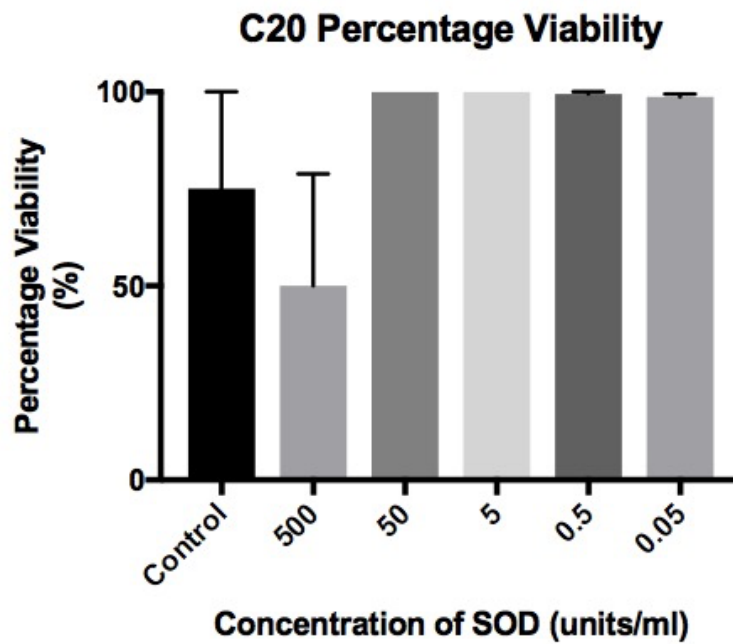


Fig. 3.1. Percentage viability of C20 cells after 7 days of treatment, using a range of concentrations of SOD. The number of viable cells are expressed as a percentage. Results are derived from the mean of four cultures (technical replicates) for each treatment group (n=1). Error bars signify \pm SEM. The SEM is a measure of the variability of internal replicates.

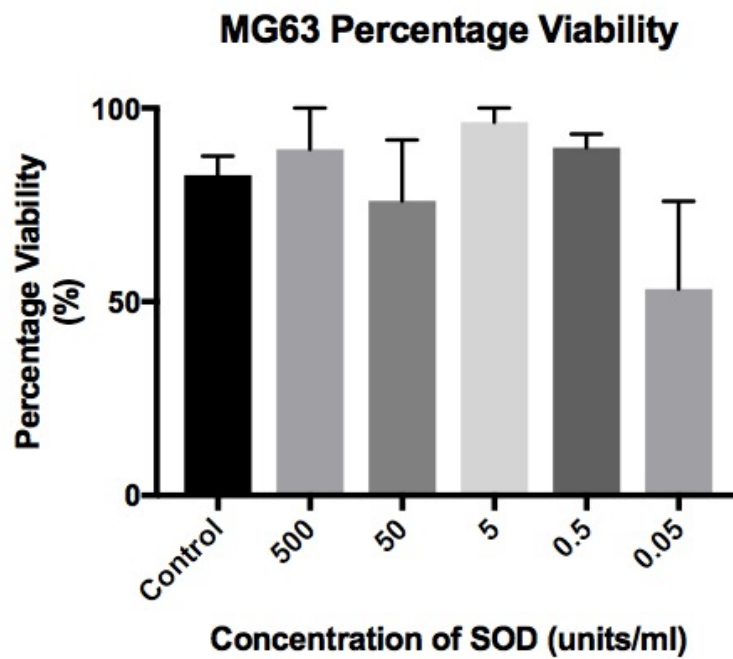


Fig. 3.2. Percentage viability of MG63 cells after 7 days of treatment, using a range of concentrations of SOD. The number of viable cells are expressed as a percentage. Results are derived from the mean of four cultures (technical replicates) for each treatment group ($n=1$). Error bars signify \pm SEM. The SEM is a measure of the variability of internal replicates.

The results suggest that in C20 cell lines (Fig. 3.1), SOD has no effect on percentage cell viability following seven days of treatment. This is seen across the concentration range 50 – 0.05 units/ml, which shows a greater percentage viability than the control. The only concentration to have a lower viability than the control was 500 units/ml, the highest concentration tested.

The MG63 cell line (Fig. 3.2) also suggests that SOD has minimal effect on cell viability. The data shows there are minimal differences seen across the concentration ranges 500-0.5 units/ml, when compared to control cultures. The concentrations 500, 5 and 0.5 units/ml have a higher viability when compared to the control. The concentrations 50 and 0.05 units/ml however, have lower viability in comparison to control cultures, with viability at 0.05 units/ml being lower than 50 units/ml. However, the data suggests no differences in viability between treatment groups, due to the overlap of error bars.

The results suggest that the various levels of SOD have no detrimental impact on cell viability in both cell lines. However, when considering a single concentration to be implemented, either 5 or 0.5 units/ml can be considered appropriate, as these concentrations show the closest levels of viability when compared to control cultures in both cell lines.

3.2 Summary of Results

The results indicate that in C20 and MG63 cell lines, SOD has no effect on percentage cell viability following seven days of treatment. 5 or 0.5 units/ml of SOD are considered the most appropriate concentrations, as they show the closest level of viability to control cultures. There is limited data on the physiological range of SOD in articular cartilage. A study has

shown that cartilage has a ten-fold higher concentration of SOD than lung tissue, suggesting the presence of large quantities of SOD in articular cartilage (63). This study, therefore is the first to assess the dose-response relationship of SOD in osteoarticular cells.

Chapter 4 – Results II

4.1 The Effects of SOD on an *in vitro* Model of Ochronosis

Having established a suitable working concentration of 0.5 units/ml of SOD, experiments were set up to observe the effects of SOD in an *in vitro* model of AKU.

The first experiment conducted was a cell viability assay using trypan blue, as described in Chapter 2 section 2.4.1.

Two additional 24 well plates, one for each cell line, were set up alongside the plates used to assess cell viability. In the additional plates, 13mm glass cover slips were added and cells seeded onto them as previously described. At days 7 and 14, the cover slips were removed and stained using Schmorl's stain. This method highlights any pigmentation present in cultures, by staining pigments an intense blue-green colour, contrasting ochronotic pigment with the surrounding cells and matrix. The results from this experiment will then be used to assess if pigment production is reduced/prevented in the presence of SOD (25, 48).

The following experiments aim to gain some new insights into the pathophysiological mechanism of ochronosis. This study will aim to determine if SOD can prevent ochronosis in C20 and MG63 cell lines upon addition of HGA.

4.1.1 C20 – Cell Viability and Histological Analysis

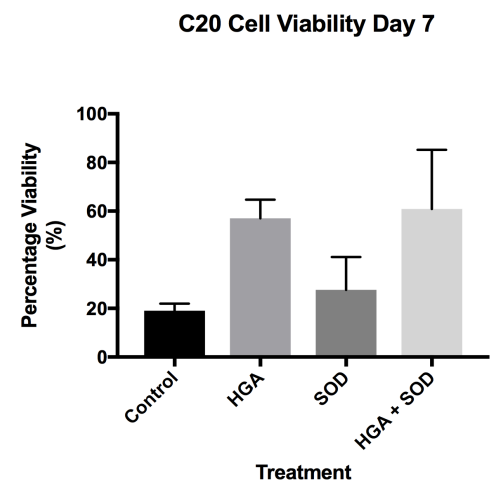


Fig. 4.1. Percentage viability of day 7 C20 cultures supplemented with HGA and SOD. The number of viable cells expressed as a percentage ($n=1$). Error bars signify \pm SEM. The SEM is a measure of the variability of internal replicates.

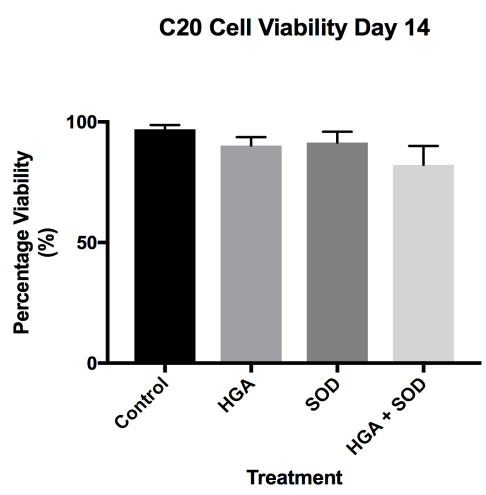


Fig. 4.2. Percentage viability of day 14 C20 cultures supplemented with HGA and SOD. The number of viable cells expressed as a percentage ($n=1$). Error bars signify \pm SEM. The SEM is a measure of the variability of internal replicates.

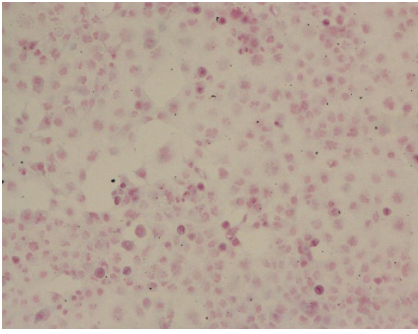
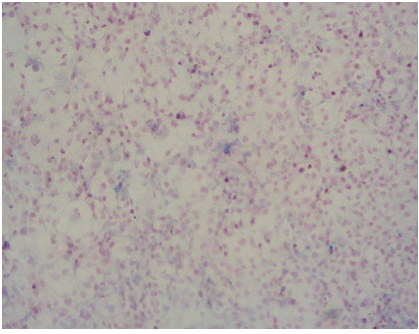
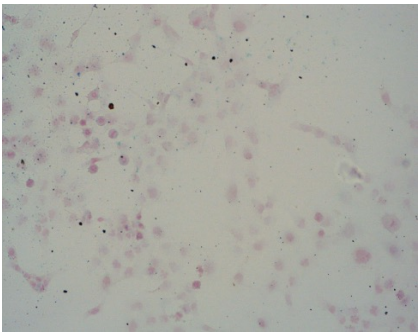
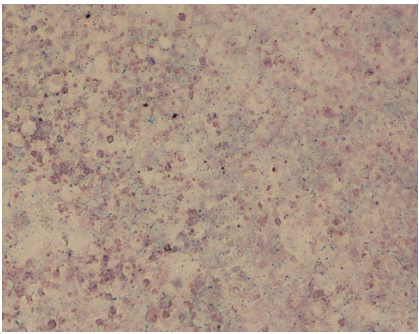
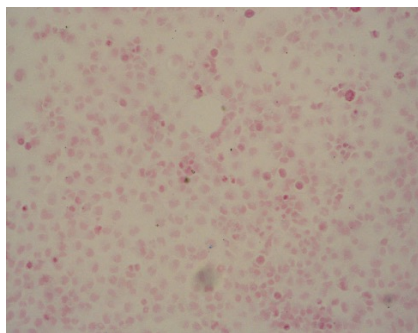
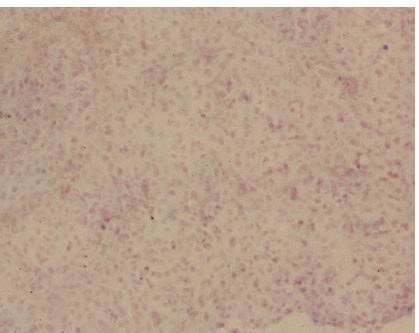
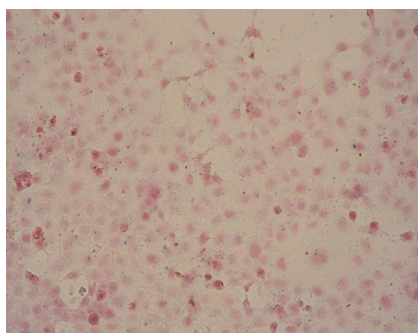
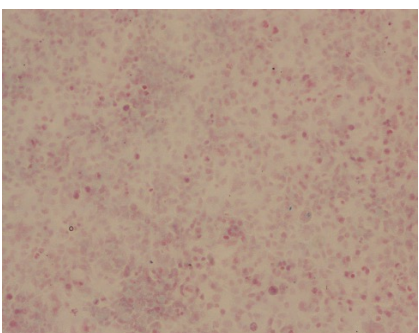
| C20 Cells x10 Magnification | | Day | |
|--------------------------------|-----------|---|--|
| | | Day 7 | Day 14 |
| Treatment | Control |  |  |
| | HGA |  |  |
| | SOD |  |  |
| | HGA + SOD |  |  |

Fig. 4.3. Light microscopy images at x10 magnification of C20 cultures supplemented with HGA and SOD.

Images of C20 cell cultures were taken at day 7 and day 14.

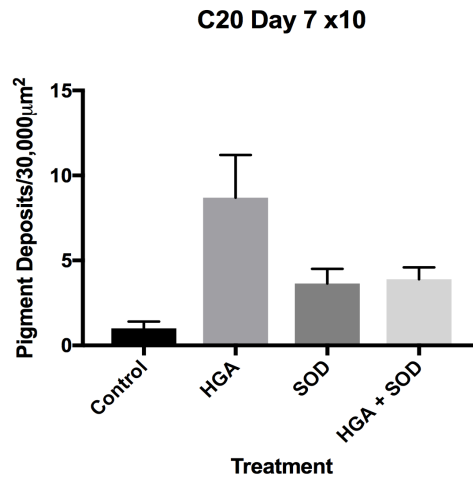


Fig. 4.4. Mean number of pigment deposits at day 7 in C20 cultures supplemented with HGA and SOD. Pigment counts from x10 magnification images expressed as number of pigment deposits per unit area ($n=1$). Error bars signify \pm SEM. The SEM is a measure of the variability of internal replicates.

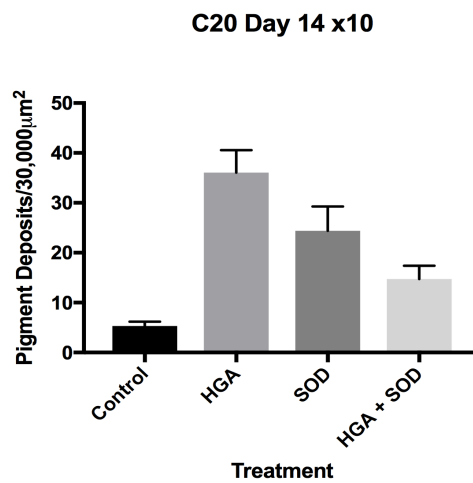


Fig. 4.5. Mean number of pigment deposits at day 14 in C20 cultures supplemented with HGA and SOD. Pigment counts from x10 magnification images expressed as number of pigment deposits per unit area ($n=1$). Error bars signify \pm SEM. The SEM is a measure of the variability of internal replicates.

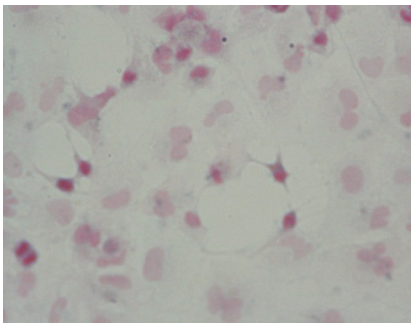
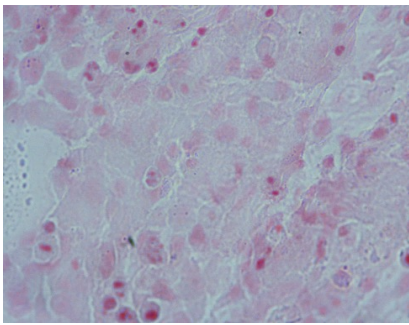
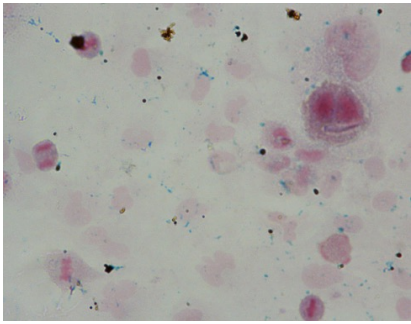
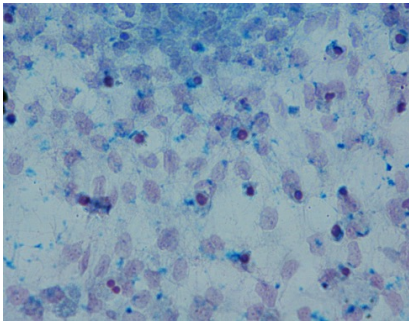
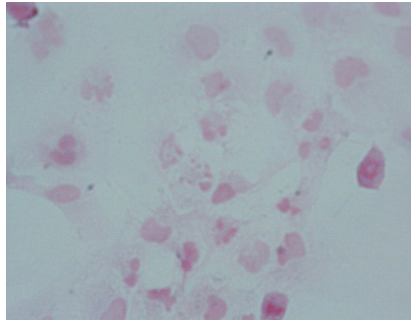
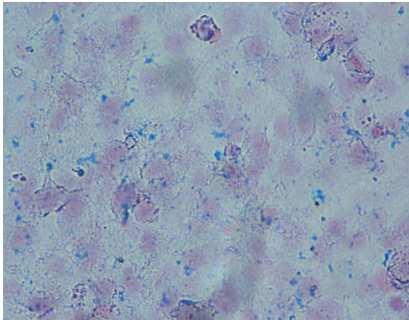
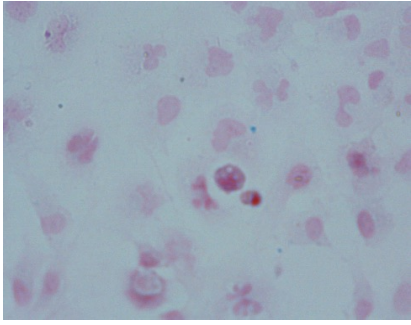
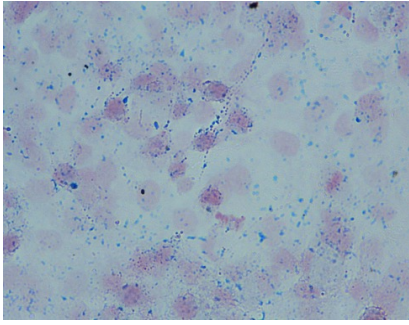
| C20 Cells x40 Magnification | | Day | |
|--------------------------------|-----------|---|--|
| | | Day 7 | Day 14 |
| Treatment | Control |  |  |
| | HGA |  |  |
| | SOD |  |  |
| | HGA + SOD |  |  |

Fig. 4.6. Light microscopy images at x40 magnification of C20 cultures supplemented with HGA and SOD.

Images of C20 cell cultures were taken at day 7 and day 14.

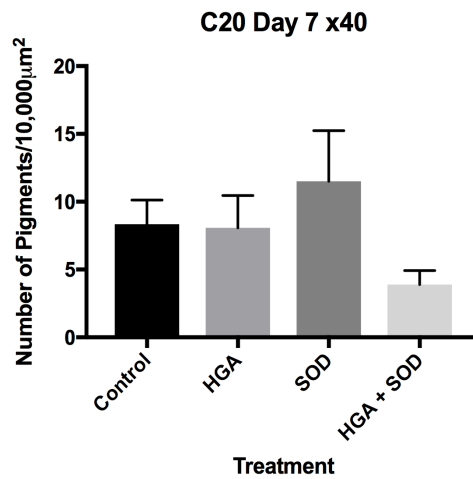


Fig. 4.7. Mean number of pigment deposits at day 7 in C20 cultures supplemented with HGA and SOD. Pigment counts from x40 magnification images expressed as number of pigment deposits per unit area ($n=1$). Error bars signify \pm SEM. The SEM is a measure of the variability of internal replicates.

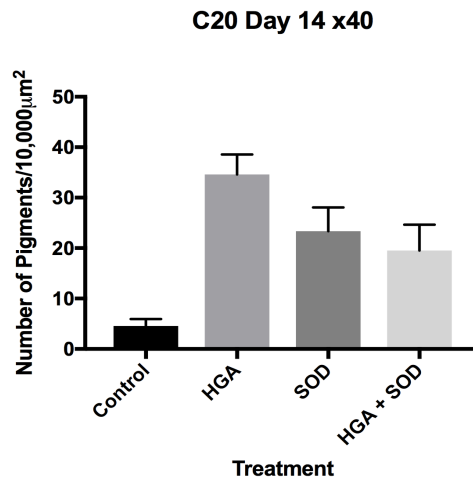


Fig. 4.8. Mean number of pigment deposits at day 14 in C20 cultures supplemented with HGA and SOD. Pigment counts from x40 magnification images expressed as number of pigment deposits per unit area ($n=1$). Error bars signify \pm SEM. The SEM is a measure of the variability of internal replicates.

After 7 days, C20 cells show differences in their viability (Fig. 4.1). Cultures containing HGA show an increased viability compared to control and SOD only cultures. There appears to be no difference in the data between HGA and HGA+SOD. After 14-days (Fig. 4.2), C20 cells show no differences in their levels of viability across all treatment conditions. The results therefore suggest C20 cells are able to tolerate medium containing SOD and HGA.

Histological examination at x10 magnification, shows increased levels of ochronotic pigment present in HGA only cultures at day 7 (Fig. 4.4). The presence of SOD in cultures with HGA+SOD shows a decrease in pigmentation compared to HGA alone, reducing it to a level equal to that of cultures without HGA. Similarly, by day 14 (Fig. 4.5), C20 cells treated with HGA only, show an increase in the number of pigment deposits compared to other treatments. Cultures containing HGA+SOD demonstrate a reduction in the amount of pigmentation.

At x40 magnification, the results suggest there are no differences between treatment conditions at day 7 (Fig. 4.7). By day 14 however (Fig. 4.8), it is indicated that cells treated with HGA only, show an increase in the amount of pigmentation compared to control cultures. Cultures containing HGA+SOD show a decrease in pigmentation compared to HGA only cultures. This suggests that by day 14 SOD influences pigmentation in C20 cells.

These results suggest that the presence of SOD in C20 cultures has an effect on the pigmentation process, whilst having no effect on the viability of cells.

4.1.2 MG63 – Cell Viability and Histological Analysis

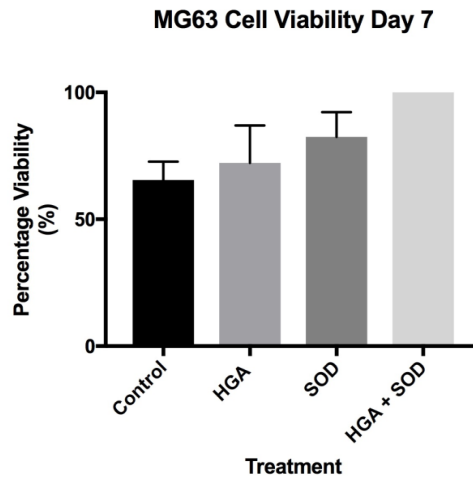


Fig. 4.9. Percentage viability of day 7 MG63 cultures supplemented with HGA and SOD. The number of viable cells expressed as a percentage ($n=1$). Error bars signify \pm SEM. The SEM is a measure of the variability of internal replicates.

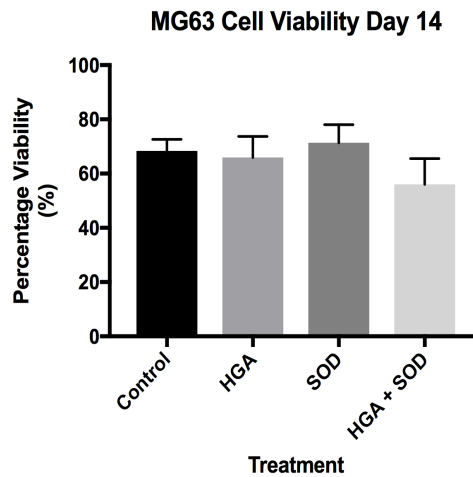


Fig. 4.10. Percentage viability of day 14 MG63 cultures supplemented with HGA and SOD. The number of viable cells expressed as a percentage ($n=1$). Error bars signify \pm SEM. The SEM is a measure of the variability of internal replicates.

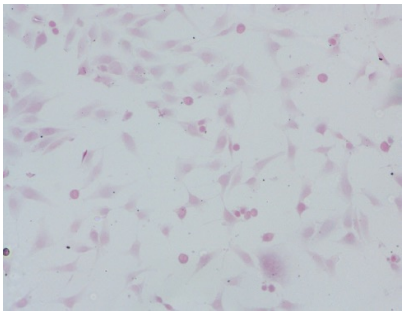
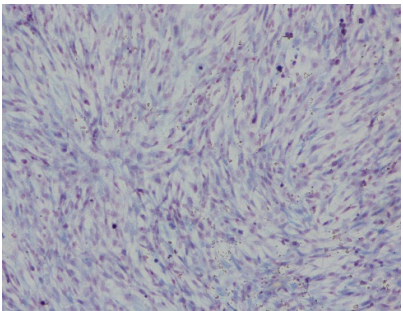
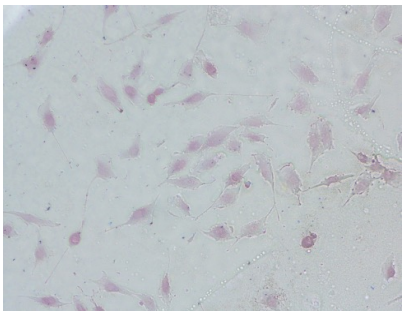
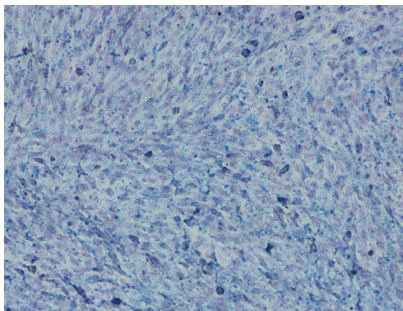
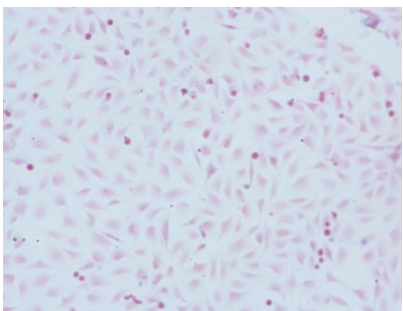
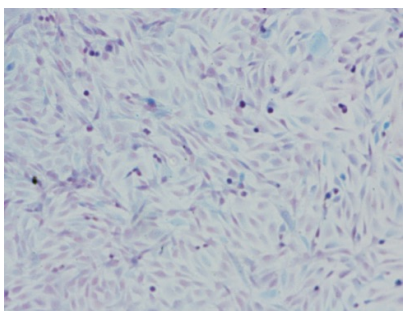
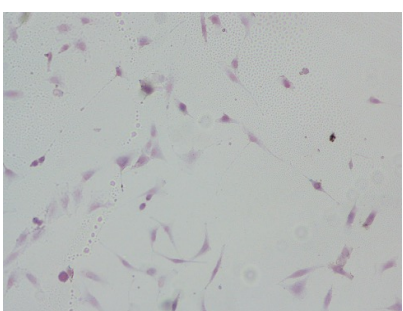
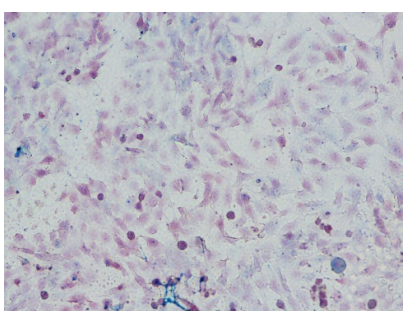
| MG63 Cells x10 Magnification | | Day | |
|---------------------------------|-----------|---|--|
| | | Day 7 | Day 14 |
| Treatment | Control |  |  |
| | HGA |  |  |
| | SOD |  |  |
| | HGA + SOD |  |  |

Fig. 4.11. Light microscopy images at x10 magnification of MG63 cultures supplemented with HGA and SOD. Images of MG63 cell cultures were taken at day 7 and day 14.

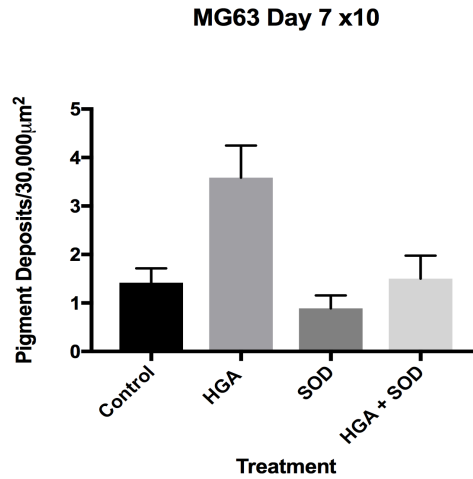


Fig. 4.12. Mean number of pigment deposits at day 7 in MG63 cultures supplemented with HGA and SOD. Pigment counts from x10 magnification images expressed as number of pigment deposits per unit area ($n=1$). Error bars signify \pm SEM. The SEM is a measure of the variability of internal replicates.

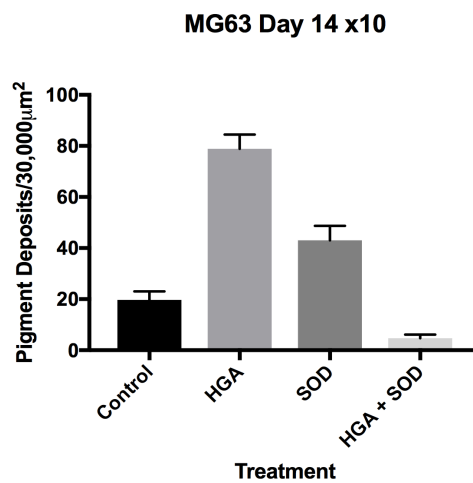


Fig. 4.13. Mean number of pigment deposits at day 14 in MG63 cultures supplemented with HGA and SOD. Pigment counts from x10 magnification images expressed as number of pigment deposits per unit area ($n=1$). Error bars signify \pm SEM. The SEM is a measure of the variability of internal replicates.

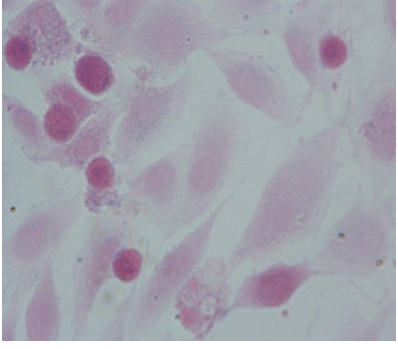
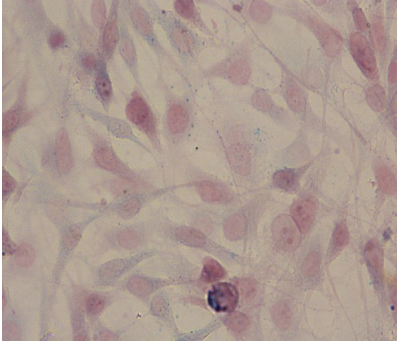
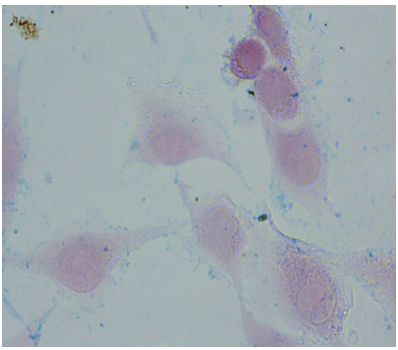
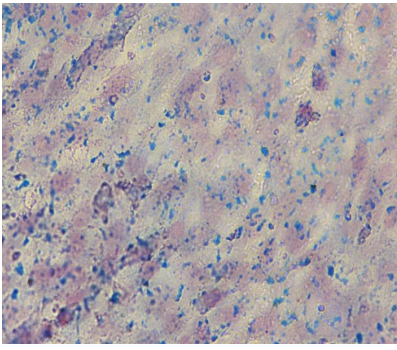
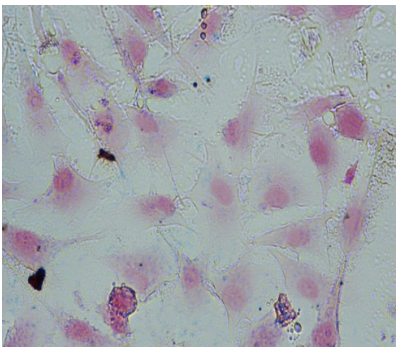
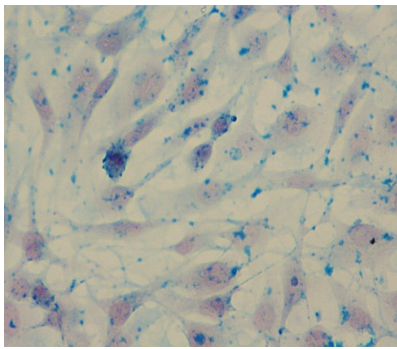
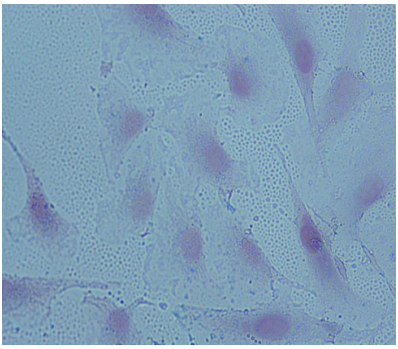
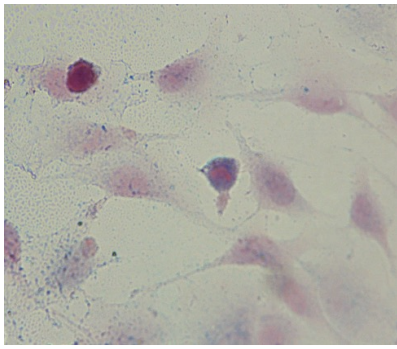
| MG63 Cells x40 Magnification | | Day | |
|---------------------------------|-----------|---|--|
| | | Day 7 | Day 14 |
| Treatment | Control |  |  |
| | HGA |  |  |
| | SOD |  |  |
| | HGA + SOD |  |  |

Fig. 4.14. Light microscopy images at x40 magnification of MG63 cultures supplemented with HGA and SOD. Images of MG63 cell cultures were taken at day 7 and day 14.

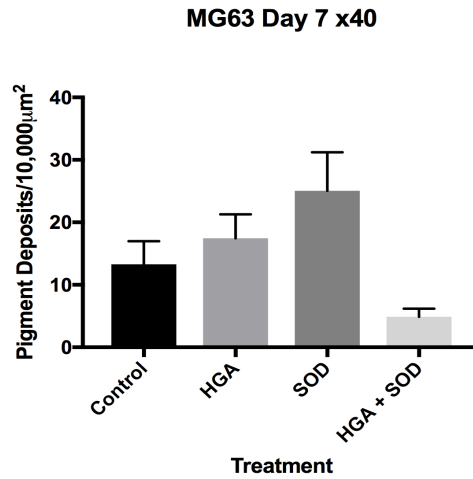


Fig. 4.15. Mean number of pigment deposits at day 7 in MG63 cultures supplemented with HGA and SOD. Pigment counts from x40 magnification images expressed as number of pigment deposits per unit area ($n=1$). Error bars signify \pm SEM. The SEM is a measure of the variability of internal replicates.

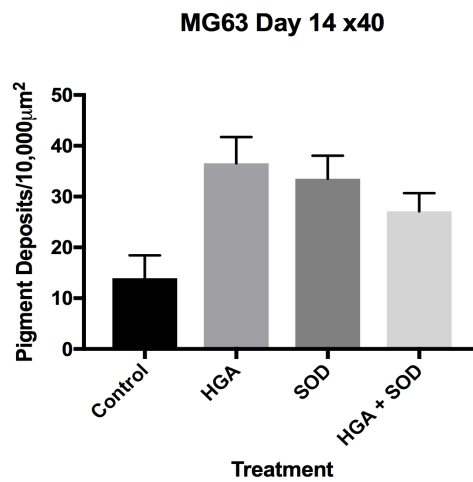


Fig. 4.16. Mean number of pigment deposits at day 14 in MG63 cultures supplemented with HGA and SOD. Pigment counts from x40 magnification images expressed as number of pigment deposits per unit area ($n=1$). Error bars signify \pm SEM. The SEM is a measure of the variability of internal replicates.

MG63 cultures indicate no differences between treatment groups in percentage viability at days 7 and 14 (Fig. 4.9 and Fig. 4.10). All treatments display similar levels of viability to control cultures. These results suggest that like C20 cultures, MG63 cells are able to tolerate medium supplemented with SOD and HGA.

The results of the MG63 pigment deposit counts show similar results to C20 cultures at x10 magnification (Fig. 4.12 and Fig. 4.13). At 7 days, the cells treated with only HGA show a significant number of pigment deposits, whereas there is a large decrease in pigmentation observed in cultures containing HGA+SOD. This trend continues on day 14, with an even larger difference in pigmentation seen between cultures treated with HGA and HGA+SOD, suggesting SOD is effective in reducing pigmentation.

Analysis of pigment deposits at x40 magnification, suggests that there is no difference in pigmentation levels between HGA only cultures and HGA+SOD, for both days 7 and 14 (Fig. 4.15 and Fig. 4.16). Although the amount of pigmentation in HGA+SOD cultures is lower than HGA cultures, the results suggest a difference may not be observed, as the error bars are likely to overlap.

The results at x10 magnification show that the presence of SOD has an effect on the pigmentation process. However, at x40 magnification the efficacy of SOD appears to have reduced. The results therefore suggest that MG63 cells respond differently to C20 cells, when exposed to cultures containing HGA+SOD.

4.2 Summary of Results

The results from the cell viability assay show that following 14 days of treatment, C20 and MG63 cultures are able to tolerate culture medium supplemented with SOD and HGA. Histological examination of C20 cultures shows that there is a decrease in the number of pigment deposits in HGA+SOD cultures, in comparison to HGA only cultures. This effect is observed at both time points at x10 magnification. At x40, a decrease in pigmentation is seen by day 14. MG63 cultures show similar results at x10 magnification to C20 cultures. At x40 magnification however, the results suggest SOD is less effective in reducing pigmentation. The results for C20 cultures suggest that SOD may have a role in the prevention of ochronosis in chondrocytes. MG63 cultures show contrasting results to C20 cultures, at x40. This may provide further evidence to suggest that in comparison to C20 cells, MG63 cells respond differently in the presence of HGA (48).

Chapter 5 – Results III

5.1 Analysis of Sulphated GAG Release in an *in vitro* Model of Ochronosis, Following Treatment with SOD

Cell supernatants from the experiments undertaken in Chapter 4 were analysed via DMMB assay, an assay used to detect loose sulphated GAG complexes in culture medium. Ultrastructural examination has shown sulphated GAGs to be a major component of ECM in bone, as well as in articular cartilage. It is therefore feasible to assess sulphated GAG release in both cell lines (93). Studies have shown that SOD binds to proteoglycans and collagen, and in early stages of OA there is a known decrease in proteoglycans and therefore an associated decrease in SOD (54, 63). It is hypothesised in AKU that proteoglycans are a protective barrier against pigment deposits on collagen fibrils (1). This theory can be furthered by suggesting that the SOD present on proteoglycans are the barrier to ochronosis, by preventing oxidative damage to proteoglycans (1). This study will aim to measure the quantity of sulphated GAG released in culture medium, as an indirect method of assessing damage to proteoglycan structures.

5.1.1 C20 – DMMB Assay

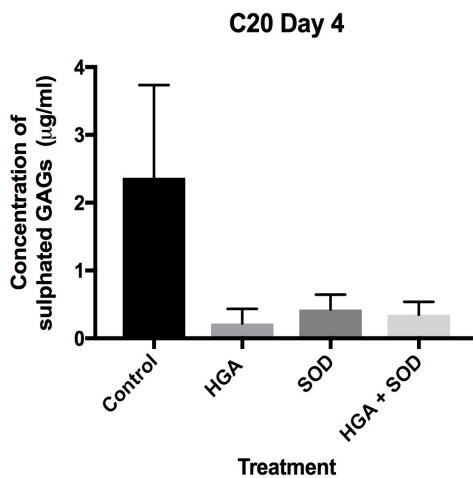


Fig. 5.1. Concentration of sulphated GAG complexes in C20 cultures supplemented with HGA and SOD at day 4 ($n=1$). Error bars signify \pm SEM. The SEM is a measure of the variability of internal replicates.

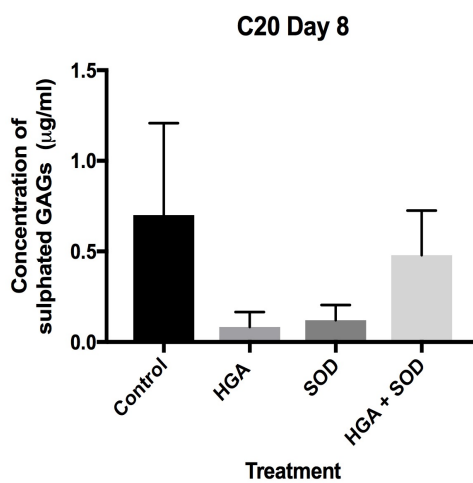


Fig. 5.2. Concentration of sulphated GAG complexes in C20 cultures supplemented with HGA and SOD at day 8 ($n=1$). Error bars signify \pm SEM. The SEM is a measure of the variability of internal replicates.

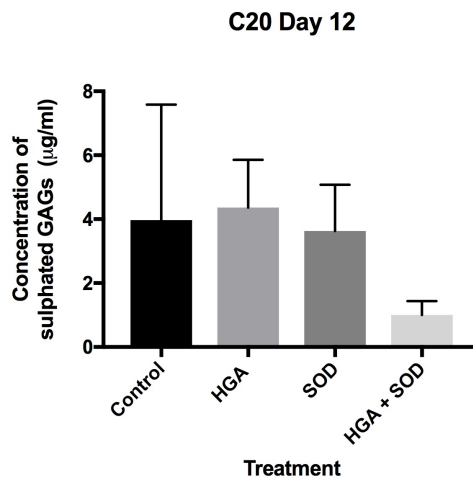


Fig. 5.3. Concentration of sulphated GAG complexes in C20 cultures supplemented with HGA and SOD at day 12 ($n=1$). Error bars signify \pm SEM. The SEM is a measure of the variability of internal replicates.

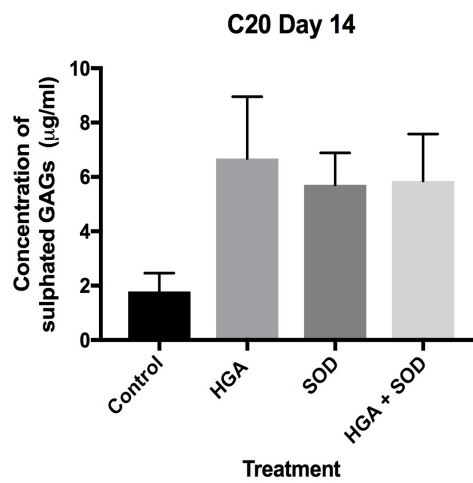


Fig. 5.4. Concentration of sulphated GAG complexes in C20 cultures supplemented with HGA and SOD at day 14 ($n=1$). Error bars signify \pm SEM. The SEM is a measure of the variability of internal replicates.

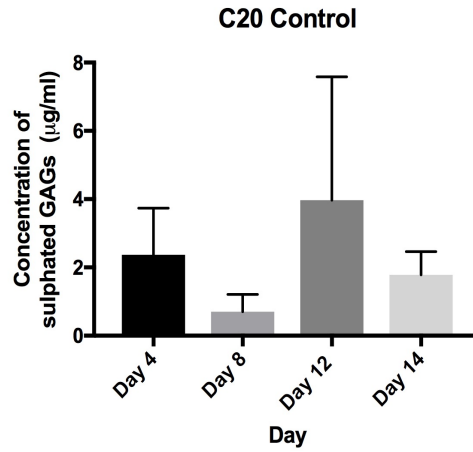


Fig. 5.5. A comparison of sulphated GAG concentrations in C20 control cultures across the 14-day treatment period ($n=1$). Error bars signify \pm SEM. The SEM is a measure of the variability of internal replicates.

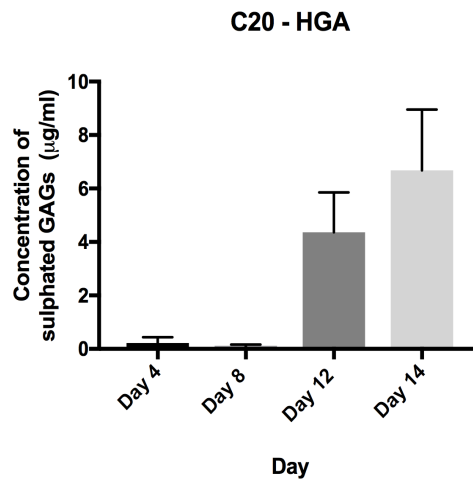


Fig. 5.6. A comparison of sulphated GAG concentrations in C20 HGA cultures across the 14-day treatment period ($n=1$). Error bars signify \pm SEM. The SEM is a measure of the variability of internal replicates.

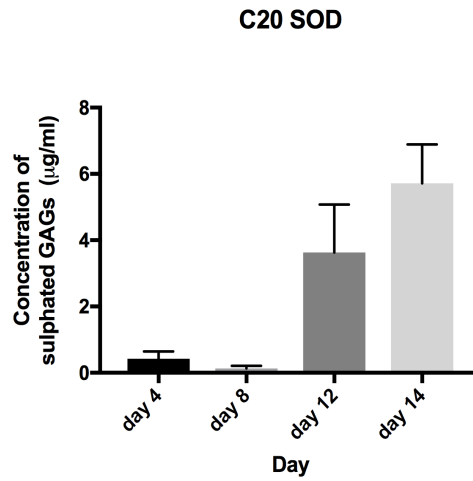


Fig. 5.7. A comparison of sulphated GAG concentrations in C20 SOD cultures across the 14-day treatment period ($n=1$). Error bars signify \pm SEM. The SEM is a measure of the variability of internal replicates.

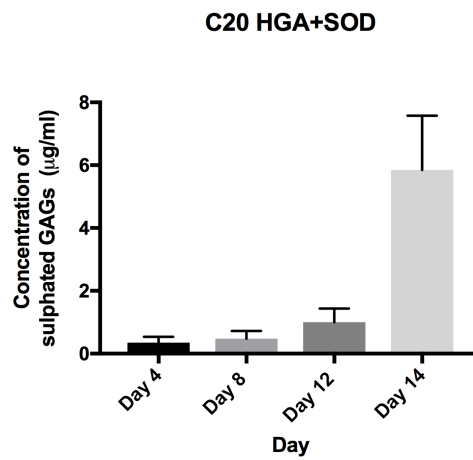


Fig. 5.8. A comparison of sulphated GAG concentrations in C20 HGA+SOD cultures across the 14-day treatment period ($n=1$). Error bars signify \pm SEM. The SEM is a measure of the variability of internal replicates.

The results suggest that in C20 cultures there are no differences in sulphated GAG release between treatment groups, at any of the time points analysed (Fig. 5.1 - Fig. 5.4). However, cultures supplemented with SOD and/or HGA show a general rise in levels of sulphated GAG, in comparison to control cultures over the treatment period. By day 14 treated cultures produce a greater level of sulphated GAGs than control cultures, however due to the large internal variance in each culture group a difference is unlikely to be observed.

When comparing the same culture conditions over the 14-day treatment period (Fig. 5.5 – Fig. 5.8), control cultures appear to consistently produce similar levels of sulphated GAG at each time point (Fig. 5.5). However, a difference is indicated within treatment cultures (Fig. 5.6 - Fig. 5.8). Cultures with HGA and/or SOD show increases in sulphated GAG production by day 14, compared to day 4. SOD cultures also show an increase by day 12, suggesting SOD may induce an earlier release of sulphated GAG in cultures.

When comparing treatment cultures to control cultures on each day (Fig. 5.1 – Fig. 5.4), the results indicate that there are no effects on sulphated GAG release. However, when each treatment is examined across the 14-day treatment period (Fig. 5.5 – Fig. 5.8), the cultures appear to release more sulphated GAGs during the later stages. This suggests that if left for longer than 14 days, there may be some differences observed in sulphated GAG levels between control and treatment cultures.

5.1.2 MG63 – DMMB Assay

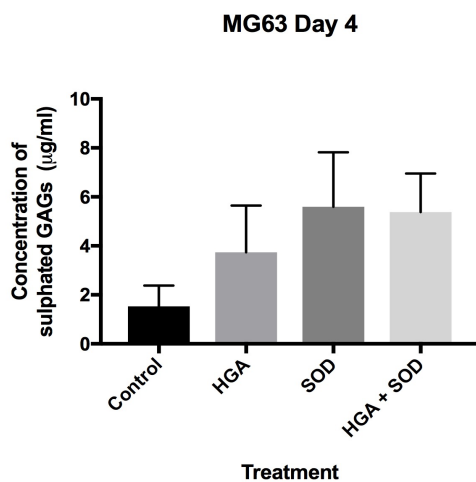


Fig. 5.9. Concentration of sulphated GAG complexes in MG63 cultures supplemented with HGA and SOD at day 4 ($n=1$). Error bars signify \pm SEM. The SEM is a measure of the variability of internal replicates.

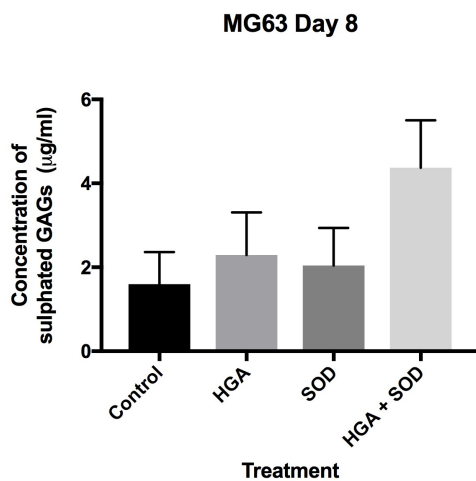


Fig. 5.10 Concentration of sulphated GAG complexes in MG63 cultures supplemented with HGA and SOD at day 8 ($n=1$). Error bars signify \pm SEM. The SEM is a measure of the variability of internal replicates.

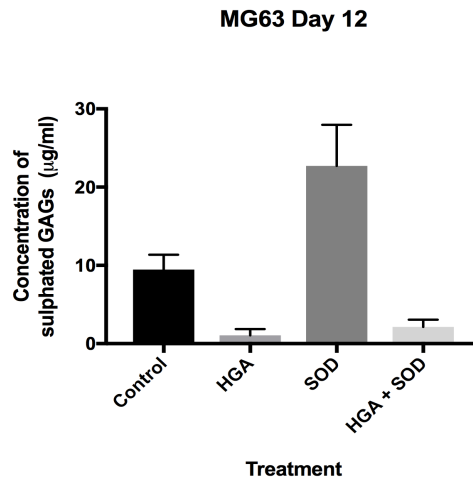


Fig. 5.11. Concentration of sulphated GAG complexes in MG63 cultures supplemented with HGA and SOD at day 12 ($n=1$). Error bars signify \pm SEM. The SEM is a measure of the variability of internal replicates.

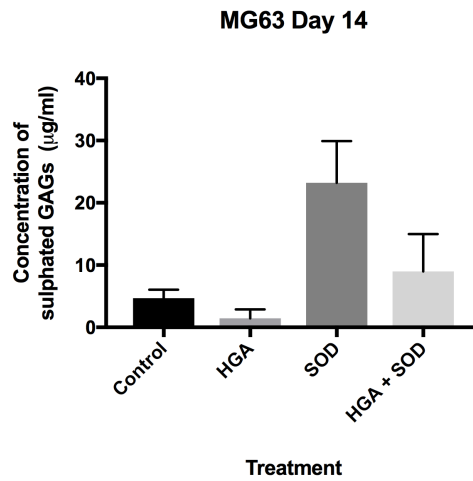


Fig. 5.12 Concentration of sulphated GAG complexes in MG63 cultures supplemented with HGA and SOD at day 14 ($n=1$). Error bars signify \pm SEM. The SEM is a measure of the variability of internal replicates.

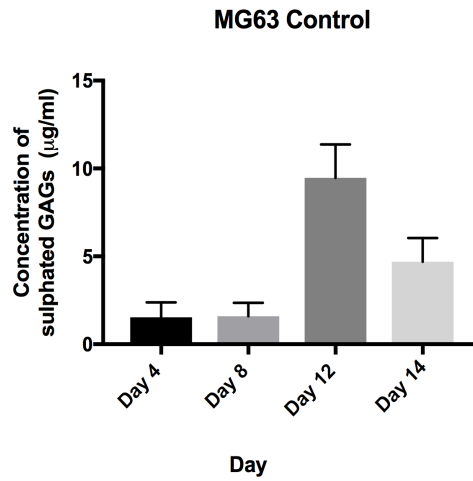


Fig. 5.13 A comparison of sulphated GAG concentrations in MG63 control cultures across the 14-day treatment period ($n=1$). Error bars signify \pm SEM. The SEM is a measure of the variability of internal replicates.

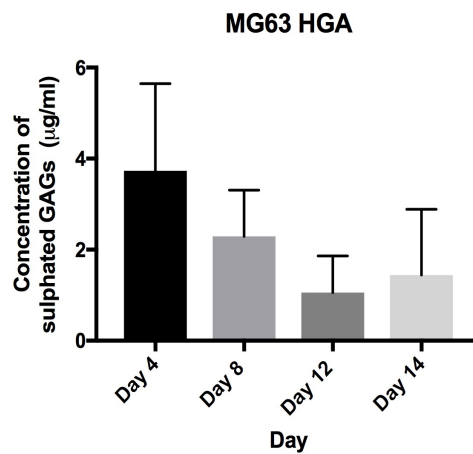


Fig. 5.14. A comparison of sulphated GAG concentrations in MG63 HGA cultures across the 14-day treatment period ($n=1$). Error bars signify \pm SEM. The SEM is a measure of the variability of internal replicates.

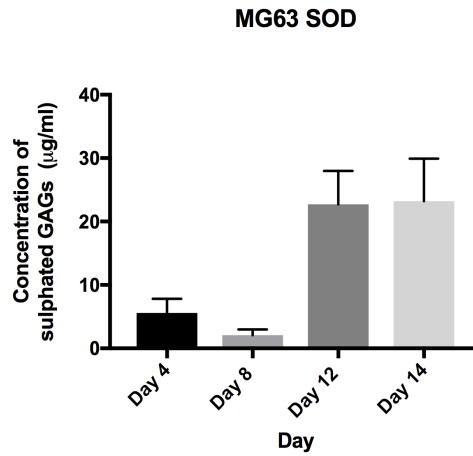


Fig. 5.15. A comparison of sulphated GAG concentrations in MG63 SOD cultures across the 14-day treatment period ($n=1$). Error bars signify \pm SEM. The SEM is a measure of the variability of internal replicates.

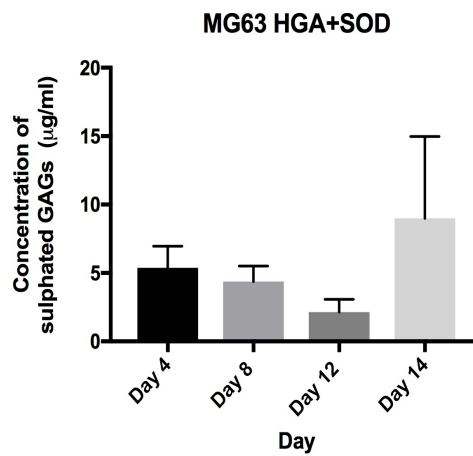


Fig. 5.16. A comparison of sulphated GAG concentrations in MG63 HGA+SOD cultures across the 14-day treatment period ($n=1$). Error bars signify \pm SEM. The SEM is a measure of the variability of internal replicates.

The data indicates that there are no differences between the treatment groups at day 4 and day 8 (Fig. 5.9 and Fig. 5.10), due to the large variances observed. However, by day 12 (Fig. 5.11 and Fig. 5.12) cultures containing SOD show an increase in sulphated GAG release in comparison to other treatment conditions. Cultures that were treated with HGA and HGA+SOD show similar levels of sulphated GAG release. Both cultures produced lower levels of Sulphated GAGs than control cultures.

Comparison of control culture across the 14-day treatment period (Fig. 5.13), shows an increase in sulphated GAG release at day 12. This decreases at day 14, and the data indicates similar levels of sulphated GAG are seen in comparison to days 4 and 8 cultures. Cultures containing SOD only (Fig. 5.15), also show an increase in sulphated GAG release at day 12 and 14. Cultures containing HGA indicate no differences are seen across the days (Fig. 5.14 and Fig. 5.16).

The results suggest that in MG63 cultures, SOD induces a greater release of sulphated GAG complexes compared to controls. The data suggests that cultures containing HGA and HGA+SOD have no impact on GAG release, as no differences are indicated, when compared to control cultures.

5.2 Summary of Results

C20 cultures appear to show no differences in sulphated GAG release between treatment groups across the 14-day treatment period. This suggests that ROS are not involved in the breakdown of proteoglycans. It can therefore be suggested that other factors are involved in the breakdown of proteoglycans, enabling ochronosis (1). MG63 cells show similar results at days 4 and 8 to C20 cultures; there are no differences between treatment groups. However, cultures treated with SOD at days 12 and 14, showed an increase in sulphated GAG, in comparison to other treatment conditions. This indicates that SOD may have a detrimental impact on aspects of the ECM of bone.

Chapter 6 – Results IV

6.1 Raman Spectroscopy of an *in vitro* Model of Ochronosis

Structural analysis of AKU cartilage has enabled a detailed understanding of the progression of AKU following the deposition of ochronotic pigment (1, 31). This has provided evidence which shows similarities between AKU and OA in the form of high density mineralised protrusions. Originally thought to be disease specific to AKU, these protrusions were later found in OA cartilage, suggesting a new mechanism of cartilage degradation in OA (1, 60, 80, 94, 95). Ochronotic osteoarthropathy represents an extreme form of OA. This means that discoveries made from research in AKU can also have potential implications for the understanding of the pathophysiology of OA (1). Further structural analysis has shown a distinct pattern of binding of ochronotic pigment on collagen fibrils (32). This has enabled the proposal of the exposed collagen hypothesis, as this binding pattern shows similarities to proteoglycan binding (1).

Structural analysis has enabled significant advancement in AKU research. There is further potential using another novel analytical technique, to provide new insights into the pathogenesis of AKU. Raman spectroscopy is a non-destructive method with the ability to analyse chemical structures and perform quantitative analyses of samples. To do this, each cell line (C20 and MG63) was passaged and grown to confluence for three days, in two 25cm³ culture flasks containing sterilised CaF₂ disks. One flask was left untreated and the other treated with 33µM of HGA. Following three days of treatment, spectroscopic measurements were carried out to determine the presence, if any, of structural differences between treatment and non-treatment groups. Quantitative analysis was also carried out with the aim

of providing information about any changes to the amount of cartilage and osteoid components present in cultures.

This study will aim to use Raman spectroscopy to observe any differences in the structural composition of *in vivo* cell cultures, with and without the presence of HGA. Through this, it may be possible to identify the matrix components associated with the ochronotic pigment and elucidate any changes in structural composition. The study will also attempt to provide evidence for the exposed collagen hypothesis via quantitative analysis of proteoglycans among treatment groups.

Average Raman Spectra of Treated and Untreated Chondrocytes

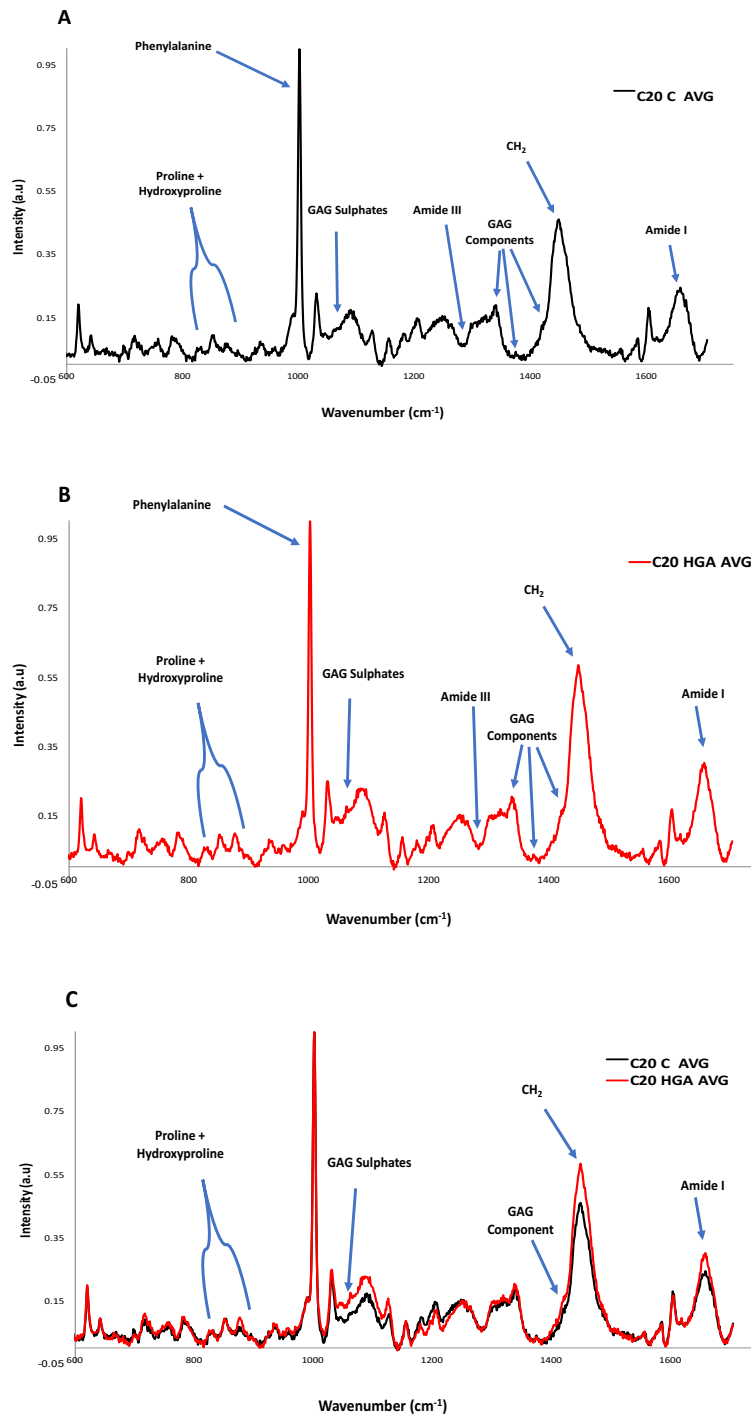


Fig. 6.1. **A)** Average spectra of C20 control cultures, with labels for key components of cell and matrix. **B)** Average spectra of C20 HGA treated cultures, with labels for key components of cell and matrix **C)** Average spectra of C20 control (Black) and HGA treated (Red) cultures. The labels highlight components which demonstrate a difference in intensity between the two treatment groups (96-98).

Average Raman Spectra of Treated and Untreated Osteoblasts

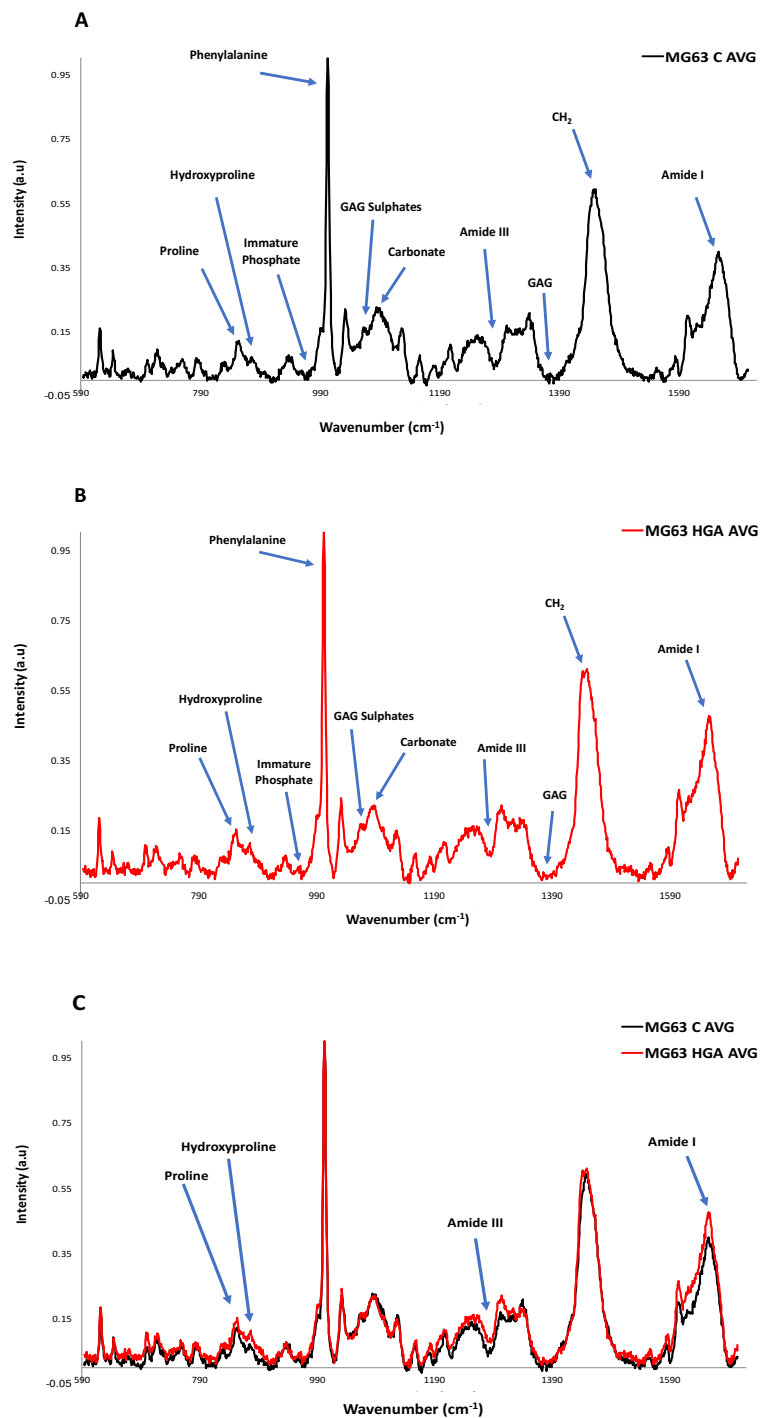


Fig. 6.2. A) Average spectra of MG63 control cultures, with labels for key components of cell and matrix. **B)** Average spectra of MG63 HGA treated cultures, with labels for key components of cell and matrix **C)** Average spectra of MG63 control (Black) and HGA treated (Red) cultures. The labels highlight components which demonstrate a difference in intensity between the two treatment groups (99, 100).

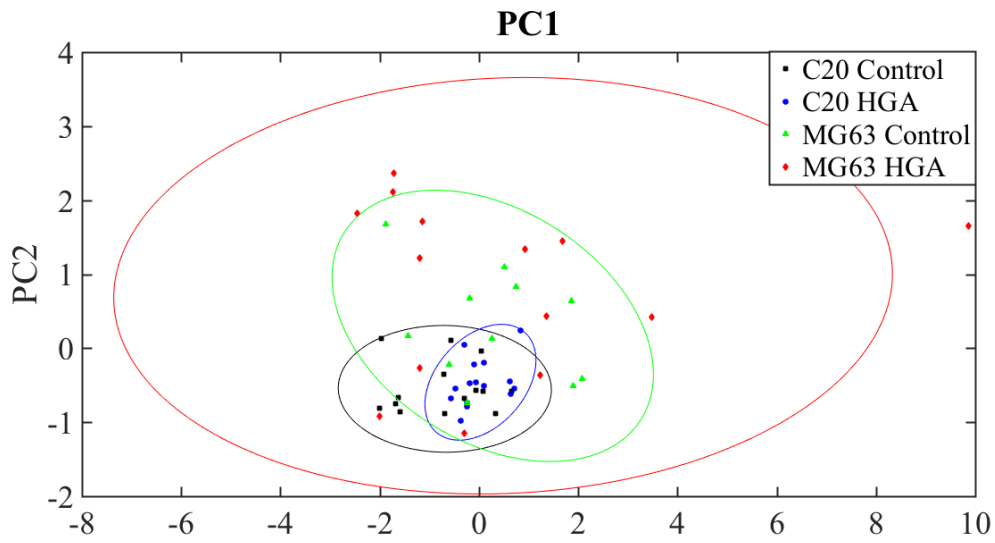


Fig. 6.3. PCA analysis of all C20 and MG63 cultures. Plots represent cell type and treatment and are colour and shape coordinated. Ellipses represent a 95% Confidence Interval for their respective cell culture.

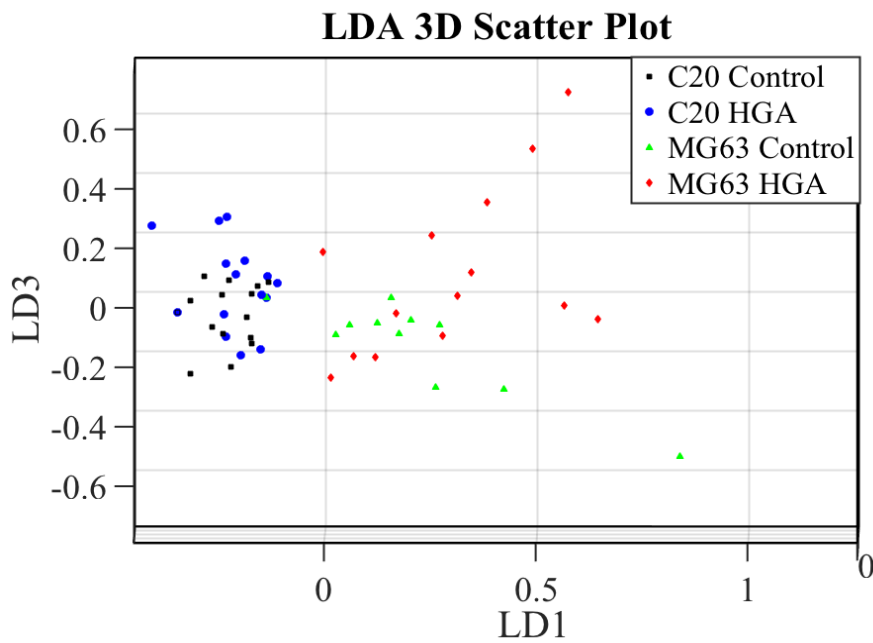
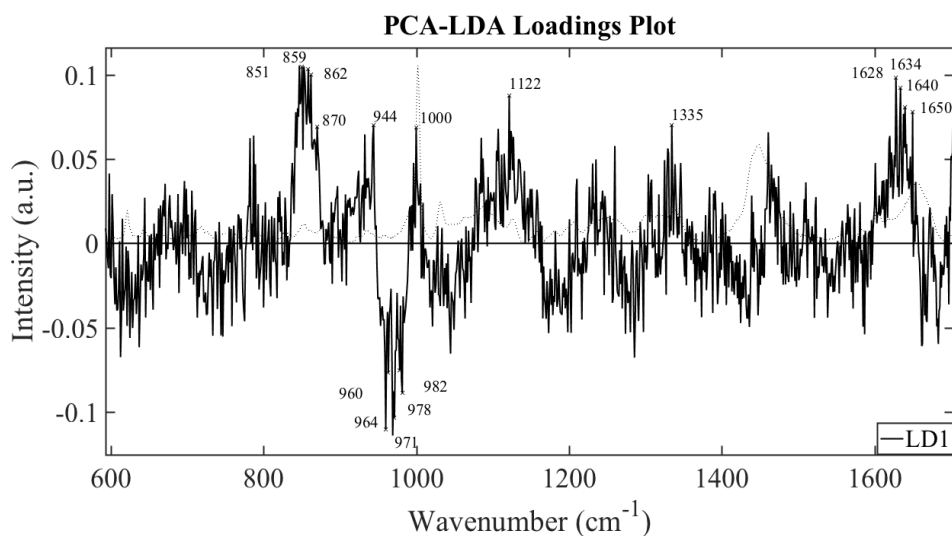
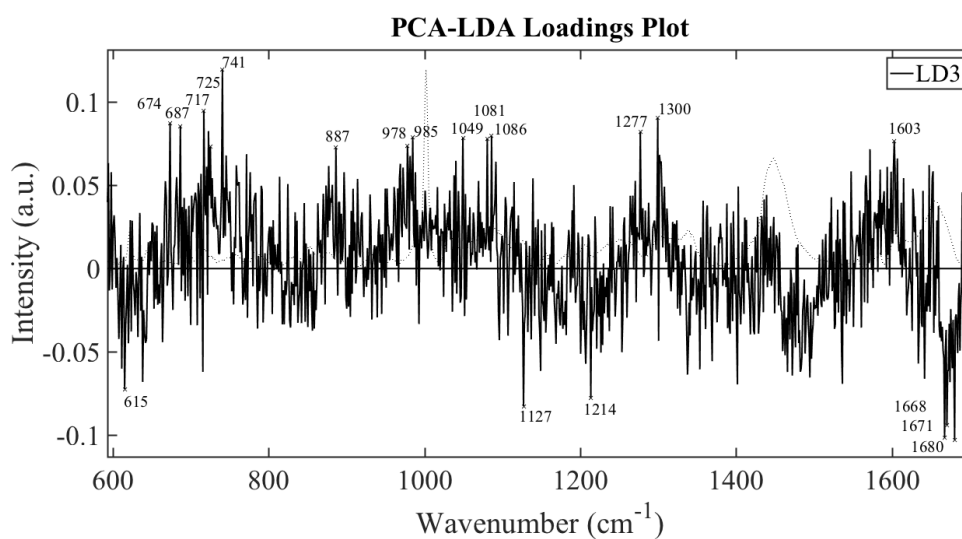


Fig. 6.4. PCA-LDA analysis of all C20 and MG63 cultures. Plots represent cell type and treatment and are colour and shape coordinated.



| Wavenumber | Associated Structure | Biological Function |
|----------------------------|----------------------------|---|
| 850-870 cm^{-1} | Proline and Hydroxyproline | Components of cartilage. Type 2 cartilage produced by C20 cell and Type 1 cartilage produced by MG63. |
| 1620-1650 cm^{-1} | Amide I | |
| 960-990 cm^{-1} | Phosphate | Mineralising agents produced in MG63 cultures but not in C20 cultures |

Fig. 6.5. Loadings plot of LD1 following PCA-LDA analysis of all C20 and MG63 cultures. A loadings plot distinguishes wavenumbers, which separate classes along LD1. Separation along LD1 is likely due to differences in cell type. Table correlates wavenumbers from the loadings plot to their associated structures. The differences observed on the loadings plot are then related to potential biological function.



| Wavenumber | Associated Structure | Biological Function |
|---------------------------|----------------------|---|
| 610-750cm ⁻¹ | Unknown | No identifiable structures associated with C20 and MG63. Possibly associated with structures present in HGA and its pigment polymer |
| 880-1090cm ⁻¹ | Unknown | |
| 1277cm ⁻¹ | Amide III | Collagen components. Structural alterations to collagen components, due to the presence of HGA. |
| 1603cm ⁻¹ | Phenylalanine | |
| 1660-1680cm ⁻¹ | Amide I | |

Fig. 6.6. Loadings plot of LD3 following PCA-LDA analysis of all C20 and MG63 cultures. A loadings plot distinguishes wavenumbers, which separate classes along LD3. Separation along LD3 is likely due to the presence of HGA. Table correlates wavenumbers from the loadings plot to their associated structures. The differences observed on the loadings plot are then related to potential biological function.

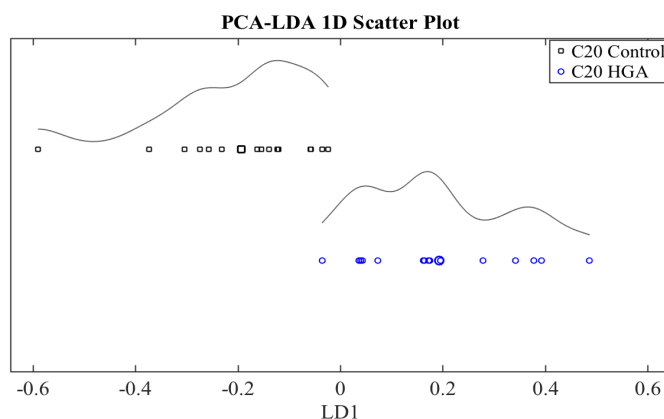
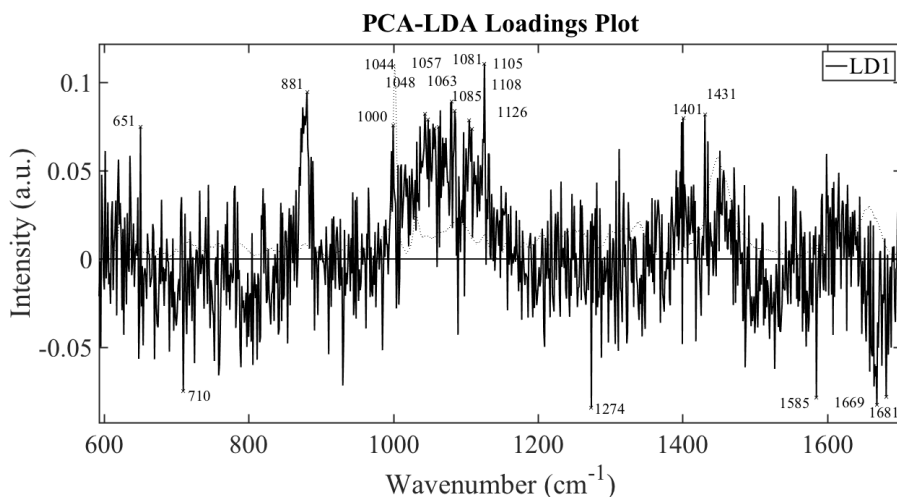


Fig. 6.7. PCA-LDA analysis of C20 Control and HGA cultures. Plots represent cell type and treatment and are colour and shape coordinated.



| Wavenumber | Associated Structure | Biological Function |
|---------------------------|----------------------|--|
| 600-800cm ⁻¹ | Unknown | No identifiable structures associated with C20. Possibly associated with structures present in HGA and its pigment polymer |
| 1063cm ⁻¹ | GAG Sulphate | Structural alteration to GAG components due to the presence of HGA |
| 1000cm ⁻¹ | Phenylalanine | Collagen components. Suggested structural alterations to collagen components, due to the presence of HGA. |
| 1274cm ⁻¹ | Amide III | |
| 1660-1690cm ⁻¹ | Amide I | |

Fig. 6.8. Loadings plot of LD1 following PCA-LDA analysis of C20 Control and HGA cultures. A loadings plot distinguishes wavenumbers, which separate classes along LD1. Separation is likely due to the presence of HGA. Table correlates wavenumbers from the loadings plot to their associated structures. The differences observed on the loadings plot are then related to potential biological function.

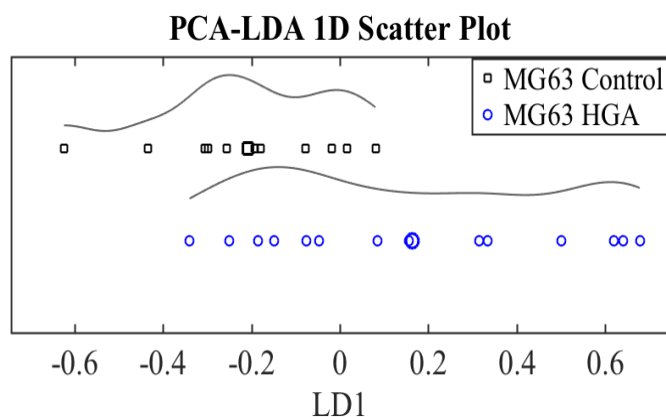
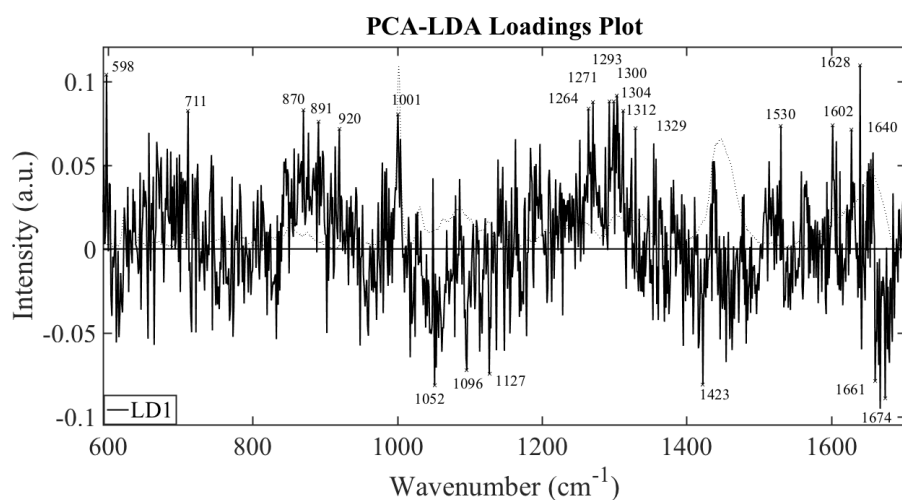


Fig. 6.9. PCA-LDA analysis of MG63 Control and HGA cultures. Plots represent cell type and treatment and are colour and shape coordinated.



| Wavenumber | Associated Structure | Biological Function |
|----------------------------|-----------------------|---|
| 870-920 cm^{-1} | Proline | Collagen components. Suggested structural alterations to collagen components, due to the presence of HGA. |
| 1001 cm^{-1} | Hydroxyproline | |
| 1260-1330 cm^{-1} | Phenylalanine | |
| 1640-1680 cm^{-1} | Amide I and Amide III | |

Fig. 6.10. Loadings plot of LD1 following PCA-LDA analysis of MG63 Control and HGA cultures. A loadings plot distinguishes wavenumbers, which separate classes along LD1. Separation is likely due to the presence of HGA. Table correlates wavenumbers from the loadings plot to their associated structures. The differences observed on the loadings plot are then related to potential biological function.

The graph displaying average spectra of C20 cultures (Fig. 6.1), highlights key peaks for cartilage components. The results show that both cultures produce Raman signatures at all key peaks, suggesting no alterations or change in presence to key structures. However, at certain wavelengths there are variations in intensity between C20 control and C20 HGA cultures. Hydroxyproline at 875cm^{-1} , GAG Sulphates at 1063cm^{-1} and 1420cm^{-1} , CH_2 at 1450cm^{-1} and Amide I at 1660cm^{-1} in cultures treated with HGA, produce a higher intensity peak than control cultures. Similar observations are seen in MG63 cultures (Fig. 6.2). Both cultures show peaks at similar wavelengths, suggesting there are no structural alterations due to HGA. Unlike C20 cultures however, there are no differences in intensity at the GAG sulphate peaks. Proline, Hydroxyproline, Amide III and Amide I at 850cm^{-1} , 875cm^{-1} , 1280cm^{-1} and 1660cm^{-1} respectively, show a visually observable difference in intensity.

PCA is a statistical analysis technique which identifies components of high variance within a dataset. PCA is an unsupervised technique which focuses on the wavenumbers with the greatest variance, rather than aiming to separate based on cell type and treatment. All four cell cultures were compared to identify any differences. The results show that there is overlap at the 95% confidence interval between all four cultures (Fig. 6.3). This suggests there are no differences between the structures of all four cultures. However, it appears this is due to the large confidence intervals seen from MG63 cultures. The plots for MG63 control and MG63 HGA are widely spread, with a few of the plots among C20 control and C20 HGA. This large spread of data suggests variations in structural composition among both MG63 cultures. On the other hand, C20 cultures show narrower confidence intervals. It is interesting to note that C20 cultures treated with HGA have the narrowest confidence interval, suggesting the least variance among cells. It is also interesting to note that while there is overlap between control

cultures and respective treated cultures, it appears that separate clusters are beginning to form, suggesting that differences in structures due to cell type and treatment are starting to appear.

Following PCA analysis, LDA was used on the data output from PCA. This method aimed to maximise the differences between groups (cell type and cell treatment) whilst minimising inter-category variance. The results show that MG63 cell cultures and C20 cell cultures are different along LD1 (Fig. 6.4). The differences observed along LD3 appears to be due to the presence of HGA. Between C20 control and C20 HGA cultures, there are some overlaps along LD3. However, it appears that C20 controls are clustered lower than C20 HGA, suggesting a separation between the two classes (treatment conditions) could be seen if observed over a longer treatment period. This separation along LD3 is more pronounced between MG63 control and MG63 HGA cultures (Fig. 6.4).

The loadings plot of the PCA-LDA analysis, shows the wavenumbers which have contributed the most in discriminating categories along LD1 and LD3 (Fig. 6.5 and Fig. 6.6). The loadings plot for LD1 mainly highlights peaks for Proline and Hydroxyproline between $850-870\text{cm}^{-1}$, Phosphate between $960-990\text{cm}^{-1}$ and Amide I between $1620-1650\text{cm}^{-1}$ (Fig. 6.5). The loadings plot therefore provides further evidence to suggest that the differences observed along LD1 on the PCA-LDA graph, are due to the differences in structural composition between the two cell types. The peaks highlighted between $610-750\text{cm}^{-1}$ and $880-1090\text{cm}^{-1}$ on the loadings plot for LD3, show no correlation to key band signatures for chondrocytes or osteoblasts, suggesting they are likely to be associated with HGA and its pigment polymer (Fig. 6.6). The peaks at 1277cm^{-1} , 1603cm^{-1} and between $1660-1680\text{cm}^{-1}$ for LD3 correlate to Amide III,

Phenylalanine and Amide I respectively. This indicates that HGA is influencing the structural composition of C20 and MG63 cell cultures. The results therefore show that there are a variety of structures which contribute to the differences observed in the PCA-LDA graph along LD1 and LD3.

PCA-LDA analysis of individual cell lines was then performed (Fig. 6.7 and Fig. 6.9). C20 control cultures were compared against C20 HGA cultures. The results show that there are differences between the two treatment groups, with only a minor overlap seen along LD1 (Fig. 6.7). The loadings plot highlights peaks between $600\text{-}800\text{cm}^{-1}$, $1000\text{-}1130\text{cm}^{-1}$, $1400\text{-}1440$ and $1580\text{-}1690\text{cm}^{-1}$, as contributing to the differences between the two groups (Fig. 6.8). Among these were peaks for key band signatures for chondrocytes. The peaks at 1000cm^{-1} , 1063cm^{-1} , 1274cm^{-1} and $1660\text{-}1690\text{cm}^{-1}$ correspond to Phenylalanine, GAG sulphate, Amide III and Amide I respectively. MG63 cultures show more overlap between control and HGA treated cultures along LD1 (Fig. 6.9). However, it does appear a separation is beginning to form between the two treatment types. Like the results from the PCA analysis, a large variance is seen among MG63 cultures, suggesting variations in structural composition within both treatment groups. The peaks at $870\text{-}920\text{cm}^{-1}$, 1001cm^{-1} , $1260\text{-}1330\text{cm}^{-1}$ and $1640\text{-}1680\text{cm}^{-1}$ are highlighted as peaks which contribute to the differences observed along LD1 (Fig. 6.10). These peaks correspond to Proline, Hydroxyproline, Phenylalanine, Amide III and Amide I respectively, which are key components present in osteoblasts. These results therefore suggest there are structural differences between control and HGA treated cultures, which can be detected via Raman spectroscopy.

6.2 Summary of Results

The graphs displaying average spectra, highlight key structures present in chondrocyte and osteoblast cultures. Both treatment groups (control and HGA) for C20 and MG63 cultures, produced Raman signatures at all key peaks, suggesting no alterations to key structures in both cultures when treated with HGA. However, following this, multivariate analyses were performed. All four cultures were initially analysed with PCA. LDA was then implemented on the data output from PCA, resulting in a PCA-LDA analysis. PCA-LDA analysis revealed differences in structural composition between the two cell types (C20 and MG63), and suggested a separation between the two treatment groups could be seen if observed over a longer treatment period. PCA-LDA of individual cell lines was then performed, comparing control cultures against HGA cultures. The results indicated there are structural differences between control and HGA treated cultures, with C20 cultures showing less overlap between treatment groups than MG63 cultures.

Chapter 7 - Discussion

The aim of this thesis was to further existing knowledge of AKU by:

1. Observing the effects of SOD in an AKU disease model.
2. Observing any structural changes to cell cultures in a disease model of AKU via Raman spectroscopy.

The research was conducted in four stages:

1. The assessment of the effects of SOD on C20 and MG63 cell lines.
2. The assessment of the effects of SOD on an *in vitro* model of ochronosis.
3. The analysis of sulphated GAG release in an *in vitro* model of ochronosis, following treatment with SOD.
4. Raman spectroscopy of an *in vitro* model of ochronosis.

7.1 The Effects of SOD on C20 and MG63 Cell Lines

The pigmentation process in AKU is known to require molecular oxygen to allow the polymerisation process to proceed (15). However, consideration must be given to normal articular cartilage, which is avascular and aneural and therefore has a hypoxic environment (45, 68). It is therefore sensible to consider that HGA utilises ROS such as superoxide anions, for the oxidation process within this environment (69). Previous therapies, for example ASC, have attempted to target this oxidative process. Although ASC prevents the polymerisation process, it also causes an accumulation of HGA, leading to increased risk of renal stones. As a result of this severe side effect it is not considered a viable treatment option (2). It is therefore worth observing the effects of alternative antioxidants on HGA, with the aims of establishing

a novel therapeutic approach and elucidating pathophysiological mechanisms involved in the polymerisation process.

Similarities between AKU and OA in their pathogenic mechanisms present novel study opportunities for greater understanding of AKU (1). Oxygen free radicals are involved in the OA disease process. An increase in the presence of ROS is associated with a downregulation/decrease in the presence of SOD in articular cartilage (63). AKU is considered a rapidly progressing form of OA, which shows similar clinical and microscopic presentations. A potential deficit of SOD in articular cartilage of patients with AKU may therefore be a contributing factor to its pathogenesis. It has been shown that cartilage is initially resistant to ochronosis, and ochronosis is only seen from the third decade and onwards. It could be that a decline in SOD, as seen in OA, initiates joint ochronosis (2, 31, 63). This would suggest SOD has a protective role in cartilaginous tissues, specifically preventing ochronosis.

At 500 units/ml C20 cells, displayed a lower level of viability in comparison to control cultures. Studies have shown that ROS are essential molecules in articular cartilage due to their intracellular signalling properties (69). It is therefore possible to suggest that at extremely high doses, SOD may have an adverse effect on articular cartilage through the prevention of metabolic processes. This would suggest that further studies are required to observe the effects of SOD in osteoarticular cells at high concentrations. The results for the cell viability assays between 0 – 50 units/ml, show that human osteoarticular cells are able to tolerate SOD. It is therefore possible to implement SOD in an *in vitro* model of ochronosis, with the aims of observing its effects on the polymerisation process of HGA. If SOD does prevent the formation of ochronotic pigment, the results suggest articular cartilage will be able to tolerate

SOD as a possible therapy. It is likely that SOD at viable concentrations will have fewer side effects in comparison to existing therapies when administered, as it is produced endogenously in a variety of tissues (64).

The results indicate that 5 and 0.5 units/ml are viable concentrations for the *in vitro* model. These cultures, show the closest levels of viability in comparison to control cultures. As 5 and 0.5 units/ml show similar results, 0.5 units/ml will be used for further experiments, with the aims of minimising resource consumption.

7.2 The Effects of SOD on an *in vitro* Model of Ochronosis

The purpose of conducting another cell viability assay was to compare how cells tolerate different treatment conditions. Specifically, this experiment was used to observe if HGA+SOD in combination had a detrimental impact in comparison to control cultures. The results indicate that C20 and MG63 cultures are able to tolerate medium treated with HGA and SOD, enabling further experimentation via histological analysis.

Upon addition of SOD, a reduction is thought to be seen in the amount of pigmentation in both cultures of osteoblasts and chondrocyte cells at x10 magnification. Little is still known about the factors which protect, or fail, within tissues that are subject to ochronosis. However, the literature on AKU is absent of reports of ochronosis in muscles, this may be due to the presence of high levels of SOD in muscular tissues within the body (101, 102). These results therefore suggest that SOD has a protective role in the pigmentation process.

HGA appears relatively stable in *in vivo* samples as seen in fresh serum and urine samples from AKU patients, suggesting ochronosis only occurs in collagenous areas such as articular cartilage (8, 66, 67). Considering the pigmentation process in AKU is known to require molecular oxygen, and normal articular cartilage has a hypoxic environment, it is possible to suggest that HGA utilises ROS within this environment to undergo polymerisation (15, 45, 68, 69). Research has shown that the pigmentation process commences in articular cartilage in the pericellular matrix (12, 13, 31). The reason for this is not yet clear, but trauma or focal damage may be a key factor (1). Degenerative change in response to trauma and focal damage changes the whole extracellular milieu and releases a variety of cytokines, as part of an inflammatory response. In response to these stimuli, chondrocytes have been shown to produce IL-6, a catabolic cytokine. Research has shown that IL-6 plays a role in the pigmentation process. IL-6 has been shown to dysregulate antioxidant defences in chondrocytes (25, 33, 34). Furthermore it is known that superoxide anions are produced in excess during an inflammatory response (65). It is possible that IL-6 inhibits the action of SOD present in articular cartilage, enabling HGA to utilise superoxide anions during the polymerisation process.

At x40 magnification, upon addition of SOD, the results indicate chondrocyte cultures show a reduction in pigmentation at day 14 only. However, osteoblast cultures do not show any differences in pigmentation at both days 7 and 14. These results contrast with analysis at x10 magnification, which suggests a reduction in pigmentation is seen in both cell lines at days 7 and 14. Cell lines have differential capacities in inducing ochronosis. This is especially seen *in vivo*, where cartilage is much more detrimentally affected by ochronosis than bone (2, 31, 48). It has been shown that C20 cultures are susceptible to a greater level of pigmentation

than osteoblasts, suggesting a greater number of pigments per unit area to be more likely present in chondrocyte cultures (48). Therefore, there is a greater likelihood of observing a difference upon addition of SOD in C20 cultures, than in MG63 cultures. Furthermore, analysis at x40 magnification was carried out with a smaller sample size in comparison to x10 magnification. This suggests further reasons a difference is not seen in MG63 cultures and only seen at day 14 for C20 cells.

The results suggest that SOD shows more pigment reduction in C20 cells than in MG63 cells. The experiments were conducted using extracellular SOD, which means SOD is only likely to prevent pigmentation from occurring in the ECM. *In vivo*, the ECM of bone is mineralised and therefore is resistant to pigmentation. Pigment deposition only occurs within osteocytes, extracellular SOD therefore is unlikely to be beneficial as a therapy in bone (2, 42, 63). Chondrocytes however produce an unmineralised ECM, which is affected by ochronosis. As a major symptom of AKU is an early onset debilitating OA, SOD can potentially be implemented as a targeted therapeutic strategy (1, 2).

It is interesting to note that in both cell lines, all results showed the presence of stained pigment deposits in cultures treated with SOD only. Schmorl's stain, originally used to identify melanin, is also used to identify ochronotic pigment. This suggests ochronotic pigment shares structural similarities to melanin. The non-specific nature of Schmorl's stain therefore suggests it may have reacted with other tyrosine metabolites, produced by the cell lines or present in the culture medium (48). It is therefore likely that pigments present in SOD only cultures are likely due to this non-specific staining. Further evidence to suggest that tyrosine metabolites are produced by cell lines or present in the culture medium is the presence of

pigment deposits in all control groups. This suggests that all treatment groups are likely to be equally affected by non-specific staining. Therefore, it is still possible to suggest that SOD inhibits/reduces the ochronotic process. However, to improve the reliability of the results, it may be beneficial to count the number of pigment deposits in replicates of control cultures. This can then be used as a baseline correction on data, prior to statistical analysis.

This experiment looked to see if there was a decrease in pigmentation between cultures treated with HGA and cultures treated with HGA+SOD. By observing a decrease in pigmentation between the two groups, it was suggested that due to the enzyme activity of SOD, a decrease in pigmentation was seen. To confirm that SOD was active in the different treatment conditions, an enzymatic assay would have been beneficial. The assay would have been able to provide further evidence to suggest SOD was the enzyme responsible for the prevention of ochronosis. However, the results still suggest that SOD plays a preventive role in the ochronotic process, indicating that HGA requires ROS for the initiation of the polymerisation process. The cell viability assays demonstrate that SOD does not have a detrimental effect on the cells. This suggests that SOD has the potential to be used as a therapeutic approach in the prevention of ochronosis in articular cartilage.

7.3 Analysis of Sulphated GAG Release in an *in vitro* Model of Ochronosis, Following Treatment with SOD

This experiment was setup to observe if SOD protected proteoglycans from damage caused by ROS. Degenerative change in response to trauma and focal damage, changes the whole extracellular milieu and releases a variety of cytokines. IL-6 has been shown to play a role in

the pigmentation process and is also known to dysregulate antioxidant defences in chondrocytes (25, 33, 34). HGA has been shown to produce ROS during the polymerisation process (15, 35). It is proposed that these ROS inflict damage to protective components in collagen such as proteoglycans. Loss of proteoglycans may enable ochronotic pigment to bind to collagen fibrils at specific areas, as proposed by Taylor *et al* (1, 32). It is therefore likely that IL-6 inhibits the action of SOD present in articular cartilage, enabling the polymerisation process. Using this exposed collagen hypothesis, a decrease in quantity of SOD in AKU cartilage, as seen in OA cartilage, can be predicted (1, 63). SOD has been shown to bind to proteoglycans; if there is loss of proteoglycans there is a subsequent loss of SOD (63, 103). This proposes a self-perpetuating mechanism, where deposition of pigment starts a nucleation event and eventually ochronotic pigment spreads throughout the entire cartilage due to inhibition and loss of SOD, and therefore proteoglycans (1, 25, 48).

The results however suggest that the treated C20 cells show no differences across the days, when compared to control cultures. This suggests that ROS are not involved in the initial breakdown of proteoglycans. It is therefore likely to be another factor, such as repetitive mechanical loading and/or ageing and degradation, which changes the composition of articular cartilage, enabling ochronosis (1).

There are also no differences indicated between HGA treatments and control cultures in MG63 cultures across all days. This suggests that proteoglycan loss in MG63 cultures is also not attributable to ROS. However, there is an increase in proteoglycan production upon addition of SOD at days 12 and 14. Studies have shown the presence of SOD in the ECM of mineralised bone (104). This suggests that the presence of SOD has no detrimental effects on

the structural composition of MG63 ECM. This is further supported from the assessment of cell viability, upon addition of SOD. Sulphated GAGs via an electrostatic interaction are attracted to SOD. As well as this, in an *in vitro* model the ECM components are not assembled correctly. The presence of SOD can therefore attract loosely formed sulphated GAGs, forming free complexes in the media. Furthermore, due to lack of mineralisation, it may be the case that MG63 cultures form a less well organised ECM than C20 cultures. This could explain why a rise in proteoglycans was seen in MG63 cultures at days 12 and 14, but not in C20 cultures (1, 48, 103).

The results indicate that ROS are not involved in the breakdown of proteoglycans. It can therefore be suggested an alternative mechanism is involved in the breakdown, such as mechanical insult, aging, changes to the cellular environment (e.g. pH), or a combination of mechanisms (1, 8). The results therefore indicate ROS are only involved in the initiation of ochronosis.

7.4 Raman Spectroscopy of an *in vitro* Model of Ochronosis

To enable the assessment of structural differences between control and HGA treated cultures, it is possible to group the highlighted peaks in the average spectra to their relevant structures. The GAG components are spectra of bonds present in proteoglycans. The spectrum produced at 1063cm^{-1} represents the sulphated bonds in a GAG complex, such as CS (96, 98). The other peaks represent bonds present in collagen. Peaks for cells are usually identified by the presence of nucleic acid peaks at 1488cm^{-1} and 1579cm^{-1} . However, they are absent in the average spectra, which is to be expected as cells are normally scattered around a dense ECM (96-98, 105).

Similar Raman peaks are produced for MG63 and C20 cultures, with peaks representing collagen and proteoglycan components present in both cultures. However, a structural difference in the two cultures, as identified by the results, is the presence of mineralised components such as phosphate and carbonate in MG63 cultures (99, 100). It is known that the ECM of MG63 cultures undergoes ochronosis due to the absence of protective factors such as minerals, which cover the ECM. However, the results suggest that minerals are still produced by the MG63 cell line. Previously, it was thought that early stage osteosarcoma cell lines did not produce minerals in cell culture conditions without the presence of appropriate stimuli, such as ascorbic acid. The results from the Raman spectra however, suggest that early stage osteoblasts produce minerals such as phosphates and carbonates, regardless of their surrounding environment. This is echoed by a study that has shown the production of hydroxyapatite, another key mineralising agent, by MG63 cells. This suggests that mineralising conditions aid in the binding of minerals to collagen fibrils, rather than in their formation (48, 82, 106, 107). The results presented here lend further evidence to the theory that *in vitro*, MG63 cell cultures do not replicate the assembly of complex structures as seen *in vivo* (48).

The results show that in the presence of HGA, certain peaks show a higher intensity for both C20 and MG63 cultures. Both cell lines in the presence of HGA produced higher intensity peaks for collagen components, suggesting more collagen is produced in this environment. HGA is thought to induce a stressful environment for chondrocytes (1, 15, 25). It has been shown that under stressful conditions chondrocytes change phenotype and become activated cells, producing greater amounts of ECM (108). Similar findings have also been shown in

MG63 cell lines when exposed to stress (109). This suggests that the presence of HGA may be the reason a higher intensity is seen in bands for collagen components, as an initial attempt is made at repairing damaged ECM (110). However, it must be noted that C20 cultures also show differences in intensity at the GAG sulphate and the CH₂ peaks, but MG63 cultures do not. This could be because C20 cells have a higher cellular activity and proliferate quicker than MG63 cells. The presence of HGA creates a stressful environment, further stimulating cellular activity of C20 cells. This results in a greater production of ECM in C20 cells, compared to MG63 cells (1, 15, 48).

The exposed collagen hypothesis predicts a loss of proteoglycans, enabling binding of HGA to collagen and polymerisation to ochronotic pigment. The results suggest there is no loss of proteoglycans following treatment with HGA. This would suggest that proteoglycans may not be the barriers to ochronosis, as originally thought. However, it is acknowledged that *in vitro* models do not assemble their ECM correctly into the organised matrix seen *in vivo*, enabling pigmentation (1). Furthermore, due to the stress response of HGA, an initial compensatory period may be seen with cells increasing production of ECM components such as proteoglycans. This could be considered as an initial attempt at repairing damaged collagen, as seen in OA (1, 15, 110, 111). If therefore a longer treatment period is observed, a decline in proteoglycans may be found.

PCA analysis shows MG63 cultures have a large confidence interval, which contrasts with confidence intervals for C20 cultures. It could be the case that MG63 cells, due to their slower cellular activity, replicate more slowly than C20 cells. This means that cells could be at several stages of the growth cycle, suggesting that cells and their surrounding ECM are at different

stages of maturity. Meanwhile C20 cell may be able to achieve cellular maturity at a faster rate, meaning that at the time of spectral acquisition, C20 cells and surrounding ECM may be fully formed into a uniform structure. This result therefore provides further evidence to suggest that C20 cells proliferate more quickly than MG63 cells (48).

PCA-LDA analysis of all four cell treatments, shows that separation was based on cell type along LD1. Further analysis using loadings plots identified that this difference was observed due to collagen and minerals. This is to be expected as the types of collagen differ between the two cells types. C20 cells produce type II collagen, whereas MG63 produce type I. Whilst both collagen structures share the same basic components, the quantity of each component in each collagen type is likely to vary (42, 46, 112). Another factor that has influenced separation between cell types is the presence of mineral components in MG63 cell cultures, which are not present in C20 cultures. This is also to be expected as MG63 cells produce minerals which, as described above, are not present on collagen (48, 107).

Analysis along LD3 shows that there may be potential to observe a distinct separation between control and HGA treated cultures, if analysed for a longer treatment period. Loadings plot analysis for LD3 shows that any differences seen can be attributed to peaks in between $610\text{-}750\text{cm}^{-1}$, and peaks corresponding to collagenous structures. It has been shown that for several biological spectra, the bands between $600\text{-}800\text{cm}^{-1}$ are a result of ring breathing vibrations. This is the simultaneous contraction of all bonds present in an aromatic ring, such as benzene (113). Whilst the structure of the ochronotic pigment is not known, it is known that a quinone intermediary is produced. As the ochronotic pigment is derived from a quinone, it is possible that aromatic compounds may be present within the pigment polymer,

also producing ring breathing vibrations (8, 113). Changes to collagenous structures is also further evidence for the presence of HGA. Ochronotic pigment is known to bind to collagen in a periodic fashion; the presence of ochronotic pigment on collagen fibres is therefore likely to alter its structure (1, 32). Alternatively, if the bands from the loadings plot are not attributable to an alteration in structure of collagen, it could be that HGA induces a stress response in cell cultures, inducing an increased production of cellular matrix, as previously mentioned (48).

Further comparison using PCA-LDA of individual cell lines (control vs treatment groups), has provided evidence to suggest that it is possible to distinguish control cultures and HGA treated cultures using Raman spectroscopy. The results from the loadings plot show that for C20 cultures, there are several peaks contributing to the differences seen between the control and treatment groups. A study has shown the presence of multiple peaks corresponding to GAG complexes within the 1000-1130 cm^{-1} range (114). This suggests that collagen and GAG components are the main contributors to the discriminant analysis (96-98, 114). Similar results are seen in the loadings plot for MG63 cultures, which shows that the peaks which contribute to the differences between treatment groups correspond to collagen components (99, 100). In both cell lines, there are peaks present in the loadings plots between 600-800 cm^{-1} , suggesting the presence of aromatic rings which could indicate the presence of ochronotic pigment (8, 113). Furthermore, there are unidentified peaks present in both cell lines, which are not related to structures in chondrocytes and osteoblasts. This could suggest these peaks are related to HGA and its ochronotic pigment. It is clear the results show that Raman spectroscopy is able to differentiate HGA treated cultures from control cultures. It is not clear however, how HGA contributes to these structural differences. As described above,

these changes could be due to the binding of ochronotic pigment to collagenous components with resulting damage to proteoglycans via ROS. Alternatively, it could be an initial stress response by cells to the presence of HGA and its pigment polymer, as indicated by the results from the average spectra (1, 48). With consideration to the results from the PCA-LDA analysis of individual cell lines (Fig. 6.7 and Fig. 6.9), and the results from the average spectra (Fig. 6.1 and Fig. 6.2), it is likely the differences seen are due to a combination of stress responses and structural alterations to the presence of HGA and its pigment polymer.

This initial experiment suggests that there is potential for Raman spectroscopy in the investigation of the pathogenesis of AKU. Raman spectroscopy has been shown to be a highly sensitive technique, capable of detecting subtle molecular changes. This ability to detect subtle changes, invisible to conventional techniques such as X-ray, has greatly enhanced the diagnosis of OA (114, 115). This has implication for using Raman spectroscopy as a potential diagnostic tool in AKU, as it may be possible to detect minor structural changes during the initial stages of ochronosis. This would enable earlier interventions, limiting progression of the disease.

7.5 Conclusion

The results from the experiments conducted in this thesis indicate that SOD does have a role in the prevention of ochronosis, and Raman spectroscopy has the potential to highlight structural differences caused by ochronosis.

The results however, demonstrate limited variability due to experimental design. The experiments conducted in this thesis were all derived from one biological replicate, with the results calculated using technical replicates (n=1). These technical replicates do not demonstrate sufficient variability to be considered as representative samples of the cell lines. Due to the lack of representative sample populations for each cell line, only the mean and SEM could be calculated for experiments I, II and III; further statistical analysis could not be conducted. It was therefore not possible to state any statistical significance from the results. Experimental repeats are required to increase sample size and improve reliability, enabling statistical certainty regarding the impact of SOD in AKU.

Several areas have been highlighted from this work, for further investigation to enable continual advancements in the understanding of AKU. The initial experiment, to assess the effects of SOD on C20 and MG63 cell lines, highlighted uncertainty in the viability of C20 cells at high concentrations of SOD. Further work should therefore be done to assess if SOD has a detrimental effect on cell viability in both cell lines, at concentrations of 500 units/ml and above. This will ensure that if SOD is targeted as a potential therapy for AKU, an effective and safe dosage with minimal side effects can be trialled.

It has been suggested that IL-6 has a role in the dysregulation of SOD. *In vitro* studies could therefore attempt to observe the effects of IL-6 in cultures containing HGA and SOD. If IL-6 does inhibit SOD, no significant differences should be expected in the quantity of ochronotic pigments between cultures containing HGA, SOD and IL-6, and cultures containing HGA only.

The results indicate that SOD has the ability to reduce/prevent ochronosis in an *in vitro* model of AKU. This suggests that SOD can have therapeutic benefits for AKU patients. However, no research has been conducted on the administration of SOD as a targeted therapy *in vivo*. Therefore, further work needs to be conducted into the methods of targeting SOD as a therapy. Studies have shown SOD mimetics injected into the articular cartilage, have beneficial effects on rats induced with arthritis. SOD mimetics are currently undergoing research with the aims of clinical implementation, in the treatment of inflammatory conditions such as arthritis (65, 116). This suggests that SOD mimetics may have a potential application in the treatment of AKU. Nevertheless, advancing research with SOD in trials involving animal models and humans, may have several challenges. Examples of this may be, finding the optimum method of administration, and identifying and reducing side effects and interactions.

The Raman spectroscopy results showed that whilst structural differences were observed, there was still a degree of overlap in both cultures. If cultures were therefore treated for a longer period prior to analysis, and repeat experiments had been conducted, a clearer distinction may have been observed. Furthermore, if both cell lines were seeded at a set number of cells/ml, a quantitative comparison would have been possible between cell lines. This may provide evidence to support the theory that C20 cells replicate and mature at a faster rate than MG63 cells.

Using Raman spectroscopy, it would be interesting to compare cartilage samples from AKU patients against control cartilage samples. If results show that it is possible to discriminate between normal cartilage and AKU cartilage, this would provide further evidence to suggest

that Raman spectroscopy could be used in the clinical setting. Studies have shown that spectral acquisitions can be made up to 4mm below the surface of the skin, using a technique known as spatially offset Raman spectroscopy. Therefore, this technique can be applied in the clinical setting to assess efficacy of treatment in AKU patients. For example, the ear can be used for clinical tests as the cartilage of the ear is commonly affected in AKU. It would be feasible to suggest that using non-invasive Raman spectroscopy techniques, the cartilage of the ear can be used to observe if treatments such as Nitisinone reduce the accumulation of HGA and prevent subsequent ochronosis (1, 79).

It is clear significant advancements have been made in the study of AKU. Furthermore, these advancements have had a significant impact on OA research. Findings from this thesis add further pieces to the puzzle, in an attempt to gain a better understanding of AKU and its disease process.

References

1. Gallagher JA, Dillon JP, Sireau N, Timmis O, Ranganath LR. Alkaptonuria: An example of a "fundamental disease"--A rare disease with important lessons for more common disorders. *Seminars in Cell & Developmental Biology*. 2016;52:53-7.
2. Mistry JB, Bukhari M, Taylor AM. Alkaptonuria. *Rare Diseases*. 2013;1:e27475.
3. Nemethova M, Radvanszky J, Kadasi L, Ascher DB, Pires DE, Blundell TL, et al. Twelve novel HGD gene variants identified in 99 alkaptonuria patients: focus on 'black bone disease' in Italy. *European Journal of Human Genetics*. 2016;24(1):66-72.
4. Ranganath L, Taylor AM, Shenkin A, Fraser WD, Jarvis J, Gallagher JA, et al. Identification of alkaptonuria in the general population: a United Kingdom experience describing the challenges, possible solutions and persistent barriers. *Journal of Inherited Metabolic Disease*. 2011;34(3):723-30.
5. Al-sbou M, Mwafi N. Nine cases of Alkaptonuria in one family in southern Jordan. *Rheumatology International*. 2012;32(3):621-5.
6. Knox WE. Sir Archibald Garrod's "Inborn Errors of Metabolism". II. Alkaptonuria. *American Journal of Human Genetics*. 1958;10(2):95-124.
7. Mannoni A, Selvi E, Lorenzini S, Giorgi M, Airo P, Cammelli D, et al. Alkaptonuria, ochronosis, and ochronotic arthropathy. *Seminars in Arthritis and Rheumatism*. 2004;33(4):239-48.

8. Taylor AM, Kammath V, Bleakley A. Tyrosinase, could it be a missing link in ochronosis in alkaptonuria? *Medical Hypotheses*. 2016;91:77-80.
9. Virchow RL. Rudolph Virchow on ochronosis.1866. *Arthritis & Rheumatology*. 1966;9(1):66-71.
10. La Du BN, Zannoni VG, Laster L, Seegmiller JE. The nature of the defect in tyrosine metabolism in alcaptonuria. *Journal of Biological Chemistry*. 1958;230(1):251-60.
11. Stenn FF, Milgram JW, Lee SL, Weigand RJ, Veis A. Biochemical identification of homogentisic acid pigment in an ochronotic egyptian mummy. *Science*. 1977;197(4303):566-8.
12. Taylor AM, Preston AJ, Paulk NK, Sutherland H, Keenan CM, Wilson PJ, et al. Ochronosis in a murine model of alkaptonuria is synonymous to that in the human condition. *Osteoarthritis and Cartilage*. 2012;20(8):880-6.
13. Preston AJ, Keenan CM, Sutherland H, Wilson PJ, Wlodarski B, Taylor AM, et al. Ochronotic osteoarthropathy in a mouse model of alkaptonuria, and its inhibition by nitisinone. *Annals of the Rheumatic Diseases*. 2014;73(1):284-9.
14. Ranganath LR, Milan AM, Hughes AT, Dutton JJ, Fitzgerald R, Briggs MC, et al. Suitability Of Nitisinone In Alkaptonuria 1 (SONIA 1): an international, multicentre, randomised, open-label, no-treatment controlled, parallel-group, dose-response study to investigate the effect of once daily nitisinone on 24-h urinary homogentisic acid excretion in patients with alkaptonuria after 4 weeks of treatment. *Annals of the Rheumatic Diseases*. 2016;75(2):362-7.

15. Braconi D, Millucci L, Bernardini G, Santucci A. Oxidative stress and mechanisms of ochronosis in alkaptonuria. *Free Radical Biology and Medicine*. 2015;88, Part A:70-80.
16. Peker E, Yonden Z, Sogut S. From darkening urine to early diagnosis of alkaptonuria. *Indian Journal of Dermatology, Venereology and Leprology*. 2008;74(6):700.
17. Noll WW, Glass DD. Causes of dark urine. *JAMA*. 1980;243(23):2398.
18. Slawson M. Thirty-three drugs that discolor urine and/or stools. *RN*. 1980;43(1):40-1.
19. Bory C, Bouliou R, Chantin C, Mathieu M. Homogentisic acid determined in biological fluids by HPLC. *Clinical Chemistry*. 1989;35(2):321-2.
20. Ranganath LR, Jarvis JC, Gallagher JA. Recent advances in management of alkaptonuria (invited review; best practice article). *Journal of Clinical Pathology*. 2013;66(5):367-73.
21. Zannoni VG, Lomtevas N, Goldfinger S. Oxidation of homogentisic acid to ochronotic pigment in connective tissue. *Biochimica et Biophysica Acta*. 1969;177(1):94-105.
22. Kazancioglu R, Taylan I, Aksak F, Durak H, Kumbasar B, Yenigun M, et al. Alkaptonuria and renal failure: a case report. *Journal of Nephrology*. 2004;17(3):441-5.
23. Venkateshan VS, Chandra B, Graziano V, Steinlauf P, Marquet E, Irmiere V, et al. Alkaptonuria and renal failure: a case report and review of the literature. *Modern Pathology*. 1992;5(4):464-71.
24. Introne WJ, Phornphutkul C, Bernardini I, McLaughlin K, Fitzpatrick D, Gahl WA. Exacerbation of the ochronosis of alkaptonuria due to renal insufficiency and improvement after renal transplantation. *Molecular Genetics and Metabolism*. 2002;77(1-2):136-42.

25. Mistry JB, Jackson DJ, Bukhari M, Taylor AM. A role for interleukins in ochronosis in a chondrocyte in vitro model of alkaptonuria. *Clinical Rheumatology*. 2016;35(7):1849-56.
26. Helliwell TR, Gallagher JA, Ranganath L. Alkaptonuria--a review of surgical and autopsy pathology. *Histopathology*. 2008;53(5):503-12.
27. Ffolkes LV, Brull D, Krywawych S, Hayward M, Hughes SE. Aortic stenosis in cardiovascular ochronosis. *Journal of Clinical Pathology*. 2007;60(1):92-3.
28. Hannoush H, Introne WJ, Chen MY, Lee SJ, O'Brien K, Suwannarat P, et al. Aortic stenosis and vascular calcifications in alkaptonuria. *Molecular Genetics and Metabolism*. 2012;105(2):198-202.
29. Lok ZS, Goldstein J, Smith JA. Alkaptonuria-associated aortic stenosis. *Journal of Cardiac Surgery*. 2013;28(4):417-20.
30. Phornphutkul C, Introne WJ, Perry MB, Bernardini I, Murphey MD, Fitzpatrick DL, et al. Natural history of alkaptonuria. *The New England Journal of Medicine*. 2002;347(26):2111-21.
31. Taylor AM, Boyde A, Wilson PJ, Jarvis JC, Davidson JS, Hunt JA, et al. The role of calcified cartilage and subchondral bone in the initiation and progression of ochronotic arthropathy in alkaptonuria. *Arthritis & Rheumatology*. 2011;63(12):3887-96.
32. Taylor AM, Wlodarski B, Prior IA, Wilson PJ, Jarvis JC, Ranganath LR, et al. Ultrastructural examination of tissue in a patient with alkaptonuric arthropathy reveals a distinct pattern of binding of ochronotic pigment. *Rheumatology (Oxford, England)*. 2010;49(7):1412-4.

33. Mathy-Hartert M, Hogge L, Sanchez C, Deby-Dupont G, Crielaard JM, Henrotin Y. Interleukin-1beta and interleukin-6 disturb the antioxidant enzyme system in bovine chondrocytes: a possible explanation for oxidative stress generation. *Osteoarthritis and Cartilage*. 2008;16(7):756-63.
34. Guerne PA, Carson DA, Lotz M. IL-6 production by human articular chondrocytes. Modulation of its synthesis by cytokines, growth factors, and hormones in vitro. *The Journal of Immunology*. 1990;144(2):499-505.
35. Braconi D, Millucci L, Ghezzi L, Santucci A. Redox proteomics gives insights into the role of oxidative stress in alkaptonuria. *Expert Review of Proteomics*. 2013;10(6):521-35.
36. Forslind K, Wollheim FA, Akesson B, Rydholm U. Alkaptonuria and ochronosis in three siblings. Ascorbic acid treatment monitored by urinary HGA excretion. *Clinical and Experimental Rheumatology*. 1988;6(3):289-92.
37. Tinti L, Spreafico A, Braconi D, Millucci L, Bernardini G, Chellini F, et al. Evaluation of antioxidant drugs for the treatment of ochronotic alkaptonuria in an in vitro human cell model. *Journal of Cellular Physiology*. 2010;225(1):84-91.
38. Spreafico A, Millucci L, Ghezzi L, Geminiani M, Braconi D, Amato L, et al. Antioxidants inhibit SAA formation and pro-inflammatory cytokine release in a human cell model of alkaptonuria. *Rheumatology (Oxford, England)*. 2013;52(9):1667-73.
39. Suwannarat P, O'Brien K, Perry MB, Sebring N, Bernardini I, Kaiser-Kupfer MI, et al. Use of nitisinone in patients with alkaptonuria. *Metabolism*. 2005;54(6):719-28.

40. Noble-Jamieson G, Barnes N. Diagnosis and management of late complications after liver transplantation. *Archives of Disease in Childhood*. 1999;81(5):446-51.
41. Ross MH, Pawlina W. *Histology : a Text and Atlas, with Correlated Cell and Molecular Biology*. 5th ed. Baltimore, Md: Lippincott Williams & Wilkins; 2006.
42. Bates P, Ramachandran M. Basics of Bone. In: Ramachandran M, editor. *Basic Orthopaedic Sciences : The Stanmore Guide* 1st ed. London: Hodder Arnold; 2006.
43. Tortora GJ, Derrickson B. *Principles of Anatomy & Physiology*. 13th ed. Hoboken, N.J.: Wiley; 2011.
44. Underwood JCE, Cross SS. *General and Systematic Pathology*. 5th ed. Edinburgh: Churchill Livingstone; 2009.
45. Waters T, Bentley G. Articular Cartilage. In: Ramachandran M, editor. *Basic Orthopaedic Sciences : The Stanmore Guide* 1st ed. London: Hodder Arnold; 2006.
46. Sophia Fox AJ, Bedi A, Rodeo SA. The basic science of articular cartilage: structure, composition, and function. *Sports Health*. 2009;1(6):461-8.
47. Bhosale AM, Richardson JB. Articular cartilage: structure, injuries and review of management. *British Medical Bulletin*. 2008;87(1):77-95.
48. Tinti L, Taylor AM, Santucci A, Wlodarski B, Wilson PJ, Jarvis JC, et al. Development of an in vitro model to investigate joint ochronosis in alkaptonuria. *Rheumatology (Oxford, England)*. 2011;50(2):271-7.

49. Doherty M, Ralston SH. Musculoskeletal Disease. In: Colledge NR, Walker BR, Ralston SH, editors. Davidson's Principles and Practice of Medicine. 21st ed. Edinburgh: Churchill Livingstone Elsevier; 2010.
50. Goldring SR, Goldring MB. Clinical aspects, pathology and pathophysiology of osteoarthritis. *Journal of Musculoskeletal & Neuronal Interactions*. 2006;6(4):376-8.
51. Hunter DJ, Felson DT. Osteoarthritis. *BMJ*. 2006;332(7542):639-42.
52. Shipley M, Rahman A, O'Gradaigh A, Conway R. Rheumatology and bone disease. In: Kumar P, Clark M, editors. Kumar and Clark's Clinical Medicine. 8th ed. Edinburgh: Churchill Livingstone; 2012.
53. Goldring MB, Goldring SR. Articular cartilage and subchondral bone in the pathogenesis of osteoarthritis. *Annals of the New York Academy of Sciences*. 2010;1192:230-7.
54. Goldring MB. Osteoarthritis and cartilage: the role of cytokines. *Current Rheumatology Reports*. 2000;2(6):459-65.
55. Poole AR, Kobayashi M, Yasuda T, Lavery S, Mwale F, Kojima T, et al. Type II collagen degradation and its regulation in articular cartilage in osteoarthritis. *Annals of the Rheumatic Diseases*. 2002;61 Suppl 2:ii78-81.
56. Malesud CJ, Islam N, Haqqi TM. Pathophysiological Mechanisms in Osteoarthritis Lead to Novel Therapeutic Strategies. *Cells Tissues Organs*. 2003;174(1-2):34-48.
57. Goldring MB. The role of the chondrocyte in osteoarthritis. *Arthritis & Rheumatology*. 2000;43(9):1916-26.

58. Martel-Pelletier J, McCollum R, Fujimoto N, Obata K, Cloutier JM, Pelletier JP. Excess of metalloproteases over tissue inhibitor of metalloprotease may contribute to cartilage degradation in osteoarthritis and rheumatoid arthritis. *Laboratory Investigation*. 1994;70(6):807-15.
59. Ling S, M, Bathon J, M. Osteoarthritis: Pathophysiology: John Hopkins Arthritis Centre; 2012 [cited 2016 12/10]. Available from: <http://www.hopkinsarthritis.org/arthritis-info/osteoarthritis/oa-pathophysiology/> - ref.
60. Gallagher JA, Ranganath LR, Boyde A. Lessons from rare diseases of cartilage and bone. *Current Opinion in Pharmacology*. 2015;22:107-14.
61. Weydert CJ, Cullen JJ. Measurement of superoxide dismutase, catalase and glutathione peroxidase in cultured cells and tissue. *Nature Protocols*. 2010;5(1):51-66.
62. Nozik-Grayck E, Suliman HB, Piantadosi CA. Extracellular superoxide dismutase. *The International Journal of Biochemistry & Cell Biology*. 2005;37(12):2466-71.
63. Regan E, Flannelly J, Bowler R, Tran K, Nicks M, Carbone BD, et al. Extracellular Superoxide Dismutase and Oxidant Damage in Osteoarthritis. *Arthritis & Rheumatology*. 2005;52(11):3479-91.
64. Marklund SL. Extracellular superoxide dismutase in human tissues and human cell lines. *The Journal of Clinical Investigation*. 1984;74(4):1398-403.
65. Di Cesare Mannelli L, Bani D, Bencini A, Brandi ML, Calosi L, Cantore M, et al. Therapeutic Effects of the Superoxide Dismutase Mimetic Compound Me2DO2A on Experimental Articular Pain in Rats. *Mediators of Inflammation*. 2013;2013:11.

66. Curtis SL, Roberts NB, Ranganath LR. Interferences of homogentisic acid (HGA) on routine clinical chemistry assays in serum and urine and the implications for biochemical monitoring of patients with alkaptonuria. *Clinical Biochemistry*. 2014;47(7–8):640-7.
67. Hughes AT, Milan AM, Christensen P, Ross G, Davison AS, Gallagher JA, et al. Urine homogentisic acid and tyrosine: simultaneous analysis by liquid chromatography tandem mass spectrometry. *Journal of Chromatography B*. 2014;963:106-12.
68. Lafont JE. Lack of oxygen in articular cartilage: consequences for chondrocyte biology. *International Journal of Experimental Pathology*. 2010;91(2):99-106.
69. Henrotin YE, Bruckner P, Pujol JPL. The role of reactive oxygen species in homeostasis and degradation of cartilage. *Osteoarthritis and Cartilage*. 2003;11(10):747-55.
70. Calvi ENdC, Nahas FX, Barbosa MV, Calil JA, Ihara SSM, Silva MdS, et al. An experimental model for the study of collagen fibers in skeletal muscle. *Acta Cirurgica Brasileira*. 2012;27:681-6.
71. Last JA, Siefkin AD, Reiser KM. Type I collagen content is increased in lungs of patients with adult respiratory distress syndrome. *Thorax*. 1983;38(5):364-8.
72. Hitomi Y, Watanabe S, Kizaki T, Sakurai T, Takemasa T, Haga S, et al. Acute exercise increases expression of extracellular superoxide dismutase in skeletal muscle and the aorta. *Redox Report*. 2008;13(5):213-6.
73. Gill S, Wight TN, Frevert CW. Proteoglycans: Key Regulators of Pulmonary Inflammation and the Innate Immune Response to Lung Infection. *Anatomical Record*. 2010;293(6):968-81.

74. Gillies AR, Lieber RL. Structure and Function of the Skeletal Muscle Extracellular Matrix. *Muscle & Nerve*. 2011;44(3):318-31.
75. Superoxide Dismutase from bovine erythrocytes. Product Information, : Sigma Aldrich; 2011.
76. Kerns JG, Buckley K, Parker AW, Birch HL, Matousek P, Hildred A, et al. The use of laser spectroscopy to investigate bone disease in King Henry VIII's sailors. *Journal of Archaeological Science*. 2015;53:516-20.
77. Bumbrah GS, Sharma RM. Raman spectroscopy – Basic principle, instrumentation and selected applications for the characterization of drugs of abuse. *Egyptian Journal of Forensic Sciences*. 2016;6(3):209-15.
78. Smith E, Dent G. *Modern Raman Spectroscopy – A Practical Approach*. Chichester, UK: John Wiley & Sons, Ltd; 2005.
79. Kerns JG, Gikas PD, Buckley K, Shepperd A, Birch HL, McCarthy I, et al. Evidence from Raman Spectroscopy of a Putative Link Between Inherent Bone Matrix Chemistry and Degenerative Joint Disease. *Arthritis & Rheumatology*. 2014;66(5):1237-46.
80. Taylor AM, Boyde A, Davidson JS, Jarvis JC, Ranganath LR, Gallagher JA. Identification of trabecular excrescences, novel microanatomical structures, present in bone in osteoarthropathies. *European Cells & Materials*. 2012;23:300-8; discussion 8-9.
81. Goldring MB, Birkhead JR, Suen LF, Yamin R, Mizuno S, Glowacki J, et al. Interleukin-1 beta-modulated gene expression in immortalized human chondrocytes. *The Journal of Clinical Investigation*. 1994;94(6):2307-16.

82. Gartland A, Rumney RM, Dillon JP, Gallagher JA. Isolation and culture of human osteoblasts. *Methods in Molecular Biology*. 2012;806:337-55.
83. Montreal-Biotech. C-Chip Instructions.
84. Mistry JB, Jackson DJ, Bukhari M, Taylor AM. Osteoarticular cells tolerate short-term exposure to nitisinone-implications in alkaptonuria. *Clinical Rheumatology*. 2016;35(2):513-6.
85. Bancroft JD. *Theory and practice of histological techniques*. 6th ed. Gamble M, editor: Philadelphia, Pa. : Churchill Livingstone Elsevier; 2008.
86. Mistry JB. *The role of osteoarthritic cytokines in the development of ochronotic osteoarthropathy (Thesis)*. Lancaster University.2013.
87. Mort JS, Roughley PJ. Measurement of Glycosaminoglycan Release from Cartilage Explants. In: Cope AP, editor. *Arthritis Research: Methods and Protocols Volume 1*. Totowa NJ: Humana Press; 2007.
88. Smith R, Wright KL, Ashton L. Raman spectroscopy: an evolving technique for live cell studies. *Analyst*. 2016;141(12):3590-600.
89. Butler HJ, Ashton L, Bird B, Cinque G, Curtis K, Dorney J, et al. Using Raman spectroscopy to characterize biological materials. *Nature Protocols*. 2016;11(4):664-87.
90. Kelly JG, Trevisan J, Scott AD, Carmichael PL, Pollock HM, Martin-Hirsch PL, et al. Biospectroscopy to metabolically profile biomolecular structure: a multistage approach linking computational analysis with biomarkers. *Journal of Proteome Research*. 2011;10(4):1437-48.

91. Ashton L, Brewster VL, Correa E, Goodacre R. Detection of glycosylation and iron-binding protein modifications using Raman spectroscopy. *Analyst*. 2017;142(5):808-14.
92. Kelly JG, Martin-Hirsch PL, Martin FL. Discrimination of Base Differences in Oligonucleotides Using Mid-Infrared Spectroscopy and Multivariate Analysis. *Analytical Chemistry*. 2009;81(13):5314-9.
93. Salbach-Hirsch J, Ziegler N, Thiele S, Moeller S, Schnabelrauch M, Hintze V, et al. Sulfated glycosaminoglycans support osteoblast functions and concurrently suppress osteoclasts. *Journal of Cellular Biochemistry*. 2014;115(6):1101-11.
94. Boyde A, Davis GR, Mills D, Zikmund T, Cox TM, Adams VL, et al. On fragmenting, densely mineralised acellular protrusions into articular cartilage and their possible role in osteoarthritis. *Journal of Anatomy*. 2014;225(4):436-46.
95. Taylor AM, Hsueh MF, Ranganath LR, Gallagher JA, Catterall JB, Kraus VB. Analysis of cartilage biomarkers of aging and turnover in the osteoarthropathy of alkaptonuria. *Osteoarthritis and Cartilage*. 2015;23:A135.
96. Esmonde-White KA, Esmonde-White FWL, Morris MD, Roessler BJ. Fiber-optic Raman Spectroscopy of Joint Tissues. *Analyst*. 2011;136(8):1675-85.
97. Esmonde-White K. Raman Spectroscopy of Soft Musculoskeletal Tissues. *Applied Spectroscopy*. 2014;68(11):1203-18.
98. Rieppo L, Töyräs J, Saarakkala S. Vibrational spectroscopy of articular cartilage. *Applied Spectroscopy Reviews*. 2017;52(3):249-66.

99. Mandair GS, Morris MD. Contributions of Raman spectroscopy to the understanding of bone strength. *BoneKEy Reports*. 2015;4.
100. Morris MD, Mandair GS. Raman Assessment of Bone Quality. *Clinical Orthopaedics and Related Research*. 2011;469(8):2160-9.
101. Powers SK, Jackson MJ. Exercise-induced oxidative stress: cellular mechanisms and impact on muscle force production. *Physiological Reviews*. 2008;88(4):1243-76.
102. Sandstrom J, Karlsson K, Edlund T, Marklund SL. Heparin-affinity patterns and composition of extracellular superoxide dismutase in human plasma and tissues. *Biochemical Journal*. 1993;294 (Pt 3):853-7.
103. Karlsson K, Lindahl U, Marklund SL. Binding of human extracellular superoxide dismutase C to sulphated glycosaminoglycans. *Biochemical Journal*. 1988;256(1):29-33.
104. Alves RD, Demmers JA, Bezstarosti K, van der Eerden BC, Verhaar JA, Eijken M, et al. Unraveling the human bone microenvironment beyond the classical extracellular matrix proteins: a human bone protein library. *Journal of Proteome Research*. 2011;10(10):4725-33.
105. Bonifacio A, Beleites C, Vittur F, Marsich E, Semeraro S, Paoletti S, et al. Chemical imaging of articular cartilage sections with Raman mapping, employing uni- and multi-variate methods for data analysis. *Analyst*. 2010;135(12):3193-204.
106. Dillon JP, Waring-Green VJ, Taylor AM, Wilson PJM, Birch M, Gartland A, et al. Primary Human Osteoblast Cultures. In: Helfrich MH, Ralston SH, editors. *Bone Research Protocols*. Totowa, NJ: Humana Press; 2012. p. 3-18.

107. Chiang Y-H, Wu SH, Kuo Y-C, Chen H-F, Chiou A, Lee OK. Raman spectroscopy for grading of live osteosarcoma cells. *Stem Cell Research & Therapy*. 2015;6(1):81.
108. Goldring MB. Chondrogenesis, chondrocyte differentiation, and articular cartilage metabolism in health and osteoarthritis. *Therapeutic Advances in Musculoskeletal Disease*. 2012;4(4):269-85.
109. Lee DY, Li YS, Chang SF, Zhou J, Ho HM, Chiu JJ, et al. Oscillatory flow-induced proliferation of osteoblast-like cells is mediated by α v β 3 and β 1 integrins through synergistic interactions of focal adhesion kinase and Shc with phosphatidylinositol 3-kinase and the Akt/mTOR/p70S6K pathway. *Journal of Biological Chemistry*. 2010;285(1):30-42.
110. Tiku ML, Sabaawy HE. Cartilage regeneration for treatment of osteoarthritis: a paradigm for nonsurgical intervention. *Therapeutic Advances in Musculoskeletal Disease*. 2015;7(3):76-87.
111. Man GS, Mologhianu G. Osteoarthritis pathogenesis – a complex process that involves the entire joint. *Journal of Medicine and Life*. 2014;7(1):37-41.
112. Lodish HF. *Molecular cell biology*. 8th ed. New York: W.H. Freeman Macmillan Learning; 2016.
113. De Gelder J, De Gussem K, Vandenabeele P, Moens L. Reference database of Raman spectra of biological molecules. *Journal of Raman Spectroscopy*. 2007;38(9):1133-47.
114. Brezillon S, Untereiner V, Mohamed HT, Hodin J, Chatron-Colliet A, Maquart FX, et al. Probing glycosaminoglycan spectral signatures in live cells and their conditioned media by Raman microspectroscopy. *Analyst*. 2017;142(8):1333-41.

115. Kong K, Kendall C, Stone N, Notingher I. Raman spectroscopy for medical diagnostics — From in-vitro biofluid assays to in-vivo cancer detection. *Advanced Drug Delivery Reviews*. 2015;89:121-34.
116. Muscoli C, Cuzzocrea S, Riley DP, Zweier JL, Thiemermann C, Wang ZQ, et al. On the selectivity of superoxide dismutase mimetics and its importance in pharmacological studies. *British journal of pharmacology*. 2003;140(3):445-60.